The Smithian/Spathian boundary (late Early Triassic): a review of ammonoid, conodont, and carbon-isotopic criteria.

Lei Zhang, Michael J. Orchard, Arnaud Brayard, Thomas J. Algeo, Laishi Zhao, Zhong-Qiang Chen, Zhengyi Lyu

Published in Earth-Science Reviews 195 (2019) 7–36

The Smithian/Spathian boundary (late Early Triassic): a review of ammonoid, conodont, and carbon-isotopic criteria

Lei Zhang[a,b], Michael J. Orchard[a,c], Arnaud Brayard[d], Thomas J. Algeo[a,b,e,*], Laishi Zhao[a,*], Zhong-Qiang Chen[e], Zhengyi Lyu[a]

[a] *State Key Laboratory of Geological Processes and Mineral Resources, China University of Geosciences, Wuhan 430074, China*
[b] *Department of Geology, University of Cincinnati, Cincinnati, Ohio 45221-0013, U.S.A.*
[c] *Geological Survey of Canada, 1500-605 Robson St., Vancouver, B.C. V6B 5J3, Canada*
[d] *Biogéosciences, UMR 6282 CNRS, Université Bourgogne Franche-Comté, 21000 Dijon, France*
[e] *State Key Laboratory of Biogeology and Environmental Geology, China University of Geosciences, Wuhan 430074, China*

*Corresponding authors: thomas.algeo@uc.edu (T.J. Algeo); zlscug@163.com (L.S. Zhao)

Abstract

The transition from the Smithian substage to the Spathian substage of the Olenekian stage of the late Early Triassic was a critical time marked by a series of biological and environmental changes during the multimillion-year recovery interval following the end-Permian mass extinction. However, the Smithian/Spathian boundary (SSB) has not yet been formally defined, a shortcoming that inhibits targeted detailed studies of successive events during the Smithian-Spathian transition and the recovery of the marine ecosystem during the Early Triassic. Here, we review main biostratigraphic (i.e., ammonoid and conodont) studies of the Smithian and Spathian substages in historically important regions (e.g., the Canadian Arctic for the Boreal realm, western North America for the eastern Panthalassic Ocean) and more recently re-studied locations (e.g., Pakistan and India in the southern Tethys, South China in the eastern Tethys) as well as the carbon isotope chemostratigraphy of 29 major Smithian-Spathian sections globally. Key ammonoid genera (e.g., *Wasatchites*, *Anasibirites*, *Glyptophiceras* and *Xenoceltites* of the late Smithian, and *Bajarunia*, *Tirolites* and *Columbites* of the early Spathian), conodont species (e.g., *Scythogondolella milleri, Novispathodus waageni*, and *Borinella buurensis* of the late Smithian, and *'Triassospathodus' hungaricus*, *Neogondolella* aff. *sweeti,* and *Icriospathodus* spp. of the early Spathian), and carbonate carbon isotope excursions provide appropriate markers for constraining the SSB. Use of the first occurrence of the conodont *Novispathodus pingdingshanensis* as a potential marker of the SSB is also discussed. Based on correlations of biostratigraphic and carbon isotope data globally, we propose to revise previous placements of the SSB transition in some sections. Finally, we show that the Smithian Thermal Maximum (STM; herein named) was middle Smithian in age and not correlative with the SSB, as inferred in some earlier studies, and that the SSB coincided with a subsequent major global cooling event.

Keywords: Carbon isotopes; Olenekian; Boreal; Tethyan; Smithian Thermal Maximum; hyperwarming;

Outline

---

1. Introduction

The Early Triassic is officially divided into two stages, the Induan and Olenekian, with the latter divided into two substages, the Smithian (ca. 0.7 Myr long) and Spathian (ca. 3 Myr long) (Fig. 1; Ovtcharova et al., 2006, 2015; Lehrmann et al., 2006; Galfetti et al., 2007; Mundil et al., 2010; Baresel et al., 2017). An alternative timescale based on cyclostratigraphic analysis of successions in Germany and China has assigned durations of 1.7 and 1.4 Myr to the Smithian and Spathian substages, respectively (Li et al., 2016a). The boundary between the Smithian and Spathian substages is an important transition during the recovery of marine ecosystems following the end-Permian mass extinction (EPME). Marine faunas show major rapid changes

during the late Smithian (over <0.12 Myr; Brühwiler et al., 2010) that continued across the Smithian/Spathian boundary (SSB), including a severe loss of biodiversity among conodonts and ammonoids (Brayard et al., 2006; Orchard, 2007; Stanley, 2009), size changes among surviving conodont taxa (Chen-YL et al., 2013; Leu et al., 2016, 2018), and greater cosmopolitanism among surviving ammonoid taxa (Brayard et al., 2006, 2007a; Fig. 1). Vegetation on land was marked by a rebound of arborescent forms (gymnosperms) during the late Smithian, following a prolonged interval of dominance by shrubby disaster-type taxa following the EPME (Galfetti et al., 2007a; Schneebeli-Hermann et al., 2012; Saito et al., 2012; Hochuli et al., 2016). In addition, a significant marine transgression occurred during the Smithian, followed by a marked regression across the SSB (e.g., Embry, 1997; Twitchett and Barras, 2004; Henderson et al., 2018). In some areas, dominantly argillaceous rocks and organic-rich shales of the late Smithian were replaced by massive carbonate rocks during the early Spathian (e.g., South China, Galfetti et al., 2008). Major perturbations in the global carbon (C) cycle were recorded by a negative $\delta^{13}C$ shift during the middle Smithian (i.e., the N3 minimum; note: the numbering system of Early Triassic C-isotopic excursions is from Song-HY et al., 2013, 2014, and used here for convenience in correlation among different studied regions), followed by a large positive shift across the SSB (to the P3 maximum) (Fig. 1). These excursions represent the fluctuations in a ~1.5-Myr-long interval of rapid, large C-isotope fluctuations that commenced at the EPME, and it was followed by muted C-isotope variation during the Spathian substage (e.g., Payne et al., 2004; Tong et al., 2007). The SSB transition was also characterized by strong tropical sea-surface cooling (Sun et al., 2012; Romano et al., 2013), and a likely steepening of the latitudinal temperature gradient (Brayard et al., 2009a). It also corresponds to the establishment of first known complex and diversified biotas after the EPME (Brayard et al., 2017). This amalgam of biotic, environmental, and climatic changes at the SSB transition is known as the "SSB Event" (e.g., Galfetti et al., 2007a).

Biostratigraphic analysis of the SSB transition began with studies of ammonoids in the Alps (Austria, Italy and Bosnia), the Himalayas (India), and the Salt Range (Pakistan) by a number of workers during the late nineteenth and early twentieth centuries, including Edmund von Mojsisovics (1839-1907), Wilhelm Heinrich Waagen (1841-1900), and Carl Diener (1862-1928). A key paper was Mojsisovics et al. (1895), which presented an ammonoid biozonation that was used to define series and stages in the first complete formal subdivision of the Triassic system. Important early work on ammonoids in the western United States was undertaken by James Perrin Smith (1864-1931) and Norman John Silberling (1928-2011), among others. The substages of the Early Triassic were established based on extensive and detailed studies of ammonoids from marine faunas collected in the Canadian Arctic by geologists from the Geological Survey of Canada (Tozer, 1962, 1965, 1967, 1971, 1984, 1994). Tozer (1994) first reported an ammonoid biozonation for both the Smithian and Spathian substages. As a result of these investigations, the Triassic portion of the Standard Global Chronostratigraphic Scale was based exclusively on ammonoid biostratigraphy until the 1990s, and ammonoid studies have been continued by later researchers (e.g., Galfetti et al., 2007b; Shigeta et al., 2009; Guex et al., 2010; Jenks et al., 2015, and references therein).

The comparative scarcity of ammonoids in some Lower Triassic successions and the relative inaccessibility of ammonoid-based type sections in the Canadian Arctic, however, generated interest in the use of conodonts, which are generally abundant in both tropical and

boreal sections, for biostratigraphic subdivision of the Lower Triassic beginning in the late 1960s and 1970s (Mosher, 1968, 1970; Sweet, 1970a, b). Initially, most of this work was undertaken in the Tethyan region, for example Pakistan (Salt Range), Kashmir (Guryul Ravine) (Sweet, 1970a, b), and later in South China Craton (Yangtze area) (e.g., Yin et al., 1986, 1996) and North America (Henderson, 1997; Henderson et al., 2001). This was the case for the P/Tr and Induan/Olenekian boundaries, which now have ratified or proposed global stratotype sections and points (GSSPs) based on the first appearance datums (FADs) of *Hindeodus parvus* (Yin et al., 2001) and *Neospathodus* ex gr. *waageni* (Zhao et al., 2002, 2004, 2008a, b; Tong et al., 2003, 2004; Goudemand, 2014a), respectively. Subsequently, high-resolution conodont biozonation studies of the Lower Triassic have been undertaken broadly around the world (e.g., Krystyn et al., 2005; Henderson and Mei, 2007; Nakrem et al., 2008; Orchard, 2008; Orchard and Zonneveld, 2009; Zhao et al., 2013a; Chen-YL et al., 2015; Lyu et al., 2017).

Despite its importance and the considerable research efforts lavished on it in recent decades, the SSB has yet to be formally defined by the International Commission on Stratigraphy (ICS)'s Subcommission on Triassic Stratigraphy (STS) (www.stratigraphy.org/index.php/ics-gssps). The ICS is currently working on stage boundary definitions and substage boundaries will not be addressed for some time yet. However, there is considerable value in establishing a precise (not formal) definition for the SSB to direct future work.The present contribution has several goals: (1) we review the history of studies of the Smithian-Spathian transition by region globally, (2) we summarize known key features of ammonoid and conodont biostratigraphy as well as carbon isotope chemostratigraphy that may prove useful for future formal definition of the SSB, and (3) we examine placements of the SSB in earlier studies, considering problematic placements and offering corrections in some cases. The present study may serve as an important reference for the future formal definition of the SSB and in investigation of the major events associated with it.

2. Evolutionary history of ammonoids and conodonts during the Smithian-Spathian transition

Following the EPME, the diversity (*sensu* taxonomic richness) of ammonoids and conodonts increased and their turnover rates became more rapid than those of most other marine invertebrate clades (Brayard et al., 2006, 2009b; Orchard, 2007; Brühwiler et al., 2010a, b, c; Ware et al., 2015). They thus provide an appropriate basis for construction of a detailed, accurate biostratigraphic framework for the Early Triassic. Both ammonoids and conodonts show relatively similar patterns of rapid diversifications and extinctions during the Early Triassic: rising diversity during the Griesbachian was followed by a minimum in the middle Dienerian, and then by major radiative bursts in the early Smithian (Tozer, 1981a, b; Brayard et al., 2006, 2009b; Orchard, 2007; Brühwiler et al., 2010a, b, c; Zakharov and Abnavi, 2013; Ware et al., 2015). Both clades experienced a second deep-cutting extinction at the beginning of the late Smithian, followed by another rapid diversification in the early Spathian. The late Smithian also corresponds to a drastic reduction of the ammonoid morphological disparity with the disappearance of sphaeroconic forms (Brosse et al., 2013). These diversity (*sensu lato*) fluctuations correspond to the large carbonate C-isotope shifts and temperature fluctuations of the Early Triassic, likely reflecting the sensitivity of these clades to climatic and environmental

perturbations (Brayard et al., 2006, Orchard, 2007; Stanley, 2009; Leu et al., 2018; Goudemand et al., 2018).

The turnover among ammonoids during the late Smithian has long been recognized (e.g., Tozer, 1982). It is now dated to the base of the *Anasibirites-Wasatchites* Zone, which is globally recognized (see Jenks et al., 2015 for a review, and Jattiot et al., 2016 for discussion of the significance of the iconic taxon *Anasibirites*). Generic diversity decreased markedly from the early-middle Smithian to the SSB transition, followed by a rebound by the middle to late Spathian, as for instance inferred from Canadian (Stanley, 2009; Fig. 1) or western USA (Guex et al., 2010) ammonoid data. The Meekoceratacеae superfamily suffered deep losses at the middle/late Smithian boundary, including extinction of the Lanceolitidae, Paranannitidae and Inyoitidae families (Brayard et al., 2006; Fig. 2). Many ammonoid taxa that are important for zonation of the early late Smithian, e.g., Prionitidae such as *Anasibirites* and *Wasatchites*, show highly cosmopolitan distributions at that time (e.g., Tozer, 1994; Orchard and Tozer, 1997; Zakharov et al., 2004; Jattiot et al., 2016, 2017, 2018). They were then replaced in the latest Smithian by a few taxa, mainly belonging to the Xenoceltitidae (*Xenoceltites*, *Glyptophiceras*) and Hedenstroemiidae (*Pseudosageceras augustum*), that had also similar cosmopolitan distributions (e.g., Brühwiler et al., 2010b, c; Jenks et al., 2015; Jattiot et al., 2017). The surviving lineages underwent a new rediversification during the earliest Spathian, marked by the rapid origination of many new families (Doricranitidae, Tirolitidae, Columbitidae, Albanitidae) and several genera of uncertain phylogenetic affinities such as *Bajarunia* (e.g., Balini et al., 2010; Guex et al., 2010; Zakharov and Abnavi, 2013; Jenks et al., 2013; Shigeta et al., 2014; Fig. 2). Most of these new early Spathian ammonoid taxa are now widely used for zonation, e.g., *Columbites* and *Procolumbites* among the Columbitidae, and *Tirolites* among the Tirolitidae (see e.g., Guex et al., 2010; Jenks et al., 2015).

Among the conodonts, the SSB Event marked the largest loss of diversity prior to their complete extinction at the end of the Triassic (Orchard, 2007). The number of conodont species globally declined from >30 species in the mid-Smithian to ~8 at the SSB transition and 2 at the earliest Spathian before rebounding to >20 in the mid-Spathian (simplified estimates based on Stanley, 2009; Fig. 1). Two important clades of the Smithian, the Ellisoniidae family and Mullerinae subfamily, mostly went extinct during the late Smithian or at the SSB (Orchard, 2007; Fig. 3). In contrast, the Novispathodinae subfamily was characterized by the survival of genera that had been extant since the early Olenekian (e.g., *Novispathodus*) as well as origination of the new genus *Triassospathodus* in the early Spathian (Orchard, 2007; Fig. 3). Other taxa that are important for conodont biozonation appeared in the Spathian, including *Icriospathodus* (affinity unknown) in the early Spathian, and *Triassospathodus* (Novispathodinae subfamily) in the early to middle Spathian. Less is known about *Neogondolella*-like taxa, although they are important for biostratigraphy at high latitudes. The survival and rebound of *Novispathodus* and similar genera were maybe due in part to their high diversity prior to the SSB Event (>30 species in the mid-Smithian) (Orchard, 2007) as well as their probable survival in deep-water refugia (Song-HJ et al., 2014). However, this later hypothesis is now challenged (Leu et al., 2018). The above cited genera are among the most important for conodont biozonation in the late Smithian to early Spathian (Zhao et al., 2003a, 2007a; Krystyn et al., 2005; Chen-YL et al., 2015, 2018).

3. Global review of Smithian-Spathian sections

Historically, the Olenekian Stage (the second stage of the Early Triassic) was defined in the Boreal realm (originally on sections along the Olenek River in Siberia), in contrast to the Induan Stage (the first stage of the Early Triassic), which was defined in the tropical Tethyan realm (Salt Range, Pakistan) (Kiparisova and Popov, 1956, 1961). In the following decades, detailed ammonoid biostratigraphic studies of the Olenekian were carried out elsewhere in the Boreal realm (Canadian Arctic) (Tozer, 1967, 1994), eastern Panthalassa (western Canada and western USA) (Silberling and Tozer, 1968; Tozer, 1994, Orchard and Tozer, 1997; Lucas and Orchard, 2007; Guex et al., 2010; Brayard et al. 2013), eastern Tethys (South China) (Tong et al., 2004; Galfetti et al., 2007b, c), and southern Tethys (India and Pakistan) (Brühwiler et al., 2007, 2012a, b; Krystyn et al., 2007a, b), as reviewed in Jenks et al. (2015) (Fig. 4A-C).

By the late 1990s and early 2000s, biostratigraphic research had shifted to a large degree from Boreal and Panthalassic to Tethyan sections, due to their abundance and generally greater accessibility, in which both ammonoids and conodonts were shown to be highly useful for biozonation owing to their wide distributions and rapid evolution during the Early Triassic (Zhao et al., 2002, 2003a, b, 2005a, b, c; Tong et al., 2004; Brühwiler et al., 2007, 2012a, b; Galfetti et al., 2007b, c). The co-occurrence of ammonoids and conodonts in Lower Triassic successions makes it possible to construct parallel biozonation schemes (e.g., Canadian Arctic, Tozer, 1994, Orchard, 2008; Chaohu, Zhao et al., 2003a, 2007a, b, Tong et al., 2004; Spiti, Brühwiler et al., 2007, Krystyn et al., 2005), which facilitates global correlations. Correlations based on C-isotope chemostratigraphy have also been used, especially when fossil records are sparse, as for some sections in the Tethyan (Horacek et al., 2007a, b; Zhang et al., 2015), Boreal (Grasby et al., 2016; Wignall et al., 2016), and Panthalassic regions (Zhang et al., 2017). Below, we review ammonoid- and conodont-based biostratigraphic as well as C-isotopic chemostratigraphic studies of the Olenekian in key geographic regions, their intercalibration, and their significance for definition of the SSB.

Boreal and Tethyan faunas experienced fluctuating patterns of endemism and cosmopolitanism throughout the Early Triassic related to recurrent environmental stresses and large geographic distances (Brayard and Bucher, 2015). Boreal ammonoid faunas are generally different and less diverse than those of the Tethyan realm (Tozer, 1981b; Dagys, 1988). Brayard et al. (2006, 2007a) studied the global patterns of latitudinal diversity gradients and assemblage similarity, showing that ammonoid faunas exhibit a clear latitudinal diversity gradient during most of the Smithian and Spathian stages, and a return to cosmopolitan distributions in the late Smithian. Boreal ammonoids were characterized by peak endemism during the Spathian (Kummel, 1973; Dagys, 1997). During the Spathian, ammonoid diversity in high-latitude areas was generally lower than at low latitudes (Brayard et al., 2006; Fig. 1). In northeastern British Columbia, Boreal and Tethyan ammonoid faunas can be found together, thus facilitating correlations between high- and low-latitude regions (Tozer, 1994).

The Smithian and Spathian substages have been subdivided recently into early/middle/late subunits on the basis of global ammonoid biostratigraphy (Brühwiler et al., 2010; Guex et al., 2010; Brayard et al., 2013; Jenks et al. 2015; Fig. 5). The early Smithian corresponds to first flemingitid and kashmiritid occurrences, and the middle Smithian represents the flourishing of families such as the Paranannitidae, Inyoitidae, Aspenitidae and Lanceolitidae (Fig. 2). The

late Smithian, which began with a major extinction among several ammonoid families, corresponds to a marked diversification of highly cosmopolitan prionitids such as *Anasibirites* and *Wasatchites* followed by the occurrence of cosmopolitan xenoceltitid (*Xenoceltites* sp., *Glyptophiceras*) and hedenstroemiid (*Pseudosageceras augustum*) taxa (Fig. 2). The early Spathian is marked by the first occurrences of *Bajarunia* and *Doricranites* and continues up to the *Procolumbites* Zone. The middle and late Spathian span the *Subcolumbites* and *Neopopanoceras haugi* zones, respectively. It should be noted that some ammonoid zones/beds are of regional significance and not found globally. These ultrafine subdivisions are possible primarily due to the practice of identifying ammonoid assemblages, which provide a high level of biostratigraphic resolution (Fig. 5). It should also be noted that the basal Smithian cannot be precisely delineated until the Induan/Olenekian boundary is formalized.

The record of sedimentation during the Smithian-Spathian transition was significantly affected by contemporaneous eustatic fluctuations. Short-term eustatic variation can be due to changes in continental ice mass and thermal expansion/contraction of seawater linked to changing global climate conditions (Milne et al., 2009; Dutton et al., 2015), or to astronomically forced land–ocean watermass exchange during geologic epochs lacking ice sheets (as postulated for the Early Triassic by Li et al., 2018). Large temperature changes were the likely cause of eustatic fluctuations during the SSB transition. The middle Smithian was an interval of hyperwarming (the Smithian Thermal Maximum, or STM; see Section 5.5) that coincided with a global transgression, and the SSB interval proper was an interval of pronounced cooling that coincided with a sharp eustatic fall (Sun et al., 2012; Romano et al., 2013; Zhang et al., 2017; see Section 5.5). The eustatic fall at the SSB resulted in widespread deposition of regressive systems tracts and/or sedimentary hiatuses, as in northern Italy (Twitchett and Barras, 2004), Iran (Horacek et al., 2007b), and Japan (Zhang et al., 2017), although the SSB succession in the western USA is thought to be nearly continuous (Guex et al., 2010; Brayard et al., 2013) due to regional tectonic controls (e.g., Caravaca et al., 2018). As such, the issue of stratigraphic condensation at the SSB is one that will have to be evaluated carefully in the context of selecting a suitable section as the GSSP of the SSB. A potential way to circumvent this problem is, for instance, to give preference to deeper-water sections.

3.1 Canadian Arctic (western Boreal)

3.1.1 Ammonoid and conodont biostratigraphy

The Canadian Arctic has long been central to an ammonoid-based subdivision of the Triassic in the northern Pangea region owing to a near-continuous marine succession from the lower Griesbachian to the upper Norian (Thorsteinsson and Tozer, 1970; Tozer, 1994). Substages of the Early Triassic were named for type sections in this area, i.e., the Griesbachian, Dienerian, Smithian, and Spathian were derived from Griesbach Creek on Axel Heiberg Island, and the Diener, Smith, and Spath creeks on Ellesmere Island (Tozer, 1965, 1967) (Fig. 4B). The thick (>2000 m) Lower Triassic successions in the Arctic accumulated in the Sverdrup Basin, grading from sandstones of the Bjorne Formation on the basin margin to shaly siltstones of the Blind Fjord Formation in the basin center (Tozer, 1961; Embry, 1986, 1991). The Blind Fjord Formation consists of three members, the Confederation Point Member (Griesbachian to

Dienerian in age), Smith Creek Member (Smithian in age), and Svartfjeld Member (mostly Spathian in age) (Embry, 1986; Orchard, 2008).

Despite the discontinuous stratigraphic distribution of ammonoid-bearing beds in these units, a succession of Early Triassic ammonoid zones were recognized (Tozer, 1994) and provided a basis for broad definition of the SSB. These ammonoid zones (in ascending order) are the *Hedenstroemia hedenstroemi*, *Euflemingites romunderi*, and *Anawasatchites tardus* for the Smithian (Tozer, 1994) and the *Olenikites pilaticus* and *Keyserlingites subrobustus* for the late early and latest Spathian, respectively (Tozer, 1967; Fig. 5A). Most of the early Spathian strata in this region are devoid of ammonoids. For example, at Smith Creek, no ammonoids were found above the upper Smithian *A. tardus* beds (Fig. 6A). The Spathian *Olenikites pilaticus* Zone is found only in limited areas south of Svartevaeg on Axel Heiberg Island (Tozer, 1967), where it directly overlies *Arctoceras gigas* n. sp. beds (GSC loc. 64719 above GSC loc. 64718) that have been tentatively correlated with the *A. tardus* Zone (Tozer, 1994), but this attribution is doubtful (see Section 5.1). In this area, the SSB is thus bracketed by the late Smithian *A. tardus* Zone and the late early Spathian *Olenikites pilaticus* Zone. This represents an important information gap, but the SSB is usually placed just above the *A. tardus* Zone (e.g., Grasby et al. 2013) as it corresponds to a complex assemblage of several typical late Smithian taxa (e.g., *Anawasatchites*, *Xenoceltites*).

The most detailed biostratigraphic studies of Early Triassic conodonts in the Canadian Arctic to date were carried out by Mosher (1973) and Orchard (2008). At Smith and Spath creeks, conodonts were recovered mainly from ammonoid-bearing limestones, whereas other lithologies (e.g., shales) are conodont-poor (Orchard, 2008). In the lower Smith Creek Member, no conodont species are known from the *Hedenstroemia hedenstroemi* beds, whereas the *Euflemingites romunderi* beds are more productive of conodonts of congruent mid-Smithian age (Mosher, 1973; Orchard, 2008) (Fig. 6A). This increased diversity of conodonts was attributed to the explosive radiation that occurred during the early Smithian (Orchard, 2007; Stanley, 2009) (Fig. 1). Higher in the section, the upper Smithian *Anawasatchites tardus* beds of the upper Smith Creek Member yielded less diverse faunas, including conodonts such as *Nv. waageni, Sc. milleri* and *Sc. mosheri* (Orchard, 2008). The lower Spathian strata in this area lack carbonate and are not amenable to recovery of conodonts. Conodonts thus cannot serve to complement the ammonoid biostratigraphical scale in this area.

3.1.2 Carbon-isotope chemostratigraphy

So far, carbon isotope chemostratigraphy of the Smithian and Spathian substages in Canadian Arctic has only been reported from Smith Creek, shown as organic carbon isotopes ($\delta^{13}C_{org}$) (Grasby et al., 2013). At Smith Creek, $\delta^{13}C_{org}$ shows higher values (ca. −27 to −25 ‰) in the lower Smithian (P2*; the asterisk indicating that the timing of peaks in the organic $\delta^{13}C$ record might differ somewhat from those in the carbonate $\delta^{13}C$ record), a large negative excursion to ca. −33 ‰ in the middle Smithian (N3*), followed by recovery to a maximum of ca. −27 ‰ (P3*) at the SSB (top of the *Anawasatchites tardus* beds), and a subsequent drop to ca. −33 ‰ (N4*) much later in the Spathian (Grasby et al., 2013; Fig. 7). It should be noted that the $\delta^{13}C_{org}$ profile at Smith Creek exhibits a second positive excursion in the upper Spathian, before the Spathian/Anisian boundary.

3.2 Spitsbergen (eastern Boreal)

3.2.1 Ammonoid and conodont biostratigraphy

Triassic clastic rocks are known to crop out extensively in the Svalbard archipelago, including on the largest island−Spitsbergen (Buchan et al., 1965). Stratigraphic successions of Olenekian age consist of the Tvillingodden Formation (lower Iskletten Member and upper Kaosfjellet Member) in western Svalbard and the Vikinghøgda Formation (lower Lusitaniadalen Member and upper Vendomdalen Member) in eastern Svalbard (Hounslow et al. 2008; Mørk et al., 2013). The Tvillingodden Formation mainly consists of sandstone in the regressive part of the unit, due to closer proximity to the basin margin, whereas the Vikinghøgda Formation is a shale or mudstone without substantial sandstone or siltstone beds, which generally grades upward into mudstone with thin sandstone or siltstone beds (Mørk et al. 1982).

The ammonoid zones identified on Svalbard are, in ascending order, the *Euflemingites romunderi* and *Anawasatchites tardus* for the Smithian, and the *Bajarunia euomphala*, *Parasibirites grambergi* and *Keyserlingites subrobustus* for the Spathian (Dagys and Weitschat, 1993). Ammonoid studies of the Lusitaniadalen Member (~88 m) and Vendomdalen Member (~92 m) in the Deltadalen area (east-central Spitsbergen) yielded first occurrences of *E. romunderi* and *A. tardus* at, respectively, ~28 m and ~4 m below the base of the Vendomdalen Member (Mørk et al., 1999; Hounslow et al., 2008; Fig. 6B). The main co-occurring ammonoids in the middle Smithian *E. romunderi* Zone are *Arctoceras blomstrandi* and *Paranannites spathi* (Mørk et al., 1999). In the latest Smithian *A. tardus* Zone, which is found across central and eastern Spitsbergen (Hounslow et al., 2008), various prionitids and *Xenoceltites subevolutus* are present into the base of the Vendomdalen member indicating a late Smithian age for these levels (Mørk et al., 1999; Piazza et al., 2017). The base of the *B. euomphala* Zone of earliest Spathian age is ~17 m above the base of the Vendomdalen Member (Mørk et al. 1999; Hounslow et al. 2008), resulting in a biostratigraphic gap of ~15 m above the latest Smithian beds within which the SSB must be located. Ammonoids of middle Spathian age are apparently lacking on Spitsbergen, but late Spathian taxa are present (Hounslow et al. 2008).

The conodont *Scythogondolella mosheri* was recognized from the lower part of the Iskletten Member in Pitnerodden, indicating a Smithian age (Clark and Hatleberg, 1983; Hatleberg and Clark, 1984). Upwards in the Iskletten Member, *Eurygnathodus* sp. (assigned to *Icriospathodus collinsoni* by Hatleberg and Clark, 1984), *Borinella buurensis* and *Neogondolella elongata* (both assigned to *Ng. jubata* by Hatleberg and Clark, 1984, later, re-assigned by Nakrem et al., 2008 to *Borinella* or *Scythogondolella* taxa) of Smithian age have also been reported (Nakrem et al., 2008). Conodonts from the top of the Iskletten Member (Skilisen Bed) in Akseløya are *Borinella*? sp., *Ng.* sp. B, *Ns. pakistanensis* and *Borinella buurensis* (Nakrem et al., 2008). Only *Ng.* ex. gr. *regalis* was reported from the Kaosfjellet Member in Reinodden, co-occurring with *Keyserlingites subrobustus* and *"Posidonia" aranea* and indicating a late Spathian age (Nakrem et al., 2008).

Previous conodont studies in Milne Edwardsfjellet recognized *Novispathodus waageni*

from 2 m below the top of the Lusitaniadalen Member, co-occurring with an ammonoid fauna consisting of *Xenoceltites subevolutus*and various prionitids, within the late Smithian *A. tardus* Zone (Nakrem et al., 2008). Weitschat and Lehmann (1978) also reported a late Smithian conodont fauna with *Sc. milleri*, *Sc. mosheri*, *Borinella* aff. *buurensis* and *Nv. waageni*, from 7 m below the top of the Lusitaniadalen Member, within the *A. tardus* Zone on the southern shore of Sassenfjorden (close to Botneheia). No conodonts were recovered from the lower part of the Vendomdalen Member (lowermost Spathian), but gondolellids are present at 31 to 54.4 m above the base of the Vendomdalen Member, within the range of the late Spathian *Keyserlingites* sp. (Nakrem et al., 2008). *Neogondolella* ex. gr. *regalis* (assigned to *Ng. jubata* by Dagis and Korčinskaja, 1989) was also reported from the *Keyserlingites subrobustus* Zone (Nakrem et al., 2008). Conodont data are thus lacking for the early Spathian but overall support placement of the SSB between the *X. subevolutus* and *B. euomphala* beds.

3.2.2 Carbon-isotope chemostratigraphy

Carbon isotope studies of the Smithian and Spathian substages in Spitsbergen, shown as $\delta^{13}C_{org}$, are from Dicksonfjellet (Galfetti et al., 2007a), Festningen (Grasby et al., 2016), and Vindodden (Wignall et al., 2016) sections (Fig. 7). Ammonoid data are available in Dicksonfjellet (Weitschat and Dagys, 1989), while no biostratigraphic work has been done to date in the Festningen and Vindodden sections. At Dicksonfjellet, the $\delta^{13}C_{org}$ profile exhibits low values (ca. −34 to −33 ‰) in the middle Smithian (within the *Euflemingites romunderi* Zone), followed by a positive excursion beginning from the base of the upper Smithian to ca. −28 ‰ (P3*) in the lowermost Spathian (base of the *Euomphala* Zone), and then a gradual decrease to ca. −32 ‰ in the upper Spathian (within the *Subrobustus* Zone) (Galfetti et al., 2007a). The $\delta^{13}C_{org}$ profile at Festningen was chemostratigraphically correlated with Smith Creek by Grasby et al. (2016), who showed a $\delta^{13}C_{org}$ maximum of ca. −25 ‰ (P2*) in the lowermost Smithian, then a negative excursion to a minimum of ca. −33 ‰ (N3*) at what they considered as the SSB (but which more likely represents the middle Smithian), followed by a rebound to ca. −29 ‰ (P3*) in the lower Spathian, and a gradual decrease to ca. −32 ‰ (N4*) in the middle Spathian. The $\delta^{13}C_{org}$ profile at Vindodden was correlated with the nearby Festningen section by Wignall et al. (2016) following the same chemostratigraphic approach. They showed stable and low values (ca. −32 ‰; N3*) during the middle Smithian, then a positive excursion following a $\delta^{13}C_{org}$ minimum at their inferred SSB (however, this level is actually the N3 event, which is of middle Smithian age; see Section 5.3). The lower Spathian is characterized by a peak at ca. −28 ‰ (P3*), followed by a gradual decrease to ca. −30 ‰ in the middle Spathian.

3.3 Western Canadian Sedimentary Basin (eastern Panthalassa)

3.3.1 Ammonoid and conodont biostratigraphy

The Western Canadian Sedimentary Basin (WCSB) contains ammonoid faunas that have been used, generally in conjunction with Canadian Arctic data, in the construction of a preliminary Early Triassic biozonation scheme for northwestern Pangea (Tozer, 1994). Triassic

strata are best exposed in the eastern Cordillera (e.g., Rocky Mountains and foothills) in northeastern British Columbia (Tozer, 1982). Lower Triassic stratigraphic successions mainly consist of the Phroso Formation (siltstone) and Vega Formation (siltstone) in the south, and the Grayling Formation (gray shale and sandstone) and Toad Formation (dark gray calcareous siltstone and shale) in the north (Gibson, 1971).

The Toad Formation contains ammonoids of the middle and late Smithian *Euflemingites romunderi* and *Anawasatchites tardus* Zones and the late Spathian *Keyserlingites subrobustus* Zone, in ascending order (McLearn and Kindle, 1950; Tozer, 1965, 1967, 1994; Orchard and Tozer, 1997) (Fig. 5B). The *E. romunderi* Zone had also been reported from the Vega Formation in the southern British Columbia (Tozer, 1967). The type locality of the *A. tardus* Zone is on the Toad River of the northeastern British Columbia (McLearn and Kindle, 1950; Tozer, 1967, 1994), and it is also known from the Liard River and Ursula Creek (Orchard and Tozer, 1997). In general, Early Triassic ammonoid occurrences in western Canada correspond to the zonal divisions previously established in the Canadian Arctic region (Tozer, 1994).

In the WCSB, conodonts were recovered not only from the *Euflemingites romunderi* and *Anawasatchites tardus* beds of middle to late Smithian age, but also from overlying (?lowermost Spathian) strata in which ammonoids are apparently absent (Orchard and Tozer, 1997; Orchard and Zonneveld, 2009). The *E. romunderi* beds yielded conodonts such as *Ns. pakistanensis* and *Nv. waageni* at Mount Ludington and Liard River in northeastern British Columbia (Orchard and Tozer, 1997), and additionally *Scythogondolella lachrymiformis*, *Paullella meeki*, *Discretella discreta*, and *Wapitiodus robustus* from the Sulphur Mountain Formation in the Wapiti Lake area, western British Columbia (Orchard and Zonneveld, 2009). Orchard (2008) also reported the conodont species *Neospathodus posterolongatus*, *Ns. cristagalli*, *Guangxidella bransoni*, and *Paullella meeki* from *E. romunderi* Zone in British Columbia. The *A. tardus* beds yielded conodonts such as *Sc. milleri*, *Sc. mosheri*, *Novispathodus. ex gr. waageni* and *Borinella buurensis*, which are also similar to assemblages from correlative units at Smith Creek in the Canadian Arctic (Orchard and Tozer, 1997). *Sc. milleri* and *Sc. mosheri* have also been reported in the *Xenoceltites* beds of the *A. tardus* Zone in the Wapiti Lake area (Orchard and Zonneveld, 2009). Orchard and Zonneveld (2009) established three conodont zones of the Smithian age in the Wapiti Lake area, which are (in ascending order) the *Sc. lachrymiformis*, *Paullella meeki* and *Sc. mosheri* zones, with the last subdivided into the *Sc. phryna* and *Sc. milleri* subzones. Therefore, ammonoid-conodont assemblages of the WCSB are nearly identical to those in age-equivalent strata of the Canadian Arctic (Orchard, 2008). Just 1 m above the top of the *A. tardus* Zone at Toad River, the overlying strata yielded the conodont *Neogondolella* aff. *sweeti* (=*Ng*. n. sp. D sensu Orchard, 2007), which was suggested to be indicative of an earliest Spathian age based on correlation with Californian successions (Orchard and Tozer, 1997). These observations confine the position of the SSB above the first occurrence of *Sc. milleri* and below the first occurrence of *Ng*. aff. *sweeti*.

3.3.2 Carbon-isotope chemostratigraphy

To date, no carbon isotope profile of the Smithian and Spathian substages is available from the WCSB.

3.4 Western United States (eastern Panthalassa)

3.4.1 Ammonoid and conodont biostratigraphy

Ammonoid-bearing marine deposits are widely distributed in the western United States. Brayard et al. (2009c, 2011, 2013), Jenks et al. (2010), Jattiot et al. (2016, 2017, 2018) and Jenks and Brayard (2018) reported Smithian ammonoid faunas, which are characterized by increasing diversity from the lower Smithian to the middle Smithian. Within this basin, late Smithian ammonoid beds are, in ascending order, the *Anasibirites kingianus* and the overlying *Xenoceltitidae* beds, which contain *Glyptophiceras, Xenoceltites* and *Pseudosageceras augustum*. They correspond respectively to the UAZ5 and UAZ6 of Jattiot et al. (2017) and can be easily correlated with Tethyan sections along the North Indian Margin. The UAZ6 contains the latest Smithian ammonoids reported worldwide so far.

Guex et al. (2005a, b; 2010) and Jenks et al. (2013) identified ammonoids from Spathian successions including, in ascending order, the early Spathian *Bajarunia confusionensis* beds, *Tirolites harti* beds, *Columbites* beds, and *Procolumbites* beds, followed by the middle Spathian *Subcolumbites* Zone and the late Spathian *Neopopanoceras haugi* Zone (Fig. 5C). The Cowboy Pass site in western Utah was inferred to contain the oldest Spathian ammonoids, i.e., *B. confusionensis*, but the lack of Smithian ammonoids in these sections does not constrain placement of the SSB well (Guex et al., 2010; Brayard et al., 2013; Fig. 6C). In addition, the nearby Confusion Range in western Utah recorded a series of Smithian ammonoid assemblages, in which *Anasibirites, Wasatchites* and *Xenoceltites* sp. indet. were discovered, indicative of a late Smithian age (Brayard et al., 2013). Based on the ammonoid data in the Confusion Range area, the SSB is located between the *Anasibirites* beds and the *B. confusionensis* beds. Sampled ammonoid faunas in Idaho also show a similar scheme with the first *Bajarunia* specimens occurring above the Xenoceltitidae beds (Brayard et al., work in progress).

In the western United States, lower-middle Smithian rocks yielded not only the conodonts *Neospathodus pakistanensis*, *Novispathodus waageni*, *Discretella discreta*, but also *Conservatella conservativa, Guangxidella bransoni*, and *Paullella meeki* (Orchard and Tozer, 1997; Orchard, 2008; Orchard and Zonneveld, 2009). Conodont assemblages from the late Smithian *Anasibirites multiformis* beds are similar to those from the WCSB, containing *Scythogondolella milleri*, *Sc. mosheri*, *Nv. ex gr. waageni* and *Borinella buurensis* (Müller, 1956; Orchard and Tozer, 1997; Orchard, 2008). Moreover, Orchard and Zonneveld (2009) reported both *Nv. waageni* and *Nv. pingdingshanensis* with *Spathicuspus* sp. from *Xenoceltites* beds of the upper *A. multiformis* Zone in Georgetown, Idaho and with *Borinella buurensis* and *Sc. milleri* in the Tardus Zone at Crittenden Springs, Nevada. The latest Smithian occurrence of *Nv. pingdingshanensis* in the western United States is thus similar to that reported from the subsurface of the WCSB (Henderson et al., 2018). Although Spathian successions in the western United States are more complete and better studied than those in the WCSB, relatively few conodonts have been described (Orchard and Tozer, 1997; Lucas and Orchard, 2007; Orchard, 2008). According to Orchard and Tozer (1997), the lowermost Spathian in the Darwin Canyon section in California contains *Neogondolella* aff. *sweeti-Ns. crassatus*, which has been tentatively correlated with the post-Tardus Zone fauna on the Toad River in northeastern

British Columbia. The Darwin faunas, which are presently under review (Goudemand et al., 2006), also include *Nv. pingdingshanensis* and *Ic. zaksi* and should provide an important North American SSB reference section for conodonts. Lucas and Orchard (2007) reported the conodonts *Icriospathodus collinsoni* and *Nv. abruptus* from the lower Spathian *Tirolites* beds and *Ng. elongata* from the overlying *Columbites* beds, all of which are indicative of an early Spathian age (Orchard and Tozer, 1997). These conodont occurrences constrain the position of the SSB to between the first occurrences of *Sc. milleri* and *Ng.* aff. *sweeti*, which is comparable to its placement in the WCSB. For the western United States generally, ammonoid biozonations are more highly resolved than those for conodonts, indicating a SSB placement between the top of the Xenoceltitidae beds and the base of the *Bajarunia* beds.

3.4.2. Carbon-isotope chemostratigraphy

In the western United States, detailed continuous C-isotope profiles of the Smithian-Spathian transition are available for the Mineral Mountains section in Utah (Thomazo et al. 2016; Fig. 7) and the Hot Springs section in southeastern Idaho (Caravaca et al., 2017). At Mineral Mountains, the $\delta^{13}C_{carb}$ profile exhibits values close to 0 ‰ in the lowermost Smithian, a gradual negative excursion to a minimum of ca. −4 ‰ (N3) in the middle Smithian (*Owenites* ammonoid beds), and a rebound through the *Anasibirites kingianus* and Xenoceltitidae 'gen. indet.' A. beds to a maximum of ca. +2 ‰ (P3) in the early Spathian (Thomazo et al., 2016; Fig. 7). A similar trend is observed at Hot Springs, with the most negative values recorded in the uppermost beds of the middle Smithian and a strong increase in $\delta^{13}C$ through the SSB and into the early Spathian (Caravaca et al., 2017). Biostratigraphic control is largely lacking for the SSB at the Hot Springs section, however.

3.5 Kamura and Inuyama, Japan (central Panthalassa)

3.5.1. Ammonoid and conodont biostratigraphy

The Kamura section represents a shallow-water (atoll) environment that was located in the central Panthalassic Ocean at the time of its accumulation (Zhang et al., 2017). The Triassic carbonate succession lithologically belongs to the Kamura Formation, which is composed mainly of micritic, microbial, and bioclastic limestones with some coarsely crystalline dolomite in its lower part (Kanmera and Nakazawa, 1973; Zhang et al., 2017). A thick Smithian succession consisting largely of bioclastic limestones is well-preserved, whereas the Spathian is largely or completely missing (Zhang et al., 2017). Conodont biostratigraphic work has been undertaken at Kamura, but no ammonoid data are available (Watanabe et al., 1979; Horacek et al., 2009; Zhang et al., 2017). It should be noted that ammonoid data are available from Japanese sections but in other tectonic and environmental contexts (e.g., Ehiro, 2016; Ehiro et al., 2016). The conodont taxa *Novispathodus* ex gr. *waageni*, *Parachirognathus*, *Discretella* and *Wapitiodus*(?) have been recovered from the middle part of the Kamura Formation, within the *Nv.* ex gr. *waageni-Parachirognathus* Zone, indicating a Smithian age (Zhang et al., 2017). Koike (1979) reported Spathian-age conodonts (e.g., "*Neospathodus*? sp. G. Sweet et al." (= ?*Icriospathodus collinsoni*), *Triassospathodus homeri* and *Tr. triangularis*) from this section, but they were not illustrated in that paper and have not been rediscovered in later studies. The

SSB apparently lies above the *Nv*. ex gr. *waageni-Parachirognathus* Zone and below the first occurrence of ?*Icriospathodus collinsoni*.

The Inuyama section represents a deep-water (abyssal) environment that was located in the central Panthalassic Ocean at the time of its accumulation (Sakuma et al., 2012). It consists of a series of disconnected stratal blocks scattered through the Mino Belt, composed of black shales, argillaceous cherts, and siliceous mudstones, in ascending order (Yao and Kuwahara, 1997; Tada et al., 2005; Sakuma et al., 2012). Lower Smithian to lower Spathian successions were recognized based on conodonts and radiolarians, but no ammonoid data are available (Sakuma et al., 2012). The conodont taxa *Guangxidella bransoni* and *Neogondolella milleri*, which are indicative of a late Smithian age, were recovered from the argillaceous cherts. The overlying siliceous mudstone yields *Neospathodus symmetricus* of early Spathian age. Therefore, the SSB can be constrained to within a ~2 m interval between the first occurrences of *Ng. milleri* and *Ns. symmetricus*.

3.5.2. Carbon-isotope chemostratigraphy

At Kamura, the $\delta^{13}C_{carb}$ profile shows a negative excursion from ca. +2.5 ‰ (P2) in the lowermost Smithian to ca. 0 ‰ (N3) in the middle Smithian, followed by a rebound to ca. +4 ‰ (P4) above the unconformity at which most or all of the Spathian is missing (Zhang et al., 2017; Fig. 7). Below the unconformity, the positive $\delta^{13}C_{carb}$ shift rises to a peak value of ca. +3.5 ‰ (Horacek et al., 2009), which is typical of the P3 maximum in other sections globally (e.g., Galfetti et al., 2007c; Horacek et al., 2007a, b) and thus suggests that the SSB and earliest Spathian may be present just below the unconformity.

At Inuyama, the $\delta^{13}C_{org}$ profile shows a negative excursion from ca. −27 ‰ in the lower Smithian to ca. −32 ‰ (N3*) in the middle Smithian, followed by a positive excursion to ca. −27 ‰ across the SSB (Sakuma et al., 2012; Fig. 7). Above the SSB, the $\delta^{13}C_{org}$ profile exhibits fluctuations between ca. −27 ‰ and −29 ‰ in the lower Spathian and a negative excursion to ca. −30 ‰ (N4*?) in the early to middle Spathian.

3.6. Chaohu area, eastern China (eastern Tethys)

3.6.1. Ammonoid and conodont biostratigraphy

The Chaohu area of eastern Anhui Province, eastern China, has come under intense investigation in recent years, including studies of its sedimentology (Li et al., 2007; Chen-ZQ et al., 2011), geochemistry (Tong et al., 2002, 2007; Zuo et al., 2006; Horacek et al., 2007c; Chen-JB et al., 2015; Zhao and Zheng, 2015), cyclostratigraphy (Li et al., 2007; Li et al., 2016a, b), and other topics (Chen-ZQ et al., 2010; Motani et al., 2015; Huang et al., 2017). During the Early Triassic, it was situated on a deep ramp on the northern margin of the Yangtze Platform, eastern China (Tong et al., 2004). At Chaohu, the Lower Triassic consists of the Yinkeng, Helongshan and Nanlinghu formations, in ascending order, in which are developed a multilevel hierarchy of mudstone and limestone cycles (Li et al., 2007; Tong et al., 2007). The Yinkeng and Helongshan formations comprise interbedded mudstone and (muddy) limestone, whereas the Nanlinghu Formation is composed of thin shale and interbedded thin and thick limestone

(Zhao et al., 2005b). The Olenekian successions in the Chaohu area extend from the middle of the Yingkeng Formation to the top of the Nanlinghu Formation. The SSB transition is present in three closely spaced sections (<1 km apart): West Pingdingshan (31°38□00□□N, 117°49□43□□E), North Pingdingshan (31°38□14□□N, 117°49□53□□E), and South Majiashan (31°37□33□□N, 117°49□21□□E). They provide a continouous and complete succession from the lowermost Smithian to the upper Spathian, and the West Pingdingshan section has been nominated as a candidate for the GSSP of the Induan/Olenekian boundary (Zhao et al., 2002, 2003a, 2007a, b, 2008a, b; Tong et al., 2003, 2004, 2005, 2007).

The Olenekian successions in the Chaohu area have received detailed study of both their ammonoid and conodont faunas. Tong et al. (2004, 2005, 2007) reported four ammonoid zones in the Olenekian Stage, including the *Flemingites-Euflemingites* and *Anasibirites* zones of Smithian age and the *Tirolites-Columbites* and *Subcolumbites* zones of Spathian age, in ascending order (Fig. 5D). Numerous ammonoids recovered at South Majiashan provide constraints on the SSB, limiting it to an ~8-m stratal interval between occurrences of the late Smithian *Anasibirites* (including *A. kingianus, A. onoi* and *A. plicatus*; note: all these determinations will have to be revised per e.g., Jattiot et al., 2016) in the upper Helongshan Formation (Beds 6 and 13) and the early Spathian *Tirolites-Columbites* (including *C.* cf. *parisianus, C. contractus, T. latumbilicatus, T.* ?cf. *spinosus* and *Xenoceltites* sp.) in the lower Nanlinghu Formation (Bed 18) (Tong et al., 2004, 2005, 2007) (Fig. 8). *Euflemingites* and *Anasibirites* cf. *kwangsiana* were also recovered from the middle Helongshan Formation at North Pingdingshan (Beds 56-57) and the upper Helongshan Formation at West Pingdingshan (Beds 50-51) (Figs. 9-10). However, these two genera do not co-occur elsewhere as they are respectively of middle and late Smithian age. One issue at Chaohu is the relatively poor preservation of ammonoid fossils, which makes firm taxonomic assignments difficult. Further work on the Chaohu ammonoid fauna will be needed to resolve inconsistencies.

This area contains an especially rich and diverse conodont fauna of the tropical biogeographic province that accumulated in an open-shelf setting at intermediate water depths (of a few hundred meters). Conodont biozonation offers narrower constraints on placement of the SSB in the Chaohu area. Zhao et al. (2007a, 2008a, b) reported five conodont zones in the Olenekian Stage, including the *Novispathodus waageni eowaageni* and *Nv. waageni waageni* of Smithian age and *Nv. pingdingshanensis*, *Triassospathodus homeri* and *Neospathodus anhuinensis* of Spathian age (Fig. 5D). They defined the *Nv. pingdingshanensis* Zone as ranging from the first occurrence of *Nv. pingdingshanensis* to the first occurrence of *Triassospathodus homeri*, with the lowermost occurrence of *Nv. pingdingshanensis* representing the SSB. The first occurrences of *Nv. pingdingshanensis* recognized were located at 48 cm above the base of Bed 52 (uppermost Helongshan Formation) at West Pingdingshan, ~40 cm above the base of Bed 61 (uppermost Helongshan Formation) at North Pingdingshan, and ~120 cm above the base of Bed 15 (lowermost Nanlinghu Formation) at South Majiashan (Figs. 8-10). In a higher-resolution study of the SSB transition in the Chaohu area, Liang et al. (2011) collected 38 samples from Beds 49-54 at West Pingdingshan and recovered 4 genera and 15 species. The first specimens of *Nv. pingdingshanensis* were found at a slightly lower stratal level than in the earlier work by Zhao and others, i.e., at 30 cm above the base of Bed 52 (Fig. 10). Occurrences of the early Spathian conodont species *Tr. homeri* (Bed 64 at North Pingdingshan; Bed 56 at West Pingdingshan), *Ns. abruptus* (Beds 64 and 52, respectively), and

Ns. spathi (Beds 64 and 56, respectively) are useful in placing an upper stratigraphic limit on the position of the SSB (Tong et al., 2007; Zhao et al., 2007a). In this context, placement of the SSB in the Chaohu area at the first occurrence of *Nv. pingdingshanensis* is consistent with the existing constraints based on local ammonoid data, but it may be diachronous with respect to occurrences of *Nv. pingdingshanensis* in upper Smithian beds globally (Orchard and Zonneveld, 2009; Komatsu et al., 2016; Chen-YL et al., 2018; Leu et al., 2018; Goudemand et al., 2018).

3.6.2. Carbon-isotope chemostratigraphy

The North Pingdingshan and West Pingdingshan sections show similar $\delta^{13}C_{carb}$ profiles from the lower Smithian to the lower Spathian, and South Majiashan yields a continuous $\delta^{13}C_{carb}$ profile from the uppermost Smithian to the upper Spathian (Figs. 8-10). At North Pingdingshan and West Pingdingshan, the $\delta^{13}C_{carb}$ profiles exhibit high values (ca. 0 ‰) in the lowermost Smithian (base of the *Novispathodus waageni eowaageni* Zone; close to P2), followed by negative excursions to ca. −7 to −4 ‰ in the middle Smithian (mid-*Nv. waageni waageni* Zone; N3), and then a rebound to ca. +4 ‰ in the lowermost Spathian (lower *Nv. pingdingshanensis* Zone; P3) (Zuo et al., 2003, 2004; Tong et al., 2007). At South Majiashan, the $\delta^{13}C_{carb}$ profile also shows a positive excursion from ca. −2 ‰ in the uppermost Smithian to ca. +4 ‰ in the lowermost Spathian (lower *Nv. pingdingshanensis* Zone; P3) (Tong et al., 2007). The $\delta^{13}C_{carb}$ profiles of all three sections show relatively stable values (ca. +2 to +4 ‰) in the lower Spathian (within the *Nv. pingdingshanensis* and *Triassospathodus homeri* zones or *Columbites-Tirolites* Zone), followed by a gradual decrease to ca. −2 ‰ in the middle to upper Spathian (within the *Neospathodus anhuiensis* Zone or *Subcolumbites* Zone; approaching N4, although it is unclear whether the N4 minimum is reached).

The proximity of the three Chaohu sections allows an evaluation of the relationships between biostratigraphic markers and features of their carbon isotope profiles (Figs. 8-10). Taking *Nv. pingdingshanensis* as an example, the first occurrence of this taxon shows somewhat variable locations relative to the major features of the $\delta^{13}C$ profiles (i.e., N3 and P3). At South Majiashan, Interval II is 19.57 m thick and extends from −6.3 ‰ (N3) to +4.3 ‰ (P3), and the first occurrence of *Nv. pingdingshanensis* is located 0.90 m below P3 (Interval I-IV was divided based on Olenekian carbon isotope excursions, see Section 4.1), which corresponds to a $\delta^{13}C$ value of ~2.0 ‰ that represents ~80 % of the rise from N3 to P3 (Fig. 8). At North Pingdingshan, Interval II is 8.28 m thick and extends from −7.3 ‰ (N3) to +3.8 ‰ (P3), and the first occurrence of *Nv. pingdingshanensis* is located approximately at P3, which corresponds to a $\delta^{13}C$ value of +4.0 ‰ that represents ~100 % of the rise from N3 to P3 (Fig. 9). At West Pingdingshan, Interval II is 24.22 m thick and extends from −4.3 ‰ (N3) to +4.2 ‰ (P3), and the first occurrence of *Nv. pingdingshanensis* is at 5.33 m below P3, which corresponds to a $\delta^{13}C$ value of ~0 ‰ that represents ~50 % of the rise from N3 to P3 (Fig. 10). It is unlikely that *Nv. pingdingshanensis* was not present in all three sections simultaneously (since they are within 1 km of each other), and the differences in stratigraphic placement of its first occurrence likely results from local environmental and taphonomic controls, with the West Pingdingshan section recording the oldest first occurrence and the other two sections slightly younger first occurrences ("Signor-Lipps Effect"; Signor and Lipps, 1982; Raup, 1986). Given that this problem exists in such a limited area as at Chaohu, it must be a common phenomenon

at other locales around the world and at a more global scale, implying that many first occurrence are local and diachroneous and obviously do not represent the true first appearance of a specific taxon in a given area, especially when only limited work has been done.

3.7. Nanpanjiang Basin, southwestern China (eastern Tethys)

3.7.1. Ammonoid and conodont biostratigraphy

During the Early Triassic, the Nanpanjiang Basin (mainly northwestern Guangxi and southern Guizhou provinces) was an epicontinental sea between the Yangtze Platform and the western Panthalassic Ocean (Enos et al., 2006). In Nanpanjiang Basin, the Lower Triassic mainly consists of the Luolou Formation (limestone and limestone-shale interbeds) and part of the overlying Ziyun Formation (thick-bedded micritic and intraclastic limestone with thin argillites) (Enos et al., 2006). Studies of Olenekian ammonoid biostratigraphy have been undertaken mainly in the Jinya area (northwestern Guangxi) (Galfetti et al., 2007b, c; Brayard and Bucher, 2008) and Jiarong section (southern Guizhou) (Chen-YL et al., 2015). Detailed conodont biostratigraphic analyses have been reported from a number of sections including Guandao (Wang et al., 2005; Lehrmann et al., 2015), Mingtang (Liang et al., 2016), Jiarong (Chen-YL et al., 2015, 2018), Shitouzhai (Zhang et al., 2015), Bainyang (Yan et al., 2013) and Qingyan (Ji et al., 2011) in southern Guizhou, and Zuodeng (Tong et al., 2007, revised after Yang et al., 1984) in northwestern Guangxi.

In the Jinya area, ammonoid biostratigraphic studies led to the recognition of eleven beds/zones in the Smithian and Spathian substages (Galfetti et al., 2007b, c; Fig. 5E) of which some can be further refined (Brayard and Bucher, 2008). Olenekian conodont data from this area are largely unpublished (Goudemand, 2014a). The Smithian ammonoid beds/zones are the *Clypites* sp. indet. beds, *Kashmirites kapila* beds, *Flemingites rursiradiatus* beds, *Owenites koeneni* beds (subdivided in *Ussuria*, *Hanielites* and *Inyoites* horizons) and *Anasibirites multiformis* beds (with *Anasibirites* and *Xenoceltites-Pseudosageceras augustum* assemblages respectively at the base and top of these beds), and those from the Spathian are the Tirolitid n. gen. A beds, *Tirolites*/*Columbites* beds, *Procolumbites* beds, *Hellenites* beds, and *Neopopanoceras haugi* Zone, in ascending order (Galfetti et al., 2007b; Brayard and Bucher, 2008). The SSB was placed at the base of the Tirolitid n. gen. A. beds, ~1-2 m above the late Smithian *Xenoceltites-Pseudosageceras augustum* assemblage of the *A. multiformis* beds (Fig. 6D). Note that another ammonoid assemblage of undetermined taxa, and thus of uncertain age, occurs between the late Smithian *Xenoceltites-Pseudosageceras augustum* assemblage and the earliest Spathian *Tirolitid* n. gen. A beds (Brayard and Bucher, 2008). This undetermined assemblage could correspond either to latest Smithian or earliest Spathian ammonoid beds.

Conodont biostratigraphic studies reported only the *Novispathodus waageni* Zone within the Smithian in the Guandao, Mingtang, Shitouzhai, and Zuodeng sections (Tong et al., 2004, 2007; Zhang et al., 2015; Lehrmann et al., 2015; Liang et al., 2016) (Fig. 11). In the Jiarong section, reported Smithian conodont zones are in ascending order, the *Nv. waageni eowaageni*, *Nv.* waageni *waageni*, *Discretella discreta* and *Pachycladina-Parachirognathus* zones (Chen-YL et al., 2015; but see Chen-YL et al., 2018, for an update based on quantitative biostratigraphic methods). In the Bianyang section, they are the *Ds. discreta* and *Pachycladina-*

Parachirognathus (Yan et al., 2013). Spathian conodont zones are in ascending order, the *Nv. crassatus* and *Triassospathodus homeri* zones at Guandao (Tong et al., 2004; Lehrmann et al., 2015); the *Tr. homeri-Tr. triangularis* Zone at Mingtang (Liang et al., 2016); the *Nv. pingdingshanensis*, *Icriospathodus collinsoni*, *Tr. homeri* and *Tr. triangularis* zones at Jiarong (Chen-YL et al., 2015, 2018); the *Nv. pingdingshanensis* and *Tr. homeri* zones at Shitouzhai and Zuodeng (Tong et al., 2007; Zhang et al., 2015); and the *Ic. collinsoni* and *Tr. homeri* zones at Bianyang (Yan et al., 2013) (Fig. 11).

At Guandao and Zuodeng, the SSB was placed at the first occurrences of *Novispathodus crassatus* and *Nv. pingdingshanensis*, respectively (Tong et al., 2004, 2007; Lehrmann et al., 2015) (Fig. 11). At Jiarong, only one ammonoid zone of early Spathian age was recognized, i.e., the *Columbites* beds in the upper part of the Luolou Formation, ~5 m above the first occurrence of *Nv. pingdingshanensis* (Chen-YL et al., 2015). Chen-YL et al. (2015) inferred that some small specimens of *Nv. pingdingshanensis* were of late Smithian age (see Maekawa and Komatsu, 2014; Komatsu et al., 2016 in An Chau Basin, Section 3.8) and placed the SSB within the *Nv. pingdingshanensis* Zone, between the first occurrence of *Nv. pingdingshanensis* and the *Columbites* beds. Chen-YL et al. (2018) recently revised conodont occurrences in Jiarong and confirmed the late Smithian occurrence of *Nv. pingdingshanensis*. At Mingtang and Shitouzhai, reports of early Spathian conodonts are not well-established. Thus, the SSB was placed based only on global correlations of carbon isotope profiles (Zhang et al., 2015; Liang et al., 2016; see Section 3.7.2). At Bianyang, the SSB was not clearly located because only early Spathian *Icriospathodus collinsoni* was recovered (Yan et al., 2013). At Qingyan, the Olenekian strata were assigned to the *Nv. waageni* and *Triassospathodus homeri* conodont zones, and the FAD of *Nv. crassatus* and *Nv. pingdingshanensis* are (nearly) the same as the first occurrence of *Tr. homeri*, making placement of the SSB somewhat equivocal (Ji et al., 2011).

3.7.2. Carbon-isotope chemostratigraphy

In Nanpanjiang Basin, carbon isotope profiles of the Olenekian Stage have been generated for multiple sections, including Jinya area (Galfetti et al., 2007c), Guandao (Tong et al., 2007), Zuodeng (Tong et al., 2007), Jiarong (Chen-YL et al., 2013), Mingtang (Liang et al., 2016) and Shitouzhai (Zhang et al., 2015) (Fig. 11). Guandao and Mingtang show similar $\delta^{13}C_{carb}$ trends, with a negative excursion from high values (ca. +4 to +6 ‰) in the lowermost Smithian to ca. −2 ‰ (N3) in the middle Smithian, a rebound to ca. +2.5 ‰ in the lowermost Spathian, a long plateau in the lower Spathian, a second negative excursion to ca. −1 ‰ (N4) in the middle Spathian, and finally a positive excursion to ca. +4 ‰ in the uppermost Spathian (Tong et al., 2007; Liang et al., 2016). The $\delta^{13}C_{carb}$ profile at Jiarong is similar to that at Mingtang except for the absence of a plateau in the lower Spathian (Chen-YL et al., 2013). At Zuodeng, $\delta^{13}C_{carb}$ shows high values (ca. +4 ‰) in the lowermost Smithian, a decrease to ~0 ‰ (N3) in the middle Smithian, a rebound to ca. +3 ‰ (P3) in the lower Spathian (base of the *Nv. pingdingshanensis* Zone), a minor negative excursion (to ca. +1 ‰; N4) in the mid-Spathian, and finally fluctuations between ~0 and +4 ‰ in the upper Spathian (Tong et al., 2007). The $\delta^{13}C_{carb}$ profile at Jinya is similar to that at Zuodeng except for a gradual increase in the late Spathian (Galfetti et al., 2007c). At Shitouzhai, $\delta^{13}C_{carb}$ varies between ca. +1 ‰ and −3 ‰ (Zhang et al., 2015),

which is lower than in other Nanpanjiang Basin sections, although its plateau in the lower Spathian is comparable to those at Guandao and Mingtang.

3.8. An Chau Basin, northern Vietnam (eastern Tethys)

3.8.1. Ammonoid and conodont biostratigraphy

The An Chau Basin was another epicontinental sea connected to the Nanpanjiang Basin and bordering the western Panthalassic Ocean during the Early Triassic. In this basin, the Lower Triassic succession consists of the Lang Son Formation (siliciclastics) of Induan-early Olenekian age and the Bac Thuy Formation (fossiliferous carbonates, limestone breccia, hemipelagic basinal marl and mudstone) of Olenekian age (Komatsu and Dang 2007; Maekawa and Komatsu, 2014; Maekawa et al. 2015; Komatsu et al., 2016).

To date, only the Bac Thuy Formation has yielded both ammonoids and conodonts of Olenekian age. Komatsu et al. (2016) reported four ammonoid beds from KC-02 (in ascending order, the *Owenites koeneni* and *Xenoceltites variocostatus* beds of middle and late Smithian age, respectively, and the *Tirolites* cf. *cassianus* and *T*. sp. nov. beds of early Spathian age) and three conodont zones (the *Novispathodus* ex gr. *waageni* Zone of Smithian age, the *Nv*. ex gr. *pingdingshanensis* Zone straddling the SSB, and the *Icriospathodus collinsoni* Zone of early Spathian age) (Fig. 11). The conodont *Nv*. ex gr. *pingdingshanensis* was reported at three stratigraphic levels: (1) from the lower part of the uppermost Smithian *X. variocostatus* beds (KC02-08); (2) from the top of the basal Spathian *Tirolites* cf. *cassianus* beds (KC02-10); and (3) from strata between the *Tirolites* cf. *cassianus* and *Tirolites* sp. nov. beds (between KC02-10 and KC02-14) (Maekawa and Komatsu, 2014; Komatsu et al., 2016).

Based on ammonoid data, Komatsu et al. (2016) placed the SSB in the An Chau Basin at the base of the *T*. cf. *cassianus* beds, which is ~0.95 m above the first occurrence of the *Nv*. ex gr. *pingdingshanensis*, and proposed that the conodont *Nv*. ex gr. *pingdingshanensis* ranged from the uppermost Smithian into the lowermost Spathian. The ammonoid *Xenoceltites* sp. was also reported from the *T*. cf. *cassianus* and *Columbites* sp. beds of the An Chau Basin (i.e., Sample 14 in Komatsu et al., 2016). However, this placement of the SSB may be called into question owing to some uncertainties in taxonomic identifications in this study. After reconsideration of *Xenoceltites variocostatus* specimens from KC02-10 illustrated in Shigeta et al. (2014), these may not pertain to this late Smithian species. Some illustrated specimens of KC02-11 also resemble some early Spathian *Bajarunia* (*sensu lato*) forms. Overall, if true, these few new tentative assignments may imply that the top of the *X. variocostatus* beds has to be only slightly shifted downward, as well as their considered SSB, as other determinations of *X. variocostatus* appear robust. Thus, *Nv*. ex gr. *pingdingshanensis* in KC02-10 and overlying beds may be of earliest Spathian age. A reconsideration of *Nv*. ex gr. *pingdingshanensis* from KC02-08 suggest it may not pertain to this species. However, at NT01-07, well-preserved specimens of *X. variocostatus* specimens co-occur with *Nv*. ex gr. *pingdingshanensis*, thus supporting a FAD of *Nv*. ex gr. *pingdingshanensis* within the late Smithian as observed in other some other basins (also see discussion in Section 5.2).

3.8.2. Carbon-isotope chemostratigraphy

In the An Chau Basin, the $\delta^{13}C_{carb}$ profile exhibits stable values of ca. -2 ‰ through the middle Smithian (up to the top of the *Owenites koeneni* beds; N3), followed by a positive excursion to maximum values of ca. +6 ‰ in the uppermost Smithian (within the *X. variocostatus* beds; P3) or earliest Spathian if we took into account our potential revised assignment, and finally a negative excursion to ca. +1 ‰ from this point into the lower Spathian (Komatsu et al., 2016; Fig. 11).

3.9. Salt Range and Surghar Range, Pakistan (southern Tethys)

3.9.1. Ammonoid and conodont biostratigraphy

A highly resolved Smithian ammonoid zonation based on the quantitative Unitary Association (UA) method has been proposed by Brühwiler et al. (2010c, 2011) using sections from the North Indian Margin. A total of 14 UA zones have been defined based on material from Pakistan (Salt Range), northern India (Spiti) and Tulong (Tibet) allowing detailed calibration and correlation of Smithian $\delta^{13}C$ curves.

The Salt Range, located on the northern Gondwanan shelf in the southern Tethys Ocean during the Early Triassic, has an Olenekian succession consisting of, in ascending order, the Ceratite Beds (Ceratite Marls and Ceratite Sandstone members), Bivalve Limestone (Upper Ceratite Limestone and Bivalve Beds members), and Dolomite Group (Dolomitic Beds and Topmost Limestone members) (Waagen, 1895; Kummel and Teichert, 1973; Guex, 1978). Recently, PJRG (1985) proposed subdivision of the succession into the Mittiwali (comprising Units 1 to 5) and Narmia members in the Salt Range and the nearby Surghar Range, in which Unit 2 (mudstone) was equivalent to the Ceratite Marls, Unit 3 (shale-sandstone) to the the Ceratite Sandstone, Unit 4 (limestone) to the Upper Ceratite Limestone and lower part of the Bivalve Beds, Unit 5 (sandstone-shale) to the upper part of the Bivalve Beds and Dolomitic Beds, and the Narmia Member to the Topmost Limestone. Important sections for Lower Triassic biostratigraphic studies include the Nammal Gorge, Chiddru and Zaluch locales in the western Salt Range, and the Narmia and Chitta-Landu in the Surghar Range.

The high-resolution ammonoid zonation established from different sections in Salt Range and Surghar Range by Brühwiler et al. (2010c, 2011, 2012a) consists of 13 Smithian UA zones of which 2 are late Smithian (Fig. 5F): the *Wasatchites distractus* beds (including the iconic genus *Anasibirites*), and the *Glyptophiceras sinuatum* beds (including *Xenoceltites variocostatus*) (Fig. 6E). As in other area worldwide, the *Glyptophiceras sinuatum* beds are of latest Smithian age (e.g., Jenks et al., 2015). The SSB is thus placed just above the *G. sinuatum* Zone within the "Bivalve Beds" (BB; Brühwiler et al., 2012a).

These upper Smithian ammonoid assemblages are relatively similar to those reported in earlier studies by PJRG (1985) based on material from the Narmia, Nammal Gorge, and Chhidru sections. Late Smithian ammonoids from the lower part of Unit 4 (equivalent to the upper part of Upper Ceratite Limestone) include *Anasibirites kingianus* and *Xenoceltites* sp. (PJRG, 1985). The upper part of Unit 4 includes *A. kingianus* and *X.* aff. *evolutus* (PJRG, 1985).

Early Spathian *Tirolites* sp. was recently sampled a few meters above the BB at Chitta-Landu. *Procolumbites* was found at the top of the BB at Nammal, but as *Procolumbites* is

younger than *Tirolites* (e.g., Guex et al., 2010), a sedimentary gap at this place is likely within the BB (Hermann et al., 2011). Spathian rocks being eroded above the BB at Chhidru, this section is uninformative for Spathian biostratigraphy. Overall, these ammonoid data constrains the position of the SSB in Pakistan to between the *Glyptophiceras sinuatum* beds and the *Tirolites* sp. beds.

The first conodont study in Nammal Gorge and Narmia yielded three zones, in ascending order, the *Novispathodus waageni* and *Neogondolella elongata* zones of Smithian age and the *Triassospathodus triangularis-Tr. homeri* Zone of Spathian age (PJRG, 1985; Fig. 5F). The *Sc. milleri* Zone, occupying a narrow interval between the *Nv. waageni* and *Ng. elongata* zones, was recognized only at Chhidru. Spathian conodont species in the *Tr. triangularis-Tr. homeri* Zone, including *Tr. triangularis*, *Tr. homeri*, *Ng. elongata* and *Ng. jubata*, range through a ~40-m-thick stratigraphic interval from the top of Unit 4 to near the top of the Narmia Member (PJRG, 1985). Therefore, based on these conodont data, the SSB can be constrained to between the first occurrences of the *Ng. elongata* and *Tr. triangularis*. Recent works of Romano et al. (2013), Leu et al. (2018), and Goudemand et al. (2018) reported several new occurrences of conodonts in Nammal and especially confirmed the occurrence of *Nv. pingdingshanensis* within the late Smithian *Glyptophiceras sinuatum* ammonoids beds.

3.9.2. Carbon-isotope chemostratigraphy

Carbon isotope profiles for the Olenekian Stage have been reported from the Nammal (Baud et al., 1996; Galfetti et al., 2007c, modified after Baud et al., 1989, and Atudorei, 1999) and Chhidru of the Salt Range, and Chitta-Landu of the Surghar Range in Pakistan (Baud et al., 1996; Hermann et al., 2011) (Fig. 12). The ammonoid and carbon isotope studies at Salt Range and Surghar Range facilitate intercalibrations (Hermann et al., 2011). The $\delta^{13}C_{carb}$ profile in Nammal exhibits stable values of ca. −2 ‰ in the middle Smithian (N3), a positive excursion to ca. +2 ‰ across the SSB, and then a decrease to ca. −2 ‰ by the mid-Spathian. In the composite section (Nammal, Chhidru, Chitta-Landu and Narmia gorges) of Hermann et al. (2011, 2012), $\delta^{13}C_{carb}$ values were only reported from the middle to uppermost Smithian, showing similar variations as in Galfetti et al. (2007c). The $\delta^{13}C_{org}$ profile of the composite section exhibits high values (ca. −24 to −28 ‰) in the lower Smithian, followed by a negative excursion to ca. −33 ‰ (N3*) in the middle Smithian (*Pseudoceltites multiplicatus* beds), then back to ca. −26 ‰ (P3*) in the lowermost Spathian (Hermann et al., 2011, 2012). Within the Spathian, the $\delta^{13}C_{org}$ signal shows a slight decrease to ca. −30 ‰ (N4*?) then an increase to ca. −26 ‰ in the upper Spathian. In the Salt Range and Surghar Range, however, the $\delta^{13}C_{org}$ profile of the Smithian interval is slightly different from those of other sections globally (Figs. 7, 11-12), possibly due to unusual sedimentation rates, or diagenetic alteration or contamination of the organic carbon isotope record.

3.10. Spiti Valley, India (southern Tethys)

3.10.1. Ammonoid and conodont biostratigraphy

In the Spiti Valley of northern India, Olenekian strata belong to the Mikin Formation,

which consists of the Smithian Limestone and Shale Members, and the Spathian Niti Limestone Member (Brühwiler et al., 2010a). Lower Triassic ammonoids and conodonts have been studied in a series of sections including Mud, Guling, Lalung, and Losar (Brühwiler et al., 2007, 2012b; Krystyn et al., 2007a, b). To date, biostratigraphic works in the Spiti Valley have focused mainly on the Permian/Triassic and Induan/Olenekian boundaries, as well as Smithian ammonoids (Orchard and Krystyn, 1998, 2007; Krystyn et al., 2004; Orchard, 2007).

At Mud, Brühwiler et al. (2010a, 2012b) reported fourteen ammonoid UA zones of Smithian age, including the late Smithian *Wasatchites distractus*, *Subvishnuites posterus* and *Glyptophiceras sinuatum* beds, in ascending order (Fig. 5G and 6F). The *W. distractus* beds also contain abundant specimens of *Anasibirites*; this assemblage can be correlated worldwide (e.g., Jenks et al. 2015; Jattiot et al. 2016, 2017). The *S. posterus* beds contain *S. posterus*, *Pseudosageceras augustum*, and *Xenocelties* cf. *variocostatus*. This interval, together with the overlying *G. sinuatum* beds, are indicative of the latest Smithian (Brühwiler et al., 2010a; Jattiot et al. 2017). *Tirolites* is reported from overlying lower Spathian beds (Brühwiler et al. 2010a, 2011), but with uncertainty on its exact occurrence. Nevertheless, based on ammonoids the SSB can be placed above the *G. sinuatum* beds and below the *Tirolites* beds.

The corresponding conodont zones at Mud are the lower-middle Smithian *Novispathodus waageni eowaageni* and *Nv. waageni waageni*, the upper Smithian *Scythogondolella milleri*, and the Spathian *Icriospathodus collinsoni* and *Chiosella gondolelloides* zones, in ascending order (Bhatt et al., 1999; Krystyn et al., 2004, 2005; Orchard and Krystyn, 2007) (Fig. 5G). Therefore, the SSB could be placed at or below the first occurrence of *Ic. collinsoni*.

3.10.2. Carbon-isotope chemostratigraphy

Carbon isotope profiles have been reported from the Mud and Losar sections, Mud profile covering the upper Dienerian to lower Smithian (Krystyn et al., 2007a), and the Losar profile covering the whole Olenekian (Atudorei, 1999; Galfetti et al., 2007c) (Fig. 12). At Mud, the $\delta^{13}C_{carb}$ profile shows a gradual decrease from ca. 0 ‰ at the Induan/Olenekian boundary to ca. −2 ‰ in the lower/middle Smithian (i.e., within the *Flemingites-Euflemingites* ammonoid Zone and the *Neospathodus spitiensis* conodont Zone; close to N3). At Losar, the $\delta^{13}C_{carb}$ profile exhibits a gradual decrease from ca. +0.5 ‰ in the lowermost Smithian (close to P2) to ca. −3 ‰ in the middle Smithian (at ~1 below the *Nyalamites angustecostatus* beds; N3), a positive excursion to ca. +2.5 ‰ (P3) across the SSB, a gradual negative excursion to ca. −1 ‰ by the middle Spathian (N4), and finally a rebound to ca. +2 ‰ in the uppermost Spathian (close to P4) (Galfetti et al., 2007c; Fig. 12).

3.11. Southern Europe, Caucasus, and Middle East (western Tethys)

3.11.1. Ammonoid and conodont biostratigraphy

Various localities in southern Europe have yielded ammonoid assemblages, but most of them are poorly preserved with a rather low diversity (e.g., Romania, Cavin and Gradinaru, 2014; Hungary, Hips and Pelikan, 2002; Balkans, Kittl, 1903; Krystyn, 1974; Golubić, 1996, 2000). Additionnally, mostly reported faunas are early Spathian, and detailed biostratigraphic

zonations are rare, preventing a firm definition of the SSB within this area based on ammonoids. However, Smithian material is beginning to be described relatively finely in some places (e.g., Đacović, 2017), suggesting that future biostratigraphic improvements around the SSB are possible. Sections in the Caucasus mainly include Smithian ammonoids (e.g., Popov, 1964), whereas reported taxa from Mangyshlak are mainly early Spathian in age (e.g., Balini et al., 2000). Here again, future improvements in ammonoid biostratigraphy may help to better constrain the SSB. Detailed ammonoid zonal schemes for the SSB in the Middle East are also lacking, in part due to the limited acessibility of this area (e.g., Iran, Balini et al., 2009, Vaziri, 2011). However, some abundant and diversified assemblages are known from the Smithian and Spathian of Oman (Tozer and Calon, 1990; Brühwiler et al., 2012c), suggesting that future biostratigraphic improvements are also possible in this region.

Latest Permian-Early Triassic conodonts have been extensively studied in Europe, for example, in Italy (Huchkriede, 1958; Assereto et al., 1973; Mostler,1982; Perri, 1986; Perri and Andraghetti, 1987; Samankassou, 1995; Perri and Farabegoli, 2003), Slovenia (Kolar-Jurkovšek and Jurkovšek, 2007; Kolar-Jurkovšek et al., 2011a, b), Croatia (Aljinović et al., 2006, 2011) and Serbia (Sudar et al., 2007; Nestell et al., 2009; Crasquin et al., 2010), including conodonts of the Olenekian age (Staesche, 1964; Perri, 1991; Kolar-Jurkovšek et al., 2013, 2015, 2017; Sudar et al., 2014; Chen-YL et al., 2016). Generally, conodont data in this area are rarer (e.g., Italy) than elsewhere and also endemic. This does not facilitate correlation with other regions. For example, some classical Smithian taxa (e.g., *Novispathodus waageni*) and taxa considered as markers of the earliest/early Spathian (e.g., *Nv. pingdingshanensis*, *Icriospathodus collinsoni*) are often absent. Sudar et al. (2014) reported two lower Smithian conodont zones, in ascending order, the *Pachycladina obliqua–Foliella gardenae* and *Neospathodus planus* zones, from the Gučevo mountain area in northwestern Serbia. In northern Italy, the *Pa. obliqua* Zone ranges through almost the entire Olenekian (Perri, 1991). Posenato (2008) suggested that *F. gardenae* may have ranged from the late Dienerian to the late Smithian. A lower Smithian *Pa. obliqua* Zone was reported from Croatia by Aljinović et al. (2011), which included the conodont taxa *Hadrodontina anceps*, *Parachirognathus ethingtoni*, *Foliella* sp. or ?*Furnishius* sp. Kolar-Jurkovšek et al. (2013) and Kolar-Jurkovšek and Jurkovšek (2015) reported Olenekian conodont assemblages from the Julian Alps area in Slovenia, in which *Triassospathodus hungaricus* was regarded as indicative of an earliest Spathian age. In Chen-YL et al. (2016), nine discrete conodont UA zones were recognized in the Olenekian of the Idrija–Žiri area in Slovenia, namely the *Eurygnathodus costatus*, *Eurygnathodus hamadai*, *F. gardenae*, *Ns. robustus*, *Platyvillosus corniger*, *Pl. regularis*, *Tr. hungaricus*, *Tr. symmetricus*, and *Ns. robustispinus* UAZs. The *F. gardenae* Zone from the Žiri road section, which contains *F. gardenae*, *Pa. obliqua* and *Pa. inclinata*, was proposed as indicative of the SSB transition based on its co-occurrence with the P3 carbon-isotope maximum (Chen-YL et al., 2016) (see Section 5.3). However, the *F. gardenae* UAZ may also include the N3 carbon-isotope minimum, thus constraining the SSB to within the *F. gardenae* UAZ. Only limited Lower Triassic conodont biostratigraphic data are available for sections from the Middle East (Brühwiler et al., 2012c; Chen-YL et al., 2018) and most of them are focused on the Permian/Triassic boundary (e.g., Gallet et al., 2000; Hauser et al., 2001; Groves et al., 2005; Horacek et al., 2007b; Richoz et al., 2010).

3.11.2. Carbon-isotope chemostratigraphy

Carbon isotope studies of the Slovenian sections revealed a $\delta^{13}C_{carb}$ shift from ca. +0.5 to +7 ‰ within the *Foliella gardenae* Zone (Interval II), followed by a decrease from ca. +5 ‰ in the *Neospathodus robustus* Zone (lower Spathian; close to P3) to ca. +1 ‰ in the *Ns. robustispinus* (middle Spathian; close to N4) (Chen-YL et al., 2016). Recently, Aljinović et al. (2018) reported a continuous Olenekian $\delta^{13}C_{carb}$ curve from Croatia, showing a negative excursion of $\delta^{13}C_{carb}$ from ca. +5 ‰ in the lower Smithian (P2) to ca. −3 ‰ in the middle Smithian (N3), followed by a positive excursion to ca. +3 ‰ in the lower Spathian (P3). The $\delta^{13}C_{carb}$ curve then decreased to ca. −2 ‰ in the mid-Spathian (N4) and back to ca. +3 ‰ in the upper Spathian (close to P4). More extensive carbon-isotope work has been undertaken in Italy. At L'Uomo, the $\delta^{13}C_{carb}$ profile shows a sharp negative excursion from ca. +6 ‰ in the lowest Smithian (P2) to ca. −2 ‰ during the middle Smithian (N3), followed by a positive excursion to ca. +2 ‰ in the lower Spathian (P3) (Horacek et al., 2007a). At Lungenfrischgraben, the $\delta^{13}C_{carb}$ profile shows a gradual decrease from ca. +4 ‰ at the IOB (P2) to ca. −2 ‰ (N3) in the middle Smithian, a rebound to ca. +3 ‰ in the lowermost Spathian (P3), and finally a negative excursion to ca. −2 ‰ in the mid-Spathian (N4) (Horacek et al., 2010). The $\delta^{13}C_{carb}$ profile at Trudener Bach is similar to that at L'Uomo, showing a shift from ca. −2 ‰ in the middle Smithian (N3) to ca. +3 ‰ at the lower Spathian (P3) (Horacek et al., 2010).

In the Middle East, carbon isotope studies on the Smithian-Spathian transition have been carried out for the Zal, Abadeh and Amol sections in Iran (Horacek et al., 2007b), the Musandam section in the United Arab Emirates (Clarkson et al., 2013), the Wadi sections (i.e. Sahtan, Shuyab, Maqam, Wasit Sud) and Sal and Radio Tower sections in Oman (Hauser et al., 2001; Richoz, 2006, Chen-YL et al., 2018), and the Taşkent section in Turkey (Richoz et al., 2006; Lau et al., 2016). In the Iranian sections, the $\delta^{13}C_{carb}$ profiles show negative excursions from +5 to +8 ‰ at the Induan/Olenekian boundary (P2) to −2 to −4 ‰ in the middle Smithian (N3), sharp rebounds to +2 to +3 ‰ at the SSB (P3), and then gradual decreases to ca. −4 ‰ in the mid-Spathian (N4) (Horacek et al., 2007b; Fig. 12). At Musandam, the $\delta^{13}C_{carb}$ profile shows a gradual negative excursion from ca. +3 ‰ in the lowermost Smithian (P2) to ca. 0 ‰ in the middle Smithian (N3), a slow rebound to ca. +4 ‰ in the lower Spathian (P3), a decrease to ca. +2 ‰ in the middle to upper Spathian (N4), and finally an increase to ca. +3 ‰ in the uppermost Spathian (close to P4) (Clarkson et al., 2013; Fig. 12). In Taşkent, the $\delta^{13}C_{carb}$ profile shows a negative excursion from ca. +6 ‰ in the lowermost Smithian (P2) to ca. −2 ‰ in the middle Smithian (N3), a positive excursion to ca. +4 ‰ in the lower Spathian (P3), followed by the second negative excursion to −2 ‰ in the middle to upper Spathian (N4), and finally an increase to ca. +4 ‰ in the uppermost Spathian (close to P4) (Lau et al., 2016). In Oman, the $\delta^{13}C_{carb}$ profiles show negative shifts from +4 to +6 ‰ in the lowermost Smithian (P2) to 0 to −2 ‰ in the middle Smithian (N3), a positive excursion to a maximum of ca. +8 ‰ in the lower Spathian (P3), a gradual negative excursion to −1 to −3 ‰ in the middle to upper Spathian (N4), and finally a rebound to positive values in the upper Spathian (Richoz, 2006; Clarkson et al., 2016; Chen-YL et al., 2018). Despite the frequent lack of biostratigraphic data, the position of the SSB is generally constrained by the well-defined N3-to-P3 shift in the carbon isotope profiles of these sections, but new biostratigraphic data will likely help to better

constrain the SSB in this area (see Chen-YL et al., 2018).

4. Chemostratigraphic records for the Smithian-Spathian transition

4.1. Carbon-isotope chemostratigraphy

The Early Triassic was an interval marked by large successive secular fluctuations in carbon isotope records, beginning at the EPME and ending around the Early/Middle Triassic boundary (e.g., Payne et al., 2004; Tong et al., 2007). These high-amplitude carbon isotopic variations were often assumed to be related to rapid marine faunal overturns and to a delayed marine ecosystem recovery following the EPME (Erwin, 2001; Bottjer et al., 2008; Chen and Benton, 2012). During this time, there is evidence of recurrent extreme environmental perturbations, e.g., high tropical sea-surface temperatures (Sun et al., 2012; Romano et al., 2013), relatively widespread oceanic anoxia (Wignall and Twitchett, 1996; Grice et al., 2005; Xie et al., 2007; Galfetti et al., 2008; Algeo et al., 2010; Hermann et al., 2011; Grasby et al., 2013; Zhao et al., 2013b; Feng et al., 2014; Tian et al., 2014; Clarkson et al., 2016; Lau et al., 2016; Huang et al., 2017; Song-HY et al., 2019), and ocean acidification (Payne et al., 2010; Hinojosa et al., 2012; Clarkson et al., 2015; Silva-Tamayo et al., 2018). Following the middle Smithian hyperwarming (Sun et al., 2012; Romano et al., 2013), the Smithian-Spathian transition was marked by a climatic cooling event (Goudemand et al., 2013, 2014a, 2018), weakened ocean stratification (Song-HY et al., 2013), and increased marine productivity linked to upwelling of sequestered deep-water nutrients at some places (Takahashi et al., 2009; Zhang et al., 2015; Song-HY et al., 2019). A concurrent major perturbation to the global carbon cycle before and across the SSB resulted in the largest excursions in marine $\delta^{13}C$ records of the Early Triassic (Payne et al., 2004; Tong et al., 2007; Galfetti et al., 2007a, b, c; Horacek et al., 2007a, b; Brühwiler et al., 2009). Such excursions in Early Triassic marine $\delta^{13}C$ records have multiple proposed causes, including volcanic emissions (Galfetti et al., 2007b; Payne and Kump, 2007), soil organic matter inputs (Sephton et al., 2005), marine productivity changes (Meyer et al., 2011), or combinations of these factors (Algeo et al., 2011). In addition, regional authigenic and/or diagenetic effects can also modify carbon isotope signals depending on the environmental settings (Schobben et al., 2016; Thomazo et al., 2016; Caravaca et al., 2017).

These large global $\delta^{13}C$ fluctuations can therefore be useful for global correlation when coupled with biostratigraphic data (e.g., Galfetti et al., 2007c; Horacek et al., 2007a, b; Grasby et al., 2016; Wignall et al., 2016; Thomazo et al., 2016). Most $\delta^{13}C$ profiles exhibit a series of alternating minima (N1 to N4) and maxima (P1 to P4; Fig. 1). During the Olenekian, $\delta^{13}C$ profiles generally exhibit a positive peak (P2) close to the Dienerian/Smithian boundary, a major negative excursion in the middle Smithian (N3), a rebound across the SSB to a second positive peak (P3) in the earliest Spathian, a second negative excursion (N4) in the middle Spathian, and a third positive excursion (P4) in the lowermost Anisian, after which $\delta^{13}C$ stabilized during the Middle Triassic (e.g., Payne et al., 2004; Tong et al., 2007). The cause(s) of these large carbon-isotopic excursions are not known with certainty. For instance, the P3 excursion has been tentatively partly related to increased marine productivity during the SSB cooling event (Song-HY et al., 2013; Zhang et al., 2015; Caravaca et al., 2017; Goudemand et al., 2018).

Although nearly all Lower Triassic marine sections examined to date yield the same pattern of large-scale carbon-isotopic fluctuations, as described above, there are nonetheless small differences in $\delta^{13}C$ profiles that may have significance for global correlation of the SSB. To facilitate discussion of carbon-isotopic variations, we have divided the Olenekian into four intervals, with Interval I representing the P2 to N3 shift, Interval II the N3 to P3 shift, Interval III the P3 to N4 shift, and Interval IV the N4 to P4 shift (Fig. 13A). Furthermore, we define "mdpt(N3-P3)" as the midpoint in units of per mille PDB between the absolute $\delta^{13}C$ value of the N3 minimum and that of the P3 maximum in a given stratigraphic section. Present indications are that the SSB may slightly predate the P3 maximum, which is early Spathian. Because the N3 minimum may not be correlative between sections (owing to a slow initial rise and consequent difficulties in uniquely locating this point in some sections), it can be useful to have another pre-P3 geochemical marker. The mdpt(N3-P3) marker can serve this purpose because by the midpoint of the N3-to-P3 shift, $\delta^{13}C$ was rising rapidly in many SSB sections, and this point can therefore be roughly correlated at a global scale in the absence of biostratigraphic data.

Most SSB sections exhibit a rapid shift from N3 to P3 (i.e., Interval II; see Fig. 13A). We are particularly concerned with variation between the lowermost Smithian and lowermost Spathian (i.e., Intervals I and II), within which we identified four major different patterns of $\delta^{13}C$ variation (Fig. 13B). This variation is mainly related to the shape and position of the N3 minimum, with implications for placement of the Interval I/II contact (see discussion in Section 5.3). Pattern 1 is characterized by an N3 minimum in the middle Smithian, followed by a slow rise in $\delta^{13}C$ through the late Smithian before a rapid rise across the SSB. Pattern 2 is characterized by a protracted $\delta^{13}C$ minimum during the middle Smithian, before a rapid rise in the late Smithian. Pattern 3 is characterized by a slow decline in $\delta^{13}C$ through the early Smithian, reaching the N3 minimum during the middle Smithian, before a rapid late Smithian rise. Pattern 4 is a variant on Pattern 3, in which the decline in $\delta^{13}C$ from the P2 maximum to the N3 minimum apparently does not show distinct rapid and slow stages (as in Pattern 3; Fig. 13B).

4.2. Other chemostratigraphic records ($\Delta\delta^{13}C_{DIC}$, $\delta^{34}S$ and $^{87}Sr/^{86}Sr$)

In addition to $\delta^{13}C$, various other chemostratigraphic records show pronounced variations during the Early Triassic. Meyer et al. (2011) and Song-HY et al. (2013) documented changes in the vertical gradient of $\delta^{13}C$ of dissolved inorganic carbon (DIC) in Early Triassic seawater based on secular differences in the $\delta^{13}C_{carb}$ profiles of sections deposited at different water depths. Song-HY et al. (2013) showed that $\Delta\delta^{13}C_{DIC}$ reached high values (ca. +4 to +7 ‰) during the middle-late Smithian, when a hot climate prevailed, and subsequently declined to ca. 0 ‰ in the early Spathian, coincident with climatic cooling (Fig. 14A). Song-HY et al. (2013) linked this pattern to the influence of temperature changes on the vertical temperature structure of the water column, with warming leading to intensified water-column stratification, reduced vertical overturn, and thus higher $\Delta\delta^{13}C_{DIC}$ values (sustained by the "biological pump"), and cooling leading to reduced stratification, invigorated overturn, and lower $\Delta\delta^{13}C_{DIC}$ values.

The $\delta^{34}S$ values of carbonate-associated sulfate (CAS) and evaporites, which are used as a proxy for contemporaneous seawater sulfate $\delta^{34}S$, show large variations throughout the Early

Triassic (Marenco et al., 2008; Horacek et al., 2010; Song-HY et al., 2014; Bernasconi et al., 2017; Lyu et al., 2018; Stebbins et al., 2018a, b; Thomazo et al., 2018). $\delta^{34}S_{CAS}$ profiles in South China exhibit a negative excursion from a maximum of ca. +40 ‰ (P2s) in the earliest Smithian to a minimum of ca. +20 ‰ (N3s) in the middle Smithian, a rebound to a maximum of ~33 ‰ (P3s) in the early Spathian, and finally a slow decline in the middle to late Spathian to values of ca. +15 ‰ by the Middle Triassic (Song-HY et al., 2014; Fig. 14B; note: the 's' suffix indicates a S-isotope excursion, whereas excursion numbers without a suffix indicate a C-isotope excursion). Recent studies revealed relatively similar variations of $\delta^{34}S_{CAS}$ during the Smithian and Spathian in the Spiti Valley (India), Jesmond (Canada), and Mineral Mountains (USA) sections (Stebbins et al., 2018a, b; Thomazo et al., 2018). These fluctuations here parallel those in $\delta^{13}C$ profiles, and this relationship has been attributed to co-burial of reduced carbon (organic matter) and reduced sulfur (pyrite), both of which are isotopically light compared to their seawater sources (DIC and sulfate, respectively). In this scenario, positive (vs. negative) shifts in $\delta^{34}S_{CAS}$ and $\delta^{13}C_{carb}$ were the result of increased (vs. reduced) burial of organic matter and pyrite, due to increased (vs. reduced) primary productivity and intensity of microbial sulfate reduction controlled by climate changes. Concomittant changes in bioturbation may have also played a role (Thomazo et al., 2018). The coupling of these two isotopic systems during the Early Triassic (which is not seen in the Cenozoic) was because of the much lower concentration of seawater sulfate at that time (2.5 to 9.1 mM; Algeo et al., 2015), resulting in a shorter residence time for seawater sulfate that more closely matched that of seawater DIC (Luo et al., 2010; Stebbins et al., 2018b). The decoupling of the marine C and S cycles that occurred during the middle to late Spathian was thus probably due to increases in seawater sulfate concentrations that resulted in residence times longer than that of DIC (Song-HY et al., 2014).

Climate warming also potentially enhanced continental weathering during the Early Triassic, as revealed by a sharp increase in seawater $^{87}Sr/^{86}Sr$. This rise commenced in the early Griesbachian from a baseline of ~0.7072, reaching ~0.7076 by the earliest Smithian and then ~0.7079 by the earliest Spathian (Sedlacek et al., 2014; Song-HJ et al., 2015; Fig. 14C). Thereafter, the rise in seawater $^{87}Sr/^{86}Sr$ slowed sharply, reaching only ~0.7081 by the late Spathian. The abrupt break in the seawater $^{87}Sr/^{86}Sr$ profile at the SSB has been attributed to a sharp global cooling at that time and a consequent decrease in continental weathering rates (Algeo and Twitchett, 2010; Sedlacek et al., 2014; Zhang-L et al., 2015; Zhang-F et al., 2018).

5. Future formalization of the Smithian/Spathian boundary

Biological and environmental studies of the Smithian-Spathian transition will ultimately lead to a formal definition of the SSB, and the present study provides a first background for moving forward toward this objective. Both ammonoids and conodonts offer numerous and widely distributed biostratigraphic markers that may be useful for future definitions of the SSB. The definition of any GSSP ideally employs multiple bio-, chemo-, and physical criteria, and when fossils are rare or lacking, as is the case for some SSB sections, then alternate proxies must be sought. The SSB transition corresponds to a rapid positive shift of $\delta^{13}C$ from the middle Smithian N3 minimum to the early Spathian P3 maximum (Interval II; Fig. 13), making the $\delta^{13}C$ signal a potentially useful auxiliary proxy to locate the SSB (but not replacing

biostratigraphic data, if available). In this section, we review (1) potential ammonoid and conodont biostratigraphic as well as carbon-isotopic criteria that may prove useful for a future formal definition of the SSB, (2) placements of the SSB in earlier studies globally, and (3) the timing of the Smithian Thermal Maximum based on the criteria proposed in the present study. Note that these points can potentially evolve according to future discoveries that may be made.

5.1. Constraints from ammonoid biozonation

The successive global events recorded by ammonoids during the late Smithian and early Spathian are well-constrained and provide multiple potential criteria for definition of the SSB. The base of the late Smithian is globally well-defined by a first major ammonoid extinction event (see Section 2 and Fig. 2) and is characterized by an assemblage grouping iconic taxa, notably prionitids, showing impressive cosmopolitan distributions, such as *Anasibirites* and *Wasatchites* (AW assemblage), and representing an almost perfect global timeline. The AW assemblage thus allows correlation at very large geographic scale among localities of different paleolatitudes and oceans (e.g., USA, Jattiot et al., 2016, 2017; South China, Tong et al., 2004, Brayard and Bucher, 2008; Pakistan, Brühwiler et al., 2011). The top of the late Smithian is also rather well-defined by an assemblage of cosmopolitan taxa, much poorer in generic richness and corresponding to a last Smithian turnover event. It is mainly found at low and mid-paleolatitudes of the Tethys and Panthalassic oceans and shows co-occurring taxa such as *Glyptophiceras*, *Xenoceltites* (*X. variocostatus* and *X. subevolutus*) and *Pseudosageceras augustum* (GXP assemblage). This latest Smithian assemblage (or characteristic species) has notably been reported from the USA (Brayard et al., 2013; Jattiot et al., 2017, 2018; Jenks and Brayard, 2018), Spitsbergen (Mørk et al., 1999), South China (Tong et al., 2004; Brayard and Bucher, 2008), Vietnam (Komatsu et al., 2016), and various localities of the North Indian Margin (Brühwiler et al., 2012a, b). The GXP assemblage can thus be used to define the uppermost Smithian at a very large number of localities. Another late Smithian assemblage (*Subvishnuites* beds) that is intermediate between AW and GXP has been reported from the North Indian Margin, but it is mostly endemic and not well-documented elsewhere. Earliest Spathian assemblages are generally characterized by widespread occurrences of typical taxa belonging to e.g., the genera *Tirolites*, *Bajarunia* and *Doricranites*. The first appearances of these taxa, as well as their co-occurrences (e.g., *Bajarunia* and *Tirolites*; BT assemblage) at some places, can serve as a potential basis for definition of the base of the Spathian (e.g., Spitsbergen, Dagys and Weitschat, 1993; USA, Guex et al., 2010; Jenks et al., 2013; South China, Tong et al., 2004; Galfetti et al., 2007b; Vietnam, Komatsu et al., 2016). However, as these earliest Spathian taxa apparently exhibit rather more endemic distributions than late Smithian taxa, diagnostic assemblages or taxa may slightly vary from basin to basin. More work is needed to finely decipher earliest Spathian occurrences of these taxa at many places. Within the early Spathian, taxa co-occuring with *Columbites* are younger.

Overall, based on published ammonoid data, the SSB is constrained above the global AW assemblage and between the latest Smithian GXP and earliest Spathian BT assemblages. Such a sucession is frequently encountered and well-documented in the western USA, South China, Tibet, Vietnam and South Primorye (see Section 3). Detailed study of basins where the Smithian-Spathian transition was not affected by a eustatic regression, as is observed almost

worldwide, or from sections representing deep water settings may help to definitively determine the detailed succession of ammonoids assemblages across the SSB.

5.2. Constraints from conodont biozonation

Conodont taxa characteristic of the late Smithian substage are useful in constraining the SSB. The Ellisoniidae family (e.g., *Pachycladina*, *Foliella*, *Parachirognathus*, *Furnishius* and *Hadrodontina*) and Mullerinae subfamily (e.g., *Discretella*, *Wapitiodus*, *Guangxidella*, *Conservatella* and *Scythogondolella*) mostly went extinct before or at the SSB (Orchard, 2007). Diagnostic late Smithian taxa of the Ellisoniidae family have been identified in many areas, e.g., *Pachycladina* from southwestern China (Yan et al., 2013; Chen-YL et al., 2015), *Pa. obliqua* and *Pa. inclinata* from southern Europe (Perri, 1991; Aljinović et al., 2011; Sudar et al., 2014; Chen-YL et al., 2016); *Foliella* from Croatia (Aljinović et al., 2011), *F. gardenae* from other southern European locales (Sudar et al., 2014; Chen-YL et al., 2016); *Parachirognathus* from Japan (Zhang et al., 2017) and southwestern China (Yan et al., 2013; Chen-YL et al., 2015), *Pa. ethingtoni,* and *Furnishius* and *Hadrodontina anceps* from southern Europe (Aljinović et al., 2011). Members of the Mullerinae subfamily that are characteristic of the late Smithian include *Discretella* from Japan (Zhang et al., 2017), *Ds. discreta* from the Canadian Arctic (Mosher, 1973; Orchard, 2008), western British Columbia (Orchard and Zonneveld, 2009), western United States (Orchard and Tozer, 1997; Orchard, 2008; Orchard and Zonneveld, 2009), and southwestern China (Yan et al., 2013; Chen-YL et al., 2015); *Wapitiodus*(?) from Japan (Zhang et al., 2017), *W. robustus* from western British Columbia (Orchard and Zonneveld, 2009); *Guangxidella bransoni* from British Columbia Orchard (2008) and the western United States (Orchard and Tozer, 1997; Orchard, 2008; Orchard and Zonneveld, 2009); *Conservatella conservativa* from Canadian Arctic (Mosher, 1973; Orchard, 2008) and the western United States (Orchard and Tozer, 1997; Orchard, 2008; Orchard and Zonneveld, 2009); *Sc. lachrymiformis*, *Sc. rhomboidea*, *Sc. milleri* and *Sc. mosheri* from the Canadian Arctic (Orchard, 2008), *Sc. milleri* and *Sc. mosheri* from Spitsbergen (Weitschat and Lehmann, 1978; Clark and Hatleberg, 1983; Hatleberg and Clark, 1984) and the western United States (Müller, 1956; Orchard and Tozer, 1997; Orchard, 2008), *Sc. lachrymiformis*, *Sc. milleri*, *Sc. mosheri* and *Sc. phryna* from western British Columbia (Orchard and Zonneveld, 2009), *Sc. milleri* from the Spiti Valley (Bhatt et al., 1999; Krystyn et al., 2004, 2005; Orchard and Krystyn, 2007) and the Salt Range (PJRG, 1985).

Some genera of the Novispathodinae (e.g., *Novispathodus*, *Triassospathodus*) and Neogondolellinae (e.g., *Neogondolella*) subfamilies survived and rediversified after the late Smithian extinction (Orchard, 2007), generating key early Spathian taxa that could be used in the definition of the SSB. Commonly assumed members of this surviving and recovery fauna included '*Tr.*' *hungaricus*, *Ng.* aff. *sweeti*, and *Nv. pingdingshanensis*, which were first reported from Hungary (Kozur and Mostler, 1970), the WCSB/western USA (Orchard and Tozer, 1997), and Chaohu (Zhao et al., 2007a), respectively. Later, '*Tr*'. *hungaricus* was also reported from Sichuan Province, South China (Tian et al., 1983), the western USA (Lucas and Orchard, 2007), and various localities in Europe (Kolar-Jurkovšek et al., 2013; Chen-YL et al., 2016); *Ng.* aff. *sweeti* was reported from Chaohu (Zhao et al., 2007a); and *Nv. pingdingshanensis* was reported from multiple sections in the South China region (Tong et al.,

2007; Ji et al., 2011; Chen-YL et al., 2015; Zhang et al., 2015), the WCSB (Orchard and Zonneveld, 2009), and the An Chau Basin (Komatsu et al., 2016).

Newly evolved conodont species of Spathian age, and their intercalibrations with ammonoid biozonation data, may serve an important role in the future definition of the SSB. In North America, *Neogondolella* aff. *sweeti* is known from strata overlying the *Anawasatchites tardus* Zone in the WCSB, and is of probable Spathian age in California. This species, as yet undescribed, differs from *Ng. sweeti* associated with Smithian *Neospathodus pakistanensis* in the Mittiwali Formation of Pakistan (Orchard and Tozer, 1997). In Hungary, '*Triassospathodus*' *hungaricus* occurs in the *Tirolites* ammonoid beds (Kozur and Mostler, 1970), thus may serve as a marker for the lower Spathian, within rocks equivalent to the *Tirolites cassianus* ammonoid Zone (Kozur, 2003). Kolar-Jurkovšek et al. (2013) inferred that the '*Tr*'. *hungaricus* fauna lies within the lower Spathian in the shallow western Tethys, where the *Icriospathodus collinsoni* fauna is missing. Chen-YL et al. (2016) speculatively proposed that '*Tr*'. *hungaricus* could be correlated with *Novispathodus pingdingshanensis* because of their small size and co-occurrence with the ammonoid *Tirolites* (e.g., Hungary, Kozur and Mostler, 1970). At Chaohu, *Nv. pingdingshanensis* is found within the *Columbites-Tirolites* ammonoid Zone of the Nanlinghu Formation, between the late Smithian *Anasibirites* beds and the early Spathian *Tirolites* beds, thus leading to its proposed use as an earliest Spathian indicator (Zhao et al., 2007a, 2008a, b; Fig. 15). There, the first occurrence of *Nv. pingdingshanensis* is coincident with the first occurrence of *Ng.* aff. *sweeti* and below the first occurrence of *Ic. collinsoni* (Zhao et al., 2007a, 2008a, b). Thus, even though both *Nv. pingdingshanensis* and '*Tr*'. *hungaricus* may be indicative of the earliest Spathian, *Nv. pingdingshanensis* is the older of these two taxa in South China.

The taxon *Nv. pingdingshanensis* was first introduced by Zhao et al. (2007a), who identified it as a marker for the SSB in South China. Since its discovery, this taxon has been reported from a number of other locations globally, including the western USA (Orchard and Zonneveld, 2009), western Canada (Henderson et al., 2018), Vietnam (Komatsu et al., 2016), Salt Range (Romano et al., 2013; Leu et al., 2018; Goudemand et al., 2018), Kashmir (Leu et al., 2018), Oman (Chen-YL et al., 2018) and the Zuodeng (Tong et al., 2007; Goudemand et al., 2012), Youping (Goudemand et al.,2012) and Jiarong sections in South China (Chen-YL et al., 2015). Although the first occurrence of *Nv. pingdingshanensis* has been used to identify the SSB in South China (Zhao et al., 2007a; Tong et al., 2007; Chen-YL et al., 2015), several studies elsewhere have claimed that the oldest specimens of *Nv. pingdingshanensis* are of late Smithian age because of specimens that co-occur with *Xenoceltites* in the AW and GXP ammonoid asssemblages (Orchard and Zonneveld, 2009; Goudemand et al., 2012; Komatsu et al., 2016; Romano et al., 2013; Chen-YL et al., 2018; Leu et al., 2018; Goudemand et al., 2018). In earlier literature, the genus *Xenoceltites* ranged from the late Smithian to the early Spathian (Guex et al., 2010), but the rare early Spathian specimens assigned to this genus are now excluded from *Xenoceltites* (Brayard et al., 2019; Leu et al., 2018), thus making key *Xenoceltites* taxa found in the AW and GXP assemblages (e.g., *X. variocostatus* and *X. subevolutus*) exclusively late Smithian in age. On this basis, some studies (e.g., Leu et al., 2018) have inferred that *Nv. pingdingshanensis* may not be a suitable marker for the SSB, but more work will be needed to definitively address the issue of a possibly diachronous first occurrence of this taxon at a global scale.

Because of its morphological similarity to antecedent taxa, *Nv. pingdingshanensis* must be carefully identified, and it is uncertain at present whether all reported occurrences of this taxon are correctly attributed. Zhao et al. (2008a) inferred a phyletic lineage in which *Nv. pingdingshanensis* evolved from the earlier taxon *Nv. waageni waageni*, with the latter evolving from *Ns. dieneri* Morphotype 3. The original taxonomic description of *Nv. pingdingshanensis* was based on 23 specimens from Beds 52 and 54-55 at West Pingdingshan (including the holotype from Bed 54) and Beds 61-64 at North Pingdinshan (Zhao et al., 2007a). *Nv. pingdingshanensis* is characterized by (1) four to nine robust, wide, and mostly fused denticles; (2) a straight basal margin in the lateral view; and (3) a large, broadly expanded oval to subrounded basal cavity that is upturned on the inner margin and flat to downturned on the outer margin. Later, additional criteria of *Nv. pingdingshanensis* were proposed by Goudemand et al. (2012), based on studies of conodont assemblages from the Nanpanjiang Basin in South China. In that study, the denticle axes of P1 elements of *Nv. pingdingshanensis* are distinctively curved in the posterior direction and consequently the two or three (wide) denticles anterior of the cusp are often conspicuously asymmetrical, the posterior edge of the free tip being much shorter than the anterior one. Moreover, Goudemand et al. (2012) showed the basal margin of the P1 element is not necessarily straight, but, contrary to the original diagnosis by Zhao et al. (2007a), may vary from substraight to slightly upturned posteriorly and, thus, cannot be used as a diagnostic feature.

Apart from *Nv. pingdingshanensis*, other conodont species can assist with placement of the SSB. For example, the early Spathian *Icriospathodus crassatus*, which appears ~2 m above *Nv. pingdingshanensis* at Chaohu (Zhao et al., 2007a; Liang et al., 2011), has been used as a marker for the SSB at Guandao (Wang et al., 2005) and in the western United States (Orchard and Tozer, 1997). *Ic. collinsoni* can also be another potentially useful indicator of an early Spathian age—it is found slightly above *Ic.*? *crassatus* at Guandao (Wang et al., 2005), within the *Columbites* beds in the western USA (Orchard and Tozer, 1997), and within the *Tirolites* sp. nov. beds in the An Chau Basin (Komatsu et al., 2016).

5.3. Constraints from carbon-isotope chemostratigraphy

When fossils are absent, carbonate carbon isotope records can be useful tools in global stratigraphic correlation because of the long residence time of dissolved inorganic carbon (DIC) in seawater. The Smithian-Spathian transition is characterized by a large positive shift in $\delta^{13}C$ (from the N3 minimum to the P3 maximum) that is globally correlatable and, hence, potentially useful as a proxy for the SSB. Payne et al. (2004) first reported from South China a positive excursion of $\delta^{13}C_{carb}$ across the SSB, from N3 in the upper *Novispathodus waageni* Zone to P3 in the lower *Nv. crassatus* Zone. Later, positive excursions of $\delta^{13}C_{carb}$ or $\delta^{13}C_{org}$ were reported from SSB sections globally (see Section 4), including a number of biostratigraphically well-studied sections in the eastern Tethyan region (e.g., Galfeti et al., 2007b; Tong et al., 2007; Chen-YL et al., 2013; Zhang et al., 2015; Komatsu et al., 2016).

Most SSB sections exhibit a rapid shift from N3 to P3 (i.e., Interval II; see Figs. 7, 11-13). The early part of this shift occurred slowly in some sections (e.g., $\delta^{13}C$ Pattern 1), and it is unclear whether the point of onset is perfectly correlative at a global scale. For example, in sections on the North Indian Margin with well-constrained ammonoid zonations (Fig. 12), the

onset may be located in the middle Smithian. However, the bulk of the positive shift occurred rapidly, so both the midpoint of the shift ('mdpt(N3-P3)') and its termination (P3) in the early Spathian are likely to represent nearly synchronous datums globally. This is rather true even though the amplitude of the $\delta^{13}C$ shift (in per mille units) within Interval II varies among different sections—variable amplitudes are merely the expression of local effects superimposed on the global N3-to-P3 carbon isotope excursion. Below, we evaluate the positions of N3, mdpt(N3-P3), and P3 relative to biostratigraphic constraints on placement of the SSB in order to assess the robustness of mdpt(N3-P3) as a potential proxy for the SSB (Figs. 7, 11-12) in the case of absence of biostratigraphic data.

Based on global ammonoid biostratigraphic constraints, N3 is generally located in the middle Smithian. Specifically, N3 in $\delta^{13}C$ Pattern 1 is biostratigraphically well-constrained in the Salt Range and Surghar Ranges (within the *Pseudoceltites multiplicatus* beds; Hermann et al., 2012) and at Losar (between the *Nyalamites angustecostatus* beds and *Truempyceras compressum* beds; Galfetti et al., 2007c), and thus indicative of middle Smithian age (Fig. 12). Besides, the location of N3 within the upper part of the *Owenites koeneni* beds at Jinya ($\delta^{13}C$ Pattern 2; Galfetti et al., 2007c) and Mineral Mountains ($\delta^{13}C$ Pattern 4; Thomazo et al., 2016) also yields similar age constraints (Figs. 7 and 11). Sections showing $\delta^{13}C$ Pattern 3 are all located in the western Tethys, where biostratigraphic resolution is generally poorer (Figs. 12 and 13B) and the position of N3 thus less well-constrained. Conodonts provide limited constraints on the timing of N3, which is roughly in the middle to upper part of the *Nv. waageni* Zone, the upper part of the *Ns. discreta* Zone, or the uppermost part of the *Pachycladina obliqua* Zone (Figs. 11-12).

The documented biostratigraphic constraints for P3 are often not as good as for N3, but an early Spathian age is inferred. Ammonoid biostratigraphy constrains P3 to above the uppermost AW and GXP Smithian assemblages (e.g., at Smith Creek, Grasby et al., 2013; Dicksonfjellet, Galfetti et al., 2007a; Mineral Mountains, Thomazo et al., 2016; Salt Range and Surghar Range, Hermann et al., 2012; and Tulong, Schneebeli-Hermann et al., 2012), and to just below or at the base of the lowermost Spathian *Tirolites* beds (e.g., Jinya, Galfetti et al., 2007c and Chaohu, Tong et al., 2004; Hot Springs, Caravaca et al., 2017). It should be noted that placement of P3 within the uppermost Smithian "*Xenoceltites variocostatus*" beds in the An Chau Basin is inconsistent with its placement in other localities globally (Komatsu et al., 2016; see Section 3.8.1 and 5.1). In the eastern Tethys, conodont biostratigraphy constrains the position of P3 to be above the first occurrences of *Nv. pingdingshanensis* (at Chaohu, Zhao et al., 2007a), *Ns. crassatus* (at Guandao, Lehrmann et al., 2015), and *Ic. collinsoni* (at Jiarong, Chen-YL et al., 2015), consistent with an early Spathian age.

In the eastern Tethys, evaluation of mdpt(N3-P3) as a potential proxy for the SSB is facilitated by the highly detailed ammonoid or/and conodont zonation schemes available for many sections (Fig. 11). In the majority of sections (6 of 8), mdpt(N3-P3) coincides rather well with the SSB within existing biostratigraphic constraints. Specifically, mdpt(N3-P3) is located at the first occurrences of the *Nv. pingdingshanensis* or *Nv. crassatus*, for example, at Chaohu, Guandao, Jiarong and Zuodeng sections. At Mingtang and Shitouzhai, conodont zonations for the lowermost Spathian are lacking, but the SSB was initially constrained as being close to mdpt(N3-P3) through carbon isotope correlations in South China. At Jinya, the SSB was placed immediately below the Tirolitid n. gen. A. beds, ~2-3 m above the last occurrences of

Anasibirites and *Xenoceltites* specimens in the underlying beds. A placement of the SSB based on mdpt(N3-P3) corresponds well to ammonoid biostratigraphic constraints at Jinya and would fall into the stratigraphic interval in between the *Anasibirites* beds and the Tirolitid n. gen. A. In the An Chau Basin, the SSB was constrained to between the *Xenoceltites* and *Tirolites* beds, but the lower constraint is biostratigraphically questionable as discussed above (see Sections 3.8.1 and 5.1).

In the southern Tethyan region, the Smithian and the SSB is better constrained biostratigraphically, e.g., at Salt and Sughar Ranges (Hermann et al, 2012), Losar (Galfetti et al., 2007c) and Tulong (Brühwiler et al., 2009), than western Tethyan region which is mainly based on carbon isotope correlations (Fig. 12), e.g., L'Uomo (Horacek et al., 2007a), Lungenfrischgraben and Trudener Bach (Horacek et al., 2010), Zal, Amol and Abadeh (Horacek et al., 2007b), and Musandam (Clarkson et al., 2013). In the Salt and Sughar Ranges, Tulong, and Losar, the SSB is close to P3 and above the mdpt(N3-P3). At Amol and Abadeh, the SSB was placed close to P3; at L'Uomo, Zal and Musandam, the SSB was placed below the mdpt(N3-P3) (Fig. 12). The SSB was not defined in the Lungenfrischgraben and Trudener Bach sections (Horacek et al., 2010). Thus, in these areas, small regional inconsistencies in placement of the SSB compare to the mdpt(N3-P3) can be noticed and highlight the influences of local conditions on the observed signal. However, mdpt(N3-P3) is most of time located not far from the SSB defined by biostratigraphic markers.

In the Boreal and eastern and central Panthalassic regions, ammonoid biostratigraphic data for the SSB interval are variable in terms of temporal resolution and quantity among basins (Fig. 7). For example, ammonoid biozonation of the late Smithian and early Spathian is available in Spitsbergen (Weitschat and Dagys, 1989), whereas only late Smithian ammonoid beds are known so far from the Canadian Arctic (Tozer, 1967). Thus, adequate biostratigraphic data allowing for constraining the SSB placement are available only in a few sections, leading to variable uncertainties in placements of the SSB when compared to mdpt(N3-P3) or P3. In these regions, carbon-isotope correlations were used in some sections for placement of the SSB, but the $\delta^{13}C$ datum chosen was not consistent among different studies. For example, Grasby et al. (2013) placed the SSB at P3 in Smith Creek, Grasby et al. (2016) placed it at N3 in Festningen, Galfetti et al. (2007a) placed it near mdpt(N3-P3) in Dicksonfjellet (just above late Smithian *Anawasatchites tardus* beds), and Wignall et al. (2016) placed it between N3 and mdpt(N3-P3) in Vindodden. In the Mineral Mountains Thomazo et al. (2016) placed it near what it is mdpt(N3-P3), this one being located at the top of the late Smithian GXP assemblage. Sakuma et al. (2012) placed the SSB between mdpt(N3-P3) and P3 in Inuyama (Fig. 7).

To sum up, there is a rather good correspondence of mdpt(N3-P3) to known biostratigraphic constraints on the SSB although some regional to local influences can modulate this inference. An approximate placement of the SSB based at least partly on carbon isotope chemostratigraphy thus can help to systematize SSB placement and avoid too important miscorrelations related to inadequate biostratigraphic records (e.g., Figs. 7 and 12). Stratigraphic boundaries are not customarily based on chemostratigraphic records, but, based on present-day data, the use of mdpt(N3-P3) can be an auxiliary criterion to locate the SSB.

Obviously, the use of $\delta^{13}C$ records for correlation or auxiliary definition of the SSB should be preceded by an evaluation of stratigraphic hiatuses and facies changes in the sections under investigation. The $\delta^{13}C$ records of most SSB sections in South China are considered to be

stratigraphically continuous, including Chaohu (Tong et al., 2007), Jiarong (Chen-YL et al., 2015), and Shitouzhai (Zhang et al., 2015). In contrast, stratigraphic incompleteness is indicated by the $\delta^{13}C$ records of the SSB sections at for instance Zal, Abadeh, and Amol in Iran, where abrupt $\delta^{13}C$ shifts are associated with faults or regressive systems tracts (Horacek et al., 2007b) and at Kamura, Japan, which is characterized by a major biostratigraphically defined gap in the Spathian (Zhang et al., 2017). Moreover, the stratigraphic completeness of the Smith Creek section through the SSB transition interval is uncertain owing to a large (to ~4 ‰), abrupt positive shift in $\delta^{13}C_{carb}$ and a concurrent facies change from siliciclastic to carbonate sediments (Grasby et al., 2013). So far, no obvious stratigraphic hiatus was reported at the SSB transition in the western Tethys or localities in the Boreal and eastern Panthalassic realms, but it remains a possibility in a context of global regression.

5.4. Placement of the Smithian/Spathian boundary in earlier studies

To date, biostratigraphic studies of the SSB are especially well documented in the eastern (e.g., South China) and southern (e.g., Salt Range) Tethys. These provide a first basis for investigation of the relationships between ammonoid zonations, conodont zonations, and carbon isotope excursions through the SSB transition. Such relationships could also be used in boundary definitions especially in localities where biostratigraphic data are lacking.

Despite these existing high-resolution biostratigraphic studies, placement of the SSB is still inconsistent in some sections within these areas. For example, in the An Chau Basin, Komatsu et al. (2016) placed the SSB at the base of the *Tirolites* cf. *cassianus* beds (see discussion of biostratigraphic data in Section 3.8.1), which are stratigraphically above the P3 carbon-isotope maximum. This placement is inconsistent with other sections worldwide, in which the SSB lies close to the mdpt(N3-P3) or below P3 (Fig. 11). The underlying problem here appears to have been the potentially doubtful attribution by Komatsu et al. (2016) of some poorly preserved ammonoid specimens to *Xenoceltites variocostatus*, which is usually considered as a marker for the late Smithian (see Section 3.8.1). Thus, more work is needed at this section to confirm the placement of the SSB, which probably is actually located between mdpt(N3-P3) and P3.

In the western Tethys, limited biostratigraphic data resulted in the SSB being identified mainly on the basis of carbon-isotope correlations, but (as noted in Section 5.3) there has been no consistent placement of the SSB within the $\delta^{13}C$ chemostratigraphic framework of the Early Triassic (Fig. 12), creating the potential for global miscorrelations and misinterpretations of paleoceanographic signals. In the southern Tethys, the SSB was placed close to P3 at Salt and Surghar Ranges (Hermann et al., 2012), and Tulong (Brühwiler et al., 2009) and mdpt(N3-P3) falls in characteristic late Smithian ammonoid assemblages (Fig. 12). Compared to mdpt(N3-P3), this SSB placement is thus slightly higher stratigraphically than that favored for the eastern Tethys, but well highlight the differential local environmental and/or diagenetic conditions influencing the $\delta^{13}C$ signal.

The biostratigraphy of the SSB transition in the Boreal realm is more poorly constrained owing to e.g., scarce fossil occurrences. Thus, carbon isotope excursions can be used to constrain the location of the SSB. We suggest placement of the SSB at mdpt(N3-P3), which is at or just above the top of the *Anawasatchites tardus* beds (or GXP assemblage if found) and

just below P3. In the Mineral Mountains, western USA, the SSB was placed at the top of the *Xenoceltitidae* 'gen. indet.' A. beds and fits rather well with the mdpt(N3-P3).

5.5. Relationship to the Smithian Thermal Maximum

The lack of a formal definition for the SSB has resulted in inconsistent placements of the SSB in different published studies, with differences sometimes as large as one or two full ammonoid zones. This is particularly problematic for studies attempting to evaluate environmental or oceanographic changes accompanying the Smithian-Spathian transition, because incorrect placement of the SSB can result in incorrect conclusions concerning the timing and causes of such changes.

These problems are illustrated by the Sun et al. (2012) study, which proposed an Early Triassic tropical sea surface temperature (SST) profile based on conodont oxygen-isotope data measured in multiple sections (Jiarong, Jinya, Guandao, Zuodeng, and Bianyang) in the Nanpanjiang Basin of southwestern China. This study inferred a thermal maximum extending from the late Smithian to the earliest Spathian (i.e., spanning the SSB), followed by a cooling event later in the early Spathian (Fig. 16A). They concluded that the late Smithian extinction and associated oceanographic changes were the result of hyperthermy, although this conclusion is likely erroneous (Goudemand et al., 2013, 2018). A fundamental problem in the Sun et al. (2012) study is that the SSB, which was putatively based on the first occurrence of *Nv. pingdingshanensis*, is positioned close to the N3 carbon-isotope minimum. For example, at Jiarong, Sun et al. (2012) placed the SSB close to N3, corresponding to a $\delta^{13}C_{carb}$ value of < -1 ‰, which is lower than the ~0 ‰ for the SSB reported by Chen-YL et al. (2013). Furthermore, the placement of the SSB based on the FAD of *Nv. pingdingshanensis* in Sun et al. (2012) is stratigraphically lower than that of Chen-YL et al. (2013) based on the same criterion, and also lower than that of Chen-YL et al. (2015) (see Section 3.7). At Zuodeng, Sun et al. (2012) placed the SSB at a $\delta^{13}C_{carb}$ value of ~0 ‰, which is lower than the +2 ‰ for the SSB reported by Tong et al. (2007). The same inconsistency also occurs at Jinya, where $\delta^{13}C_{carb}$ at the SSB is ~ −2 ‰ in Sun et al. (2012) but ~+2 ‰ in Galfetti et al. (2007c). Thus, systematic misplacement of the SSB (e.g., based on the first occurrence of *Nv. pingdingshanensis*) in multiple sections is one of the underlying causes of the erroneous conclusion concerning the timing of the Smithian Thermal Maximum in Sun et al. (2012).

Inconsistent placement of the SSB has thus resulted in different interpretations of Smithian-Spathian transition events (see Sun et al., 2012, 2013; Romano et al., 2013; Goudemand et al., 2013, 2018). Goudemand et al. (2013) recompiled a subset of $\delta^{13}C$ and $\delta^{18}O_{conodont}$ data, originally from Sun et al. (2012), based on ammonoid biostratigraphic control (Fig. 16B) constraining the SSB to between the *Anasibirites* and *Tirolitid* beds, corresponding to the *Nv. pingdingshanensis* Zone (i.e., between the first occurrences of *Nv. pingdingshanensis* and *Ic. collinsoni*). Goudemand (2014b) updated the calibration between $\delta^{13}C$ and $\delta^{18}O_{conodont}$ based on conodont zonations and absolute ages, and his placement of the SSB is close to the mdpt(N3-P3), below P3 (Fig. 13; see also Goudemand et al., 2018). Based on his work and the stratigraphic framework of the present study, the Smithian Thermal Maximum (herein named) peaked in the middle Smithian, around the N3 carbon-isotope minimum, rather than close to the SSB as shown in Sun et al. (2012) (see discussion in Goudemand et al. 2013, 2018 and

Goudemand, 2014b). The SSB transition proper was characterized by a cooling trend rather than by hyperwarming (Fig. 16).

Regardless of which fossil group is used in definition of the SSB, the N3-to-P3 positive $\delta^{13}C$ excursion is a good proxy for placement of the SSB. Therefore, $\delta^{13}C$ chemostratigraphy can play an important role in the formal definition of the SSB. Re-evaluation of the timing of onset of the Smithian Thermal Maximum will help our understanding of the environmental and biotic changes across the SSB and more broadly during the Early Triassic recovery.

6. Conclusions

This contribution reviewed the history and present status of global ammonoid and conodont biostratigraphic research on the Smithian and Spathian substages, coeval chemostratigraphic records of $\delta^{13}C$, $\Delta\delta^{13}C_{DIC}$, $\delta^{34}S_{CAS}$ and $^{87}Sr/^{86}Sr$, and their relationships to climate change during the Smithian-Spathian transition.

The Smithian/Spathian boundary (SSB) potentially can be defined on the basis of ammonoid or conodont data. Ammonoid faunas show a pronounced transition from late Smithian forms belonging to e.g., the genera *Wasatchites*, *Anasibirites*, *Glyptophiceras* and *Xenoceltites* to early Spathian forms belonging to e.g., *Bajarunia*, *Tirolites* and *Columbites*. The future definition of the SSB should be fuided by existing ammonoid-based biostratigraphic constraints. Specifically, it should fall between strata containing late Smithian forms belonging to the AW and GXP assemblages and strata containing early Spathian forms belonging to the genera *Bajarunia, Doricranites*, and/or *Tirolites.* Conodont faunas change across this divide from late Smithian forms such as *Scythogondolella milleri, Borinella buurensis* and *Foliella gardenae* to early Spathian forms such as '*Triassospathodus*' *hungaricus*, *Neogondolella* aff. *sweeti*, *Icriospathodus* spp., and *Novispathodus brevissimus*. The first appearance of *Novispathodus pingdingshanensis*, which has been proposed as a marker for the SSB, occurs in several places with both ammonoids (*Xenoceltites*) and conodonts (*Sc. milleri*) regarded as traditionally of late Smithian age. The ranges of these various taxa, as well as that of other conodonts with potential for definition of the SSB, requires more work.

Carbonate carbon-isotopes ($\delta^{13}C_{carb}$) change rapidly through the Smithian-Spathian transition interval, from the middle Smithian N3 minimum to the early Spathian P3 maximum, providing potential isotopic markers that could be linked to a biostratigraphically defined SSB. In particular, the isotopic midpoint of the N3-to-P3 shift (herein termed 'mdpt(N3-P3)') is generally close to the level of the SSB based on biostratigraphic constraints and may serve as an auxiliary definition of the boundary. A test of the utility of the mdpt(N3-P3) marker as a proxy for the SSB based on biostratigraphically well-studied SSB sections shows that mdpt(N3-P3) is generally within 2 m of the accepted position of the SSB, especially for sections in the Tethys region. It should be noted that the actual $\delta^{13}C$ value of mdpt(N3-P3) is site-specific, depending on water-depth and other local environmental factors.

Stratigraphic relationships among ammonoids, conodonts, and carbon isotope excursions show that the Smithian Thermal Maximum (herein named) was approximately synchronous with the N3 carbon-isotope minimum and, thus, of middle Smithian age. The Smithian/Spathian boundary proper coincided with a pronounced relative cooling event.

Acknowledgments

This study was supported by NSFC grants (No. 41673011, 41473006, 41272025 to LSZ, 41803011 to LZ and 41821001 to XSC), by Natural Science Foundation of Hubei Province (No. 2018CFB263 to LZ), by China Postdoctoral Science Foundation (2018M642945 to ZYL) and by the Fundamental Research Funds for the Central Universities, China University of Geosciences-Wuhan (No. CUGQYZX1728 and CUGCJ1815 to LSZ, CUG170683 to LZ). This paper was started when the senior author was a visiting scholar at the University of Cincinnati during 2015-2016 with support from the China Scholarship Council (No. 201506410031). This work is also a contribution to the ANR project AFTER (ANR-13-JS06-0001-01; to A.B.) and was also supported by the French "Investissements d'Avenir" program, project ISITE-BFC (ANR-15-IDEX-03; to A.B.).

References

Algeo, T.J., Twitchett, R.J., 2010. Anomalous Early Triassic sediment fluxes due to elevated weathering rates and their biological consequences. Geology 38, 1023-1026.

Algeo, T.J., Hinnov, L., Moser, J., Maynard, J.B., Elswick, E., Kuwahara, K., Sano, H., 2010. Changes in productivity and redox conditions in the Panthalassic Ocean during the latest Permian. Geology 38, 187-190.

Algeo, T.J., Chen, Z.Q., Fraiser, M.L., Twitchett, R.J., 2011. Terrestrial-marine teleconnections in the collapse and rebuilding of Early Triassic marine ecosystems. Palaeogeography, Palaeoclimatology, Palaeoecology 308, 1-11.

Algeo, T.J., Luo, G.M., Song, H.Y., Lyons, T.W., Canfield, D.E., 2015. Reconstruction of secular variation in seawater sulfate concentrations. Biogeosciences 12(7), 2131-2151.

Aljinović, D., Kolar-Jurkovšek, T., Jurkovšek, B., 2006. The Lower Triassic shallow marine succession in Gorski Kotar region (External Dinarides, Croatia): lithofacies and conodont dating. Rivista Italiana di Paleontologia e Stratigrafia 112, 35-53.

Aljinović, D., Kolar-Jurkovšek, T., Jurkovšek, B., Hrvatović, H., 2011. Conodont dating of the Lower Triassic sedimentary rocks in the external Dinarides (Croatia and Bosnia and Herzegovina). Rivista Italiana di Paleontologia e Stratigrafia 117, 135-148.

Aljinović, D., Horacek, M., Krystyn, L., Richoz, S., Kolar-Jurkovšek, T., Smirčić, D., Jurkovšek B., 2018. Western Tethyan epeiric ramp setting in Early Triassic – an example from the central Dinarides (Croatia). Journal of Earth Sciences (China University of Geosciences-Wuhan) 29, 806-823.

Assereto, R., Bosellini, A., Fantini Sestini, N., Sweet, W.C., 1973. The Permian–Triassic boundary in the southern Alps (Italy). In: Logan, A., Hill, L.V. (Eds.), Permian and Triassic Systems and Their Mutual Boundary. Canadian Society of Petroleum Geologists Memoir 2, pp. 176-199.

Atudorei, V., 1999. Constraints on the Upper Permian to Upper Triassic marine carbon isotope curve. Case studies from the Tethys. Ph.D., University of Lausanne, Switzerland, 161 pp.

Bagherpour, B., Bucher, H., Baud, A., Brosse, M., Venneman, T., Martini, R., Kuang, G., 2017. Onset, development, and cessation of basal Early Triassic microbialites (BETM) in the Nanpanjiang pull-apart Basin, South China Block. Gondwana Research 44, 178-204.

Balini, M., Gavrilova, V.A., Nicora, A., 2000. Biostratigraphical revision of the classic Lower Triassic Dolnapa section (Mangyshlak, West Kazakhstan). Zentralblatt für Geologie und Paläontologie, Teil I 11-12, 1441-1462.

Balini, M., Nicora, A., Berra, F., Garzanti, E., Levera, M., Mattei, M., Muttoni, G., Zanchi, A., Bollati, I., Larghi, C., Zanchetta, S., Salamati., R., Mossavvari, F., 2009. The Triassic stratigraphic succession of Nakhlak (Central Iran), a record from an active margin. In: Brunet, M.-F., Wilmsen, M., Granath, J.W. (Eds.), South Caspian to Central Iran Basins, Geological Society of London Special Publication 312, pp. 287-321.

Balini, M., Lucas, S.G., Jenks, J.F., Spielmann, J.A., 2010. Triassic ammonoid biostratigraphy: an overview. In: Lucas, S.G. (Ed.), The Triassic Timescale, Geological Society of London Special Publication 334, pp. 221-262.

Baresel, B., Bucher, H., Brosse, M., Cordey, F., Guodun, K., Schaltegger, U., 2017. Precise age for the Permian–Triassic boundary in South China from high-precision U-Pb geochronology and Bayesian age–depth modeling. Solid Earth 8(2), 361-378.

Baud, A., Magaritz, M., Holser, W.T., 1989. Permian–Triassic of the Tethys: carbon isotope studies. Geologische Rundschau 78, 649-677.

Baud, A., Atudorei, V., Sharp, Z.D., 1996. Late Permian and Early Triassic evolution of the Northern Indian margin: carbon isotope and sequence stratigraphy. Geodinamica Acta 9, 57-77.

Bernasconi, S.M., Meier, I., Wohlwend, S., Brack, P., Hochuli, P.A., Hansruedi Bläsi, Wortmann, U.G., Ramseyer, K., 2017. An evaporite-based high-resolution sulfur isotope record of late Permian and Triassic seawater sulfate. Geochimica et Cosmochimica Acta, 204, 331-349.

Bhatt, D.K., Joshi, V.K., Arora, R.K., 1999. Conodont biostratigraphy of the Lower Triassic in Spiti Himalaya, India. Journal of the Geological Society of India 54, 153-167.

Bottjer, D.J., Clapham, M.E., Fraiser, M.L., Powers, C.M., 2008. Understanding mechanisms for the end-Permian mass extinction and the protracted Early Triassic aftermath and recovery. GSA Today 18, 4-10.

Brayard, A., Bucher, H., 2008. Smithian (Early Triassic) ammonoid faunas from northwestern Guangxi (South China): taxonomy and biochronology. Fossils and Strata 55, 179 pp.

Brayard, A., Bucher, H., 2015. Permian-Triassic extinctions and rediversifications. In: Klug, C., Korn, D., De Baets, K., Kruta, I., Mapes, R.H. (Eds.), Ammonoid Paleobiology: From Macroevolution to Paleogeography. Springer, Dordrecht, pp. 465-473.

Brayard, A., Bucher, H., Escarguel, G., Fluteau, F., Bourquin, S., Galfetti, T., 2006. The Early Triassic ammonoid recovery: Paleoclimatic significance of diversity gradients. Palaeogeography, Palaeoclimatology, Palaeoecology 239, 374-395.

Brayard, A., Escarguel, G., Bucher, H., 2007a. The biogeography of Early Triassic ammonoid faunas: clusters, gradients, and networks. Geobios 40, 749-765.

Brayard, A., Bucher, H., Brühwiler, T., Galfetti, T., Goudemand, N., Guodun, K., Escarguel, G., Jenks, J., 2007b. *Proharpoceras* Chao: a new ammonoid lineage surviving the end-Permian mass extinction. Lethaia 40, 175-181.

Brayard, A., Escarguel, G., Bucher, H., Brühwiler, T., 2009a. Smithian and Spathian (Early Triassic) ammonoid assemblages from terranes: Paleoceanographic and paleogeographic implications. Journal of Asian Earth Sciences 36, 420-433.

Brayard, A., Escarguel, G., Bucher, H., Monnet, C., Brüehwiler, T., Goudemand, N., Galfetti, T., Guex, J., 2009b. Good genes and good luck: ammonoid diversity and the end-Permian mass extinction. Science 325, 1118-1121.

Brayard, A., Brüehwiler, T., Bucher, H., Jenks, J., 2009c. *Guodunites*, a low-palaeolatitude and trans-Panthalassic Smithian (Early Triassic) ammonoid genus. Palaeontology 52, 471-481.

Brayard, A., Vennin, E., Olivier, N., Bylund, K.G., Jenks, J., Stephen, D.A., Bucher, H., Hofmann, R., Goudemand, N., Escarguel, G., 2011. Transient metazoan reefs in the aftermath of the end-Permian mass extinction. Nature Geoscience 4, 693-697.

Brayard, A., Bylund, K.G., Jenks, J.F., Stephen, D.A., Olivier, N., Escarguel, G., Fara, E., Vennin, E., 2013. Smithian ammonoid faunas from Utah: implications for Early Triassic biostratigraphy, correlation and basinal paleogeography. Swiss Journal of Palaeontology 132, 141-219.

Brayard, A., Krumenacker, L. J., Botting, J. P., Jenks, J. F., Bylund, K. G., Fara, E., Vennin, E., Olivier, N., Goudemand, N., Saucède, T., Charbonnier, S., Romano, C., Doguzhaeva, L., Thuy, B., Hautmann, M., Stephen, D.A., Thomazo, C., Escarguel, G., 2017. Unexpected Early Triassic marine ecosystem and the rise of the Modern evolutionary fauna. Science Advances, 3 (e1602159), 1-11.

Brayard, A., Jenks, J.F., Bylund, K.G., and the Paris Biota team, 2019. Ammonoids and nautiloids from the earliest Spathian Paris Biota and other early Spathian localities in southeastern Idaho. Geobios, in press.

Brosse, M., Brayard, A., Fara, E., Neige, P., 2013. Ammonoid recovery after the Permian–Triassic mass extinction: a re-exploration of morphological and phylogenetic diversity patterns. Journal of the Geological Society of London 170, 225-236.

Brühwiler, T., Bucher, H., Goudemand, N., Brayard, A., 2007. Smithian (Early Triassic) ammonoid successions of the Tethys: new preliminary results from Tibet, India, Pakistan and Oman. The Global Triassic Bulletin 41, 25-26.

Brühwiler, T., Goudemand, N., Galfetti, T., Bucher, H., Baud, A., Ware, D., Hermann, E., Hochuli, P.A., Martini, R., 2009. The Lower Triassic sedimentary and carbon isotope records from Tulong (South Tibet) and their significance for Tethyan palaeoceanography. Sedimentary Geology 222, 314-332.

Brühwiler, T., Ware, D., Bucher, H., Krystyn, L., Goudemand, N., 2010a. New early Triassic ammonoid faunas from the Dienerian/Smithian boundary beds at the Induan/Olenekian GSSP candidate at Mud (Spiti, Northern India). Journal of Asian Earth Sciences 39, 724-739.

Brühwiler, T., Bucher, H., Goudemand, N., 2010b. Smithian (Early Triassic) ammonoids from Tulong, South Tibet. Geobios 43, 403-431.

Brühwiler, T., Bucher, H., Brayard, A., Goudemand, N., 2010c. High-resolution biochronology and diversity dynamics of the Early Triassic ammonoid recovery: the Smithian faunas of the Northern Indian Margin. Palaeogeography, Palaeoclimatology, Palaeoecology 297, 491-501.

Brühwiler, T., Bucher, H., Roohi, G., Yaseen, A., Rehman, K., 2011. A new early Smithian ammonoid fauna from the Salt Range (Pakistan). Swiss Journal of Palaeontology 130, 187-201.

Brühwiler, T., Bucher, H., Ware, D., Schneebeli-Hermann, E., Hochuli, P.A., Roohi, G.,

Rehman, K., Yaseen, A., 2012a. Smithian (Early Triassic) ammonoids from the Salt Range, Pakistan. Special Papers in Palaeontology 88, 1-114.

Brühwiler, T., Bucher, H., Ware, D., Krystyn, L., 2012b. Middle and late Smithian (Early Triassic) ammonoids from Spiti, India. Special Papers in Palaeontology 88, 115-174.

Brühwiler, T., Bucher, H., Goudemand, N., Galfetti, T., 2012c. Smithian (Early Triassic) ammonoid faunas from Exotic Blocks from Oman: taxonomy and biochronology. Palaeontographica Abteilung A 296, 3-107.

Buchan, S.H., Challinor, A., Harland, W.B., Parker, J.R., 1965. The Triassic stratigraphy of Svalbard. Norsk Polarinstitutt Skrifter 135, 91 pp.

Burgess, S.D., Bowring, S., Shen, S.Z., 2014. High-precision timeline for Earth's most severe extinction. Proceedings of the National Academy of Sciences (U.S.A.) 111, 3316-3321.

Caravaca, G., Thomazo, C., Vennin, E., Olivier, N., Cocquerez, T., Escarguel, G., Fara, E., Jenks, J.F., Bylund, K.G., Stephen, D.A., Brayard, A., 2017. Early Triassic fluctuations of the global carbon cycle: New evidence from paired carbon isotopes in the western USA basin. Global and Planetary Change 154, 10-22.

Caravaca, G., Brayard, A., Vennin, E., Guiraud, M., Le Pourhiet, L., Grosjean, A.S., Thomazo, C., Olivier, N., Fara, E., Escarguel, G., Bylund, K.G., 2018. Controlling factors for differential subsidence in the Sonoma Foreland Basin (Early Triassic, western USA). Geological Magazine 155(6), 1305-1329.

Cavin, L., Gradinaru, E., 2014. *Dobrogeria aegyssensis*, a new early Spathian (Early Triassic) coelacanth from North Dobrogea (Romania). Acta Geologica Polonica 64, 161-187.

Chen, J.B., Algeo, T.J., Zhao, L.S., Chen, Z.Q., Cao, L., Zhang, L., Li, Y., 2015. Diagenetic uptake of rare earth elements by bioapatite, with an example from Lower Triassic conodonts of South China. Earth-Science Reviews 149, 181-202.

Chen, Y.L., Twitchett, R.J., Jiang, H.S., Richoz, S., Lai, X.L., Yan, C.B., Sun, Y.D., Liu, X.D., Wang, L., 2013. Size variation of conodonts during the Smithian-Spathian (Early Triassic) global warming event. Geology 41, 823-826.

Chen, Y.L., Jiang, H.S., Lai, X.L., Yan, C.B., Richoz, S., Liu, X.D., Wang, L.N., 2015. Early Triassic conodonts of Jiarong, Nanpanjiang Basin, southern Guizhou Province, South China. Journal of Asian Earth Sciences 105, 104-121.

Chen, Y.L., Kolar-Jurkovšek, T., Jurkovšek, B., Aljinović, D., Richoz, S., 2016. Early Triassic conodonts and carbonate carbon isotope record of the Idrija-Žiri area, Slovenia. Palaeogeography Palaeoclimatology Palaeoecology 444, 84-100.

Chen, Z.Q., Benton, M.J., 2012. The timing and pattern of biotic recovery following the end-Permian mass extinction. Nature Geoscience 5, 375-383.

Chen, Z.Q., Tong, J.N., Liao, Z.T., Chen, J., 2010. Structural changes of marine communities over the Permian–Triassic transition: ecologically assessing the end-Permian mass extinction and its aftermath. Global and Planetary Change 73, 123-140.

Chen, Z.Q., Tong, J.N., Fraiser, M.L., 2011. Trace fossil evidence for restoration of marine ecosystems following the end-Permian mass extinction in the Lower Yangtze region, South China. Palaeogeography, Palaeoclimatology, Palaeoecology 299, 449-474.

Clark, D.L., Hatleberg, E.W., 1983. Paleoenvironmental factors and the distribution of conodonts in the Lower Triassic of Svalbard and Nepal. Fossils and Strata 15, 171-175.

Clarkson, M., Kasemann, S., Wood, R., Lenton, T., Daines, S., Richoz, S., Ohnemueller, F.,

Meixner, A., Poulton, S., Tipper, E., 2015. Ocean acidification and the Permo-Triassic mass extinction. Science 348, 229-232.

Clarkson, M.O., Richoz, S., Wood, R.A., Maurer, F., Krystyn, L., Mcgurty, D.J., Astratti, D., 2013. A new high-resolution $\delta^{13}C$ record for the Early Triassic: Insights from the Arabian Platform. Gondwana Research 24, 233-242.

Clarkson, M.O., Wood, R.A., Poulton, S.W., Richoz, S., Newton, R.J., Kasemann, S.A., Bowyer, F., Krystyn, L., 2016. Dynamic anoxic ferruginous conditions during the end-Permian mass extinction and recovery. Nature Communications 7, 12236.

Crasquin, S., Sudar, M.N., Jovanović, D., Kolarjurkovšek T., 2010. Upper Permian ostracode assemblage from the Jadar Block (Vardar Zone, NW Serbia). Geološki anali Balkanskoga poluostrva 71, 23-35.

Đacović, M., 2017. New Early Triassic (Smithian) ammonoids from Gornji Brčeli (southern Montenegro). Austrian Journal of Earth Sciences 110(2), 9 pp.

Dagis, A.A., Korčinskaja, M.V., 1989. Triasovye konodonty Sval'barda. (Triassic conodonts of Svalbard.) In: Dagis, A.S., Dubatolov, V.N. (Eds.), Verhnij Paleozoj i Trias Sibiri. (Upper Paleozoic and Triassic of Siberia.) Trudy Akademija Nauk SSSR, Sibirskoe otdelenie Instituta Geologii i Geofiziki 732, 109-121.

Dagys, A.S., 1988. Major features of the geographic differentiation of Triassic ammonoids. In: Wiedmann, J., Kullmann, J. (Eds.), Cephalopods — Present and Past. Schweizerbart'sche Verlagsbuchhandlung, Stuttgart, pp. 341-349.

Dagys, A.S., 1997. A new Late Olenekian (Triassic) ammonoid of low paleolatitude affinity from Arctic Asia (Eastern Taimyr). Paläontologische Zeitschrift 71, 217–220.

Dagys, A.S., Weitschat, W., 1993. Correlation of the Boreal Triassic: Mitteilungen Geologisch-Paläontologisches Institut Universität Hamburg 75, 249-256.

Dutton, A., Carlson, A.E., Long, A.J., Milne, G.A., Clark, P.U., DeConto, R., Horton, B.P., Rahmstorf, S., Raymo, M.E., 2015. Sea-level rise due to polar ice-sheet mass loss during past warm periods. Science 349(6244), aaa4019.

Ehiro, M., 2016. Additional Early Triassic (late Olenekian) ammonoids from the Osawa Formation at Yamaya, Motoyoshi area, South Kitakami Belt, Northeast Japan. Paleontological Research 20(1), 1-6.

Ehiro, M., Sasaki, O., Kano, H., 2016. Ammonoid fauna of the upper Olenekian Osawa Formation in the Utatsu area, South Kitakami Belt, Northeast Japan. Paleontological Research 20(2), 90-104.

Embry, A.F., 1986. Stratigraphic subdivision of the Blind Fjord and Bjorne formations (Lower Triassic), Sverdrup Basin, Arctic Islands. Current Research, Part B, Geological Survey of Canada, Paper 86-1B, 329-340.

Embry, A.F., 1991. Mesozoic history of the Arctic Islands. In Trettin, H. (Ed.), Geology of the Innuitian Orogen and Arctic Platform of Canada and Greenland. Geology of Canada, vol. 3, pp. 369-433.

Embry, A.F., 1997. Global sequence boundaries of the Triassic and their identification in the Western Canada Sedimentary Basin. Bulletin of Canadian Petroleum Geology 45(4), 415-433.

Enos, P., Lehrmann, D.J., Wei, J.Y., Yu, Y.Y., Xiao, J.F., Chaikin, D.H., Minzoni, M., Berry, A.K., Montgomery, P., 2006. Triassic Evolution of the Yangtze Platform in Guizhou

Province, People's Republic of China, Geological Society of America Special Paper 417, 105 pp.

Erwin, D.H., 2001. Lessons from the past: biotic recoveries from mass extinctions. Proceedings of the National Academy of Sciences (U.S.A.) 98, 5399-5403.

Feng, Q.L., Algeo, T.J., 2014. Evolution of oceanic redox conditions during the Permo-Triassic transition: Evidence from deepwater radiolarian facies. Earth-Science Reviews 137, 34-51.

Galfetti, T., Hochuli, P.A., Brayard, A., Bucher, H., Weissert, H., Vigran, J.O., 2007a. Smithian-Spathian boundary event: Evidence for global climatic change in the wake of the end-Permian biotic crisis. Geology 35, 291-294.

Galfetti, T., Bucher, H., Ovtcharova, M., Schaltegger, U., Brayard, A., Brühwiler, T., Goudemand, N., Weissert, H., Hochuli, P.A., Cordey, F., 2007b. Timing of the Early Triassic carbon cycle perturbations inferred from new U-Pb ages and ammonoid biochronozones. Earth and Planetary Science Letters 258, 593-604.

Galfetti, T., Bucher, H., Brayard, A., Hochuli, P.A., Weissert, H., Guodun, K., Atudorei, V., Guex, J., 2007c. Late Early Triassic climate change: insights from carbonate carbon isotopes, sedimentary evolution and ammonoid paleobiogeography. Palaeogeography, Palaeoclimatology, Palaeoecology 243, 394-411.

Galfetti, T., Bucher, H., Martini, R., Hochuli, P.A., Weissert, H., Crasquin-Soleau, S., Brayard, A., Goudemand, N., Brühwiler, T., Goudun, K., 2008. Evolution of Early Triassic outer platform paleoenvironments in the Nanpanjiang Basin (South China) and their significance for the biotic recovery. Sedimentary Geology 204, 36–60.

Gallet, Y., Krystyn, L., Besse, J., Saidi, A., Ricou, L.E., 2000. New constraints on the Upper Permian and Lower Triassic geomagnetic polarity timescale from the Abadeh section (central Iran). Journal of Geophysical Research: Solid Earth B105, 2805-2815.

Gibson, D.W., 1971. Triassic stratigraphy of the Sikanni Chief River-Pine Pass region. Rocky Mountain Foothills, northeastern British Columbia. Geological Survey of Canada, Paper 70-31, 105 pp.

Golubić, V., 1996. Biostratigraphic distribution of Upper Scythian (Lower Triassic) ammonites in the river Zrmanja Area in northern Dalmatia, Croatia. Natura Croatica 5, 165-176.

Golubić, V., 2000. Biostratigraphic distribution of Upper Scythian ammonites in the referent area of Muć Gornji village, Croatia. Natura Croatica 9, 237–274.

Goudemand, N., 2014a. Note on the conodonts from the Induan-Olenekian Boundary. Albertiana 42, 49-51.

Goudemand, N., 2014b. Time calibrated Early Triassic $\delta^{13}C_{carb}$, $\delta^{18}O_{apatite}$ and SST curves from South China: an update. Albertiana 42, 41-48.

Goudemand, N., Orchard, M.J., Guobiao, L., Galfetti, T., Bucher, H., 2006. A new early Spathian (Early Triassic) conodont succession from North America. Abstracts and Proceedings, The Boreal Triassic, August 16-20, Longyearbyen, Svalbard, Norway.

Goudemand, N., Orchard, M.J., Urdy, S., Brühwiler, T., Brayard, A., Bucher, H., 2012. Early Triassic conodont clusters from South China: revision of the architecture of the 15 element apparatuses of the superfamily Gondolelloidea. Palaeontology 55, 1021-1034.

Goudemand, N., Romano, C., Brayard, A., Hochuli, P.A., Bucher, H. 2013. Comment on "Lethally hot temperatures during the Early Triassic greenhouse". Science 339, 1033.

Goudemand, N., Romano, C., Leu, M., Bucher, H., Trotter, J., Williams, I., 2018. Dynamic interplay between climate and marine biodiversity upheavals during the Early Triassic Smithian-Spathian biotic crisis. Earth-Sciences Reviews, this volume. https://doi.org/10.1016/j.earscirev.2019.01.013

Grasby, S.E., Beauchamp, B., Embry, A., Sanei, H., 2013. Recurrent Early Triassic ocean anoxia. Geology 41, 175-178.

Grasby, S.E., Beauchamp, B., Bond, D.P., Wignall, P.B., Sanei, H., 2016. Mercury anomalies associated with three extinction events (Capitanian crisis, latest Permian extinction and the Smithian/Spathian extinction) in NW Pangea. Geological Magazine 153, 285-297.

Grice, K., Cao, C., Love, G.D., Böttcher, M.E., Twitchett, R.J., Grosjean, E., Summons, R.E., Turgeon, S.C., Dunning, W., Jin, Y., 2005. Photic zone euxinia during the Permian-Triassic superanoxic event. Science 307, 706-709.

Groves, J.R., Altiner, D., Rettori, R., 2005. Extinction, survival, and recovery of Langenide foraminifers in the Permian-Triassic boundary interval, Central Taurides, Turkey. Journal of Paleontology 79, 1-38.

Guex, J., 1978. Le Trias inférieur des Salt Ranges, Pakistan: problèmes biochronologiques. Eclogae Geologicae Helvetiae 71, 105-141.

Guex, J., Hungerbühler, A., Jenks, J.F., Taylor, D.G., Bucher, H., 2005a. Dix-huit nouveaux genres d'ammonites du Spathien (Trias inférieur) de l'ouest américain (Idaho, Nevada, Utah et Californie): Note préliminaire. Bulletin de Géologie de Lausanne 362, 32 pp.

Guex, J., Hungerbühler, A., Jenks, J.F., Taylor, D.G., Bucher, H., 2005b. Dix-neuf nouvelles espèces d'ammonites du Spathien (Trias inférieur) de l'ouest américain (Idaho, Nevada, Utah et Californie): Note préliminaire. Bulletin de Géologie de Lausanne 363, 25 pp.

Guex, J., Hungerbühler, A., Jenks, J.F., O'Dogherty, L., Atudorei, V., Taylor, D.G., Bucher, H., Bartolini, A., 2010. Spathian (Lower Triassic) ammonoids from western USA (Idaho, California, Utah and Nevada). Mémoirs de Géologie (Lausanne) 49, 92 pp.

Hatleberg, E.W., Clark, D.L., 1984. Lower Triassic conodonts and biofacies interpretations: Nepal and Svalbard. Geologica et Palaeontologica 18, 101-125.

Henderson, C.M., 1997. Uppermost Permian conodonts and the Permian-Triassic boundary in the Western Canada sedimentary basin. Bulletin of Canadian Petroleum Geology 45, 693-707.

Henderson, C.M., 2018. Permian conodont biostratigraphy. In: Lucas, S.G., Shen, S.Z. (Eds.), The Permian Timescale, Geological Society of London Special Publication 450, pp. 119-142.

Henderson, C.M., Mei, S., 2007. Geographical clines in Permian and lower Triassic gondolellids and its role in taxonomy. Palaeoworld 16, 190-201.

Henderson, C.M., Dunn, L., Fossenier, K., 2001. Pennsylvanian to Permian Belloy Formation and Lower Triassic Montney Formation of the Western Canada Sedimentary Basin: Sequence Biostratigraphy, Paleogeography and Tectonics. Rock the Foundation Convention, Canadian Society of Petroleum Geologists 113-1, 495-497.

Henderson, C.M. Golding, M.L., Orchard, M.J., 2018. Conodont sequence biostratigraphy of the Lower Triassic Montney Formation. Bulletin of Canadian Petroleum Geology 66, 1-16.

Hermann, E., Hochuli, P.A., Méhay, S., Bucher, H., Brühwiler, T., Ware, D., Hautmann, M.,

Roohi, G., Yaseen, A., 2011. Organic matter and palaeoenvironmental signals during the Early Triassic biotic recovery: The Salt Range and Surghar Range records. Sedimentary Geology 234, 19-41.

Hermann, E., Hochuli, P. A., Bucher, H., Roohi, G., 2012. Uppermost Permian to Middle Triassic palynology of the Salt Range and Surghar Range, Pakistan. Review of Palaeobotany and Palynology 169, 61-95.

Hinojosa, J.L., Brown, S.T., Chen, J., DePaolo, D.J., Paytan, A., Shen, S.Z., Payne, J.L., 2012. Evidence for end-Permian ocean acidification from calcium isotopes in biogenic apatite. Geology 40, 743-746.

Hips, K., Pelikan, P., 2002. Lower Triassic shallow marine succession in the Bükk Mountains, NE Hungary. Geologica Carpathica 53, 351-367.

Hochuli, P.A., Sanson-Barrera, A., Schneebeli-Hermann, E., Bucher, H., 2016. Severest crisis overlooked—Worst disruption of terrestrial environments postdates the Permian–Triassic mass extinction. Scientific Reports 6, 28372.

Horacek, M., Brandner, R., Abart, R., 2007a. Carbon isotope record of the P/T boundary and the Lower Triassic in the Southern Alps: evidence for rapid changes in storage of organic carbon. Palaeogeography, Palaeoclimatology, Palaeoecology 252, 347-354.

Horacek, M., Richoz, S., Brandner, R., Krystyn, L., Spötl, C., 2007b. Evidence for recurrent changes in Lower Triassic oceanic circulation of the Tethys: The $\delta^{13}C$ record from marine sections in Iran. Palaeogeography, Palaeoclimatology, Palaeoecology 252, 355-369.

Horacek, M., Wang, X., Grossman E.L., Richoz, S., Cao Z., 2007c. The carbon-isotope curve from the Chaohu section, China: different trends at the Induan –Olenekian Boundary or diagenesis? Albertiana 35, 41-45.

Horacek, M., Koike, T., Richoz, S., 2009. Lower Triassic $\delta^{13}C$ isotope curve from shallow-marine carbonates in Japan, Panthalassa realm: Confirmation of the Tethys $\delta^{13}C$ curve. Journal of Asian Earth Sciences 36, 481-490.

Horacek, M., Brandner, R., Richoz, S., Povoden-Karadeniz, E., 2010. Lower Triassic sulphur isotope curve of marine sulphates from the Dolomites, N-Italy. Palaeogeography, Palaeoclimatology, Palaeoecology 290, 65-70.

Hounslow, M.W., Peters, C., Mork, A., Weitschat, W., Vigran, J.O., 2008. Biomagnetostratigraphy of the Vikinghogda Formation, Svalbard (Arctic Norway), and the geomagnetic polarity timescale for the Lower Triassic. Geological Society of America Bulletin 120, 1305-1325.

Huang, Y.G., Chen, Z.Q., Wignall, P.B., Zhao, L.S., 2017. Latest Permian to Middle Triassic redox condition variations in ramp settings, South China: Pyrite framboid evidence. Geological Society of America Bulletin 129, 229-243.

Huchkriede, R., 1958. Die conodonten der mediterranen Trias und ihr stratigraphischer Wert. Paläontologische Zeitschrift 32, 141-175.

Jattiot, R., Bucher, H., Brayard, A., Monnet, C., Jenks, J.F., Hautmann, M., 2016. Revision of the genus *Anasibirites* Mojsisovics (Ammonoidea): an iconic and cosmopolitan taxon of the late Smithian (Early Triassic) extinction. Papers in Palaeontology 2, 155-188.

Jattiot, R., Bucher, H., Brayard, A., Brosse, M., Jenks, J.F., Bylund, K.G., 2017. Smithian ammonoid faunas from northeastern Nevada: implications for Early Triassic biostratigraphy and correlation within the western USA basin. Palaeontographica A 309,

89 pp.
Jattiot, R., Brayard, A., Bucher, H., Vennin, E., Caravaca, G., Jenks, J., Bylund, K.G., Escarguel G., 2018. Palaeobiogeographical distribution of Smithian (Early Triassic) ammonoid faunas within the western USA basin and its controlling parameters. Palaeontology, 61, 963-980..
Jenks, J.F., Brayard, A., 2018. Smithian (Early Triassic) ammonoids from Crittenden Springs, Elko County, Nevada: taxonomy, biostratigraphy and biogeography. New Mexico Museum of Natural History and Science Bulletin 78, 175 pp.
Jenks, J.F., Brayard, A., Brühwiler, T., Bucher, H., 2010. New Smithian (Early Triassic) ammonoids from Crittenden Springs, Elko County, Nevada: Implications for taxonomy, biostratigraphy and biogeography. New Mexico Museum of Natural History and Science Bulletin 48, 41 pp.
Jenks, J.F., Guex, J., Hungerbühler, A., Taylor, D.G., Bucher, H., 2013. Ammonoid biostratigraphy of the early Spathian Columbites parisianus zone (Early Triassic) at Bear Lake Hot Springs, Idaho. New Mexico Museum of Natural History and Science Bulletin 61, 268-283.
Jenks, J.F., Monnet, C., Balini, M., Brayard, A., Meier, M., 2015. Biostratigraphy of Triassic ammonoids. In: Klug, C., Korn, D., De Baets, K., Kruta, I., Mapes, R.H. (Eds.), Ammonoid Paleobiology: From Macroevolution to Paleogeography. Springer, Dordrecht, pp. 329-388.
Ji, W.T., Tong, J.N., Zhao, L.S., Zhou, S.Q., Chen, J., 2011. Lower–Middle Triassic conodont biostratigraphy of the Qingyan section, Guizhou Province, Southwest China. Palaeogeography, Palaeoclimatology, Palaeoecology 308, 213-223.
Kanmera, K., Nakazawa K., 1973. Permian–Triassic relationships and faunal changes in the eastern Tethys. In: Logan, A., Hills, L.V. (Eds.), The Permian and Triassic Systems and Their Mutual Boundary, Canadian Society of Petroleum Geologists Memoir 2, pp. 100-119.
Kiparisova, L.D., Popov, I.N., 1956. The separation of the Lower Triassic system into stratums. Doklady Akademii Nauk SSSR 109, 842-845.
Kiparisova, L.D., Popov, Y.N., 1961. On the subdivision of the Lower Triassic into two stages. Bull. Interdept. Stratigr. Comm., St. Petersburg 3, 24-37.
Kittl, E., 1903: Die Cephalopoden der oberen Werfener Schichten von Muć in Dalmatien. Abhandlungen der Kaiserlich-Königlichen Geologischen Reichsanstalt 20, 1-77.
Koike, T., 1979. Conodont biostratigraphy of Triassic Taho limestone in western Shikoku, SW Japan. In: Igo, H., Koike, T. (Eds.), Biostratigraphy of Permian and Triassic Conodonts and Holothurian Sclerites in Japan, Committee of Prof. M. Kanuma Retirement Ceremony, Tokyo, Japan, pp. 115-126.
Kolar-Jurkovšek, T., Jurkovšek, B., 2007. First record of *Hindeodus–Isarcicella* population in Lower Triassic of Slovenia. Palaeogeography Palaeoclimatology Palaeoecology 252, 72-81.
Kolar-Jurkovšek, T., Jurkovšek, B., 2015. Conodont zonation of Lower Triassic strata in Slovenia. Geologija 58, 155-174.
Kolar-Jurkovšek, T, Jurkovšek, B., Aljinović, D., 2011a. Conodont biostratigraphy and lithostratigraphy across the Permian–Triassic boundary at the Lukač section in western

Slovenia. Rivista Italiana di Paleontologia e Stratigrafia 117, 115-133.
Kolar-Jurkovšek, T, Jurkovšek, B., Aljinović, D., Nestell, P.G., 2011b. Stratigraphy of Upper Permian and Lower Triassic of the Žiri area (Slovenia). Geologija 54, 193-204.
Kolar-Jurkovšek, T, Vuks, V.J., Aljinović, D., Hautmann, M., Kaim, A., Jurkovšek, B., 2013. Olenekian (Early Triassic) fossil assemblage from eastern Julian Alps (Slovenia). Annales Societatis Geologorum Poloniae 83, 213-227.
Komatsu, T., Dang, T.H., 2007. Lower Triassic bivalve fossils from the Song Da and An Chau Basins, North Vietnam. Paleontological Research 11, 135-144.
Komatsu, T., Takashima, R., Shigeta, Y., Maekawa, T., Tran, H.D., Cong, T.D, Sakata, S., Dinh, H.D., Takahashi, O., 2016. Carbon isotopic excursions and detailed ammonoid and conodont biostratigraphies around Smithian-Spathian boundary in the Bac Thuy Formation, Vietnam. Palaeogeography, Palaeoclimatology, Palaeoecology 454, 65-74.
Kozur, H., 2003. Integrated ammonoid, conodont and radiolarian zonation of the Triassic. Hallesches Jahrbuch für Geowissenschaften 25, 49-79.
Kozur, H., Mostler, H., 1970. Neue Conodonten aus der Trias. Ber. Nat.-Med. (Ver. Innsbruck) 58, 429-464.
Krystyn, L., 1974. Die *Tirolites*-Fauna (Ammonoidea) der untertriassischen Werfener Schichten Europas und ihre stratigraphische Bedeutung. Oesterreichische Akademie der Wissenschaften, Mathematisch-Naturwissenschaftliche Klasse, Abteiling I 193, 29-50.
Krystyn, L., Balini, M., Nicora, A., 2004. Lower and Middle Triassic stage and substage boundaries in Spiti. Albertiana 30, 40-53.
Krystyn, L., Om, N.B., Devendra, K.B., 2005. Muth (Spiti, Indian Himalaya) a candidate Global Stratigraphic Section and Point (GSSP) for the base of the Olenekian Stage. Albertiana 33, 51-53.
Krystyn, L., Bhargava, O.N., Richoz, S., 2007a. A candidate GSSP for the base of the Olenekian Stage: Mud at Pin Valley; district Lahul & Spiti, Himachal Pradesh (Western Himalaya), India. Albertiana 35, 5-29.
Krystyn, L., Richoz, S., Bhargava, O.N., 2007b. The Induan-Olenekian Boundary (IOB) in Mud–an update of the candidate GSSP section M04. Albertiana 36, 33-45.
Kummel, B., 1973. Lower Triassic (Scythian) molluscs. In: Hallam, A. (Ed.), Atlas of Paleobiogeography. Elsevier, Amsterdam, pp. 225-233.
Kummel, B., Teichert, C., 1973. Stratigraphic boundary problems: Permian and Triassic of West Pakistan. Journal of Geology 81, 240-241.
Lau, K.V., Maher, K., Altiner, D., Kelley, B.M., Kump, L.R., Lehrmann, D.J., Silva-Tamayo, J.C., Weaver, K.L., Yu, M., Payne, J.L., 2016. Marine anoxia and delayed Earth system recovery after the end-Permian extinction. Proceedings of the National Academy of Sciences (U.S.A.) 113, 2360-2365.
Lehrmann, D.J., Ramezani, J., Bowring, S.A., Martin, M.W., Montgomery, P., Enos, P., Payne, J.L., Orchard, M.J., Wang, H.M., Wei, J.Y., 2006. Timing of recovery from the end-Permian extinction: Geochronologic and biostratigraphic constraints from south China. Geology 34(12), 1053-1056.
Lehrmann, D.J., Stepchinski, L., Altiner, D., Orchard, M.J., Montgomery, P., Enos, P., Ellwood, B.B., Bowring, S.A., Ramezani, J., Wang, H.M., 2015. An integrated biostratigraphy (conodonts and foraminifers) and chronostratigraphy (paleomagnetic

reversals, magnetic susceptibility, elemental chemistry, carbon isotopes and geochronology) for the Permian–Upper Triassic strata of Guandao section, Nanpanjiang Basin, South China. Journal of Asian Earth Sciences 108, 117-135.

Leu, M., Bucher, H., Goudemand, N., 2018. Clade-dependent size response of conodonts to environmental changes during the late Smithian extinction. Earth-Science Reviews, this volume. https://doi.org/10.1016/j.earscirev.2018.11.003

Li, M.S., Ogg, J., Zhang, Y., Huang, C.J., Hinnov, L., Chen, Z.Q., Zou, Z.Y., 2016a. Astronomical tuning of the end-Permian extinction and the Early Triassic Epoch of South China and Germany. Earth and Planetary Science Letters 441, 10-25.

Li, M.S., Huang, C.J., Hinnov, L., Ogg, J., Chen, Z.Q., Zhang, Y., 2016b. Obliquity-forced climate during the Early Triassic hothouse in China. Geology 44, 623-626.

Li, M.S., Hinnov, L.A., Huang, C.J., Ogg, J.G., 2018. Sedimentary noise and sea levels linked to land–ocean water exchange and obliquity forcing. Nature Communications 9, 1004.

Li, S.Y., Tong, J.N., Liu, K.Y., Wang, F.J., Huo Y.Y., 2007. The Lower Triassic cyclic deposition in Chaohu, Anhui Province, China. Palaeogeography, Palaeoclimatology, Palaeoecology 252, 188-199.

Liang, D., Tong, J.N., Zhao, L.S., 2011. Lower Triassic Smithian-Spathian boundary at West Pingdingshan section in Chaohu, Anhui Province. Science in China D: Earth Sciences 54, 372-379.

Liang, L., Tong, J.N., Song, H.J., Song, T., Tian, L., Song, H.Y., Qiu, H.O., 2016. Lower-Middle Triassic conodont biostratigraphy of the Mingtang section, Nanpanjiang Basin, South China. Palaeogeography Palaeoclimatology Palaeoecology 459, 381-393.

Lucas, S.G., Orchard, M.J., 2007. Triassic lithostratigraphy and biostratigraphy north of Currie, Elko County, Nevada. New Mexico Museum of Natural History and Science Bulletin 40, 119-126.

Luo, G.M., Kump, L.R., Wang, Y., Tong, J., Arthur, M.A., Yang, H., Huang, J., Yin, H., Xie, S., 2010. Isotopic evidence for an anomalously low oceanic sulfate concentration following end-Permian mass extinction. Earth and Planetary Science Letters 300, 101-111.

Lyu, Z.Y., Orchard, M.J., Chen, Z.Q., Wang, X.D., Zhao, L.S., Han, C., 2017. Uppermost Permian to Lower Triassic conodont successions from the Enshi area, western Hubei Province, South China. Palaeogeography, Palaeoclimatology, Palaeoecology, in press. https://doi.org/10.1016/j.palaeo.2017.08.015.

Lyu, Z.Y., Zhang, L., Algeo, T.J., Zhao, L.S., Chen, Z.Q., Li, C., Ma, B., Ye, F.H., 2018. Global-ocean circulation changes during the Smithian–Spathian transition inferred from carbon-sulfur cycle records. Earth-Science Reviews, this volume. https://doi.org/10.1016/j.earscirev.2019.01.010

Maekawa, T., Komatsu, T., 2014. Conodont Succession, In: Shigeta, Y., Komatsu, T., Maekawa, T., Tran, H.D. (Eds.), Olenekian (Early Triassic) stratigraphy and fossil assemblages in Northeastern Vietnam. National Museum of Nature and Science Monographs (Tokyo, Japan) 45, 51-54.

Maekawa, T., Komatsu, T., Shigeta, Y., Huyen, D.T., Tien, D.C., 2015. First occurrence of Early Triassic conodonts from the Lang Son Formation, northeastern Vietnam. Paleontological Research 19, 312-320.

Marenco, P.J., Corsetti, F.A., Kaufman, A.J., Bottjer, D.J., 2008b Environmental and

diagenetic variations in carbonate associated sulfate: an investigation of CAS in the Lower Triassic of the western USA. Geochimica et Cosmochimica Acta 72, 1570-1582.

McLearn, F.H., Kindle, E.D., 1950. Geology of Northeast British Columbia. Geological Survey of Canada Memoir 259, 236 pp.

Meyer, K.M., Yu, M., Jost, A.B., Kelley, B.M., Payne, J.L., 2011. $\delta^{13}C$ evidence that high primary productivity delayed recovery from end-Permian mass extinction. Earth and Planetary Science Letters 302, 378-384.

Milne, G.A., Gehrels, W.R., Hughes, C.W., Tamisiea, M.E., 2009. Identifying the causes of sea-level change. Nature Geoscience 2, 471-478.

Mojsisovics, E.V., Waagen, W., Diener, C., 1895. Entwurf einer Gliederung der pelagischen Sedimente des Trias-Systems. Sitzberichte der kaiserlicher Akademie der Wissenschaften Wien 104, 1271-1302.

Mørk, A., Knarud, R., Worsley, D., 1982, Depositional and diagenetic environments of the Triassic and Lower Jurassic succession of Svalbard, In: Embry, A.F., Balkell, H.R. (Eds.), Arctic Geology and Geophysics: Canadian Petroleum Society Geological Memoir 8, pp. 371-398.

Mørk, A., Elvebakk, G., Forsberg, A.W., Hounslow, M.W., Nakrem, H.A., Vigran, J.O., Weitschat, W., 1999. The type section of the Vikinghøgda Formation: A new Lower Triassic unit in central and eastern Svalbard. Polar Research 18, 51-82.

Mørk, A., Lord, G.S., Solvi, K.H., Dallmann, W.K., 2013. Geological Map of Svalbard 1:100 000, sheet G14G Hopen. Norsk Polarinstitutt Temakart No. 50.

Mosher, L.C., 1968. Triassic conodonts from western North America and Europe and their correlation. Journal of Paleontology 42, 895-946.

Mosher, L.C., 1970. New conodont species as Triassic guide fossils. Journal of Paleontology 44, 737-742.

Mosher, L.C., 1973. Triassic conodonts from British Columbia and the northern Arctic Islands. Geological Survey of Canada Bulletin 222, 141-193.

Mostler, H., 1982. Bozener Quarzporphyr und Werfener Schichten. In: Mostler, H. (Ed.), Excursionsführer zur 4. Jahrestagung der Österreichischen Geologischen Gesellschaft, Seis am Schlern Südtirol, H. Kowatsch, Innsbruck, pp. 43-79.

Motani, R., Jiang, D.Y., Chen, G.B., Tintori, A., Rieppel, O., Ji, C., Huang, J.D., 2015. A basal ichthyosauriform with a short snout from the Lower Triassic of China. Nature 517, 485-488.

Müller, K.J., 1956. Triassic conodonts from Nevada. Journal of Paleontology 30, 818-830.

Mundil, R., Pálfy, J., Renne, P.R., Brack, P., 2010. The Triassic timescale: new constraints and a review of geochronological data. In: Lucas, S.G. (Ed.), The Triassic Timescale, Geological Society of London Special Publication 334, pp. 41-60.

Nakrem, H.A., Orchard, M.J., Weitschat, W., Hounslow, M.W., Beatty, T.W., Mørk, A., 2008. Triassic conodonts from Svalbard and their Boreal correlations. Polar Research 27, 523-539.

Nestell, G.P., Sudar, M., Jovanović, D., Kolar-Jurkovšek, T., 2009. Latest Permian foraminifers from the Vlašić Mountain area, northwestern Serbia. Micropaleontology 55, 495-513.

Orchard, M.J., 1995. Taxonomy and correlation of Lower Triassic (Spathian) segminate

conodonts from Oman and revision of some species of Neospathodus. Journal of Paleontology 69, 110-122.
Orchard, M.J., 2007. Conodont diversity and evolution through the latest Permian and Early Triassic upheavals. Palaeogeography, Palaeoclimatology, Palaeoecology 252, 93-117.
Orchard, M.J., 2008. Lower Triassic conodonts from the Canadian Arctic, their intercalibration with ammonoid-based stages and a comparison with other North American Olenekian faunas. Polar Research 27, 393-412.
Orchard, M.J., Krystyn, L., 1998. Conodonts of the lowermost Triassic of Spiti, and new zonation based on *Neogondolella* successions. Rivista Italiana di Paleontologia e Stratigrafia 104, 341-368.
Orchard, M.J., Krystyn, L., 2007. Conodonts from the Induan-Olenekian boundary interval at Mud, Spiti. Albertiana 35, 30-34.
Orchard, M.J., Tozer, E.T., 1997. Triassic conodont biochronology, its calibration with the ammonoid standard, and a biostratigraphic summary for the western Canada sedimentary basin. Bulletin of Canadian Petroleum Geology 45, 675-692.
Orchard, M.J., Zonneveld, J.P., 2009. The Lower Triassic Sulphur Mountain Formation in the Wapiti Lake area: lithostratigraphy, conodont biostratigraphy, and a new biozonation for the lower Olenekian (Smithian) Earth Science Sector (ESS) Contribution 20080714. Canadian Journal of Earth Sciences 46, 757-790.
Ovtcharova, M., Bucher, H., Schaltegger, U., Galfetti, T., Brayard, A., Guex, J., 2006. New Early to Middle Triassic U–Pb ages from South China: calibration with ammonoid biochronozones and implications for the timing of the Triassic biotic recovery. Earth and Planetary Science Letters 243(3-4), 463-475.
Ovtcharova, M., Goudemand, N., Hammer, Ø., Guodun, K., Cordey, F., Galfetti, T., Schaltegger, U., Bucher, H., 2015. Developing a strategy for accurate definition of a geological boundary through radio-isotopic and biochronological dating: The Early–Middle Triassic boundary (South China). Earth-Science Reviews 146, 65-76.
Pakistanese-Japanese Research Group (PJRG), 1985. Permian and Triassic systems in the Salt Range and Surghar Range, Pakistan. In: Nakazawa, K.D., Dickins, J.M. (Eds.), The Tethys, her Paleogeography and Paleobiogeography from Paleozoic to Mesozoic. Takai University Press, Tokyo, pp. 221-312.
Payne, J.L., Kump, L.R., 2007. Evidence for recurrent Early Triassic massive volcanism from quantitative interpretation of carbon isotope fluctuations. Earth and Planetary Science Letters 256, 264-277.
Payne, J.L., Lehrmann, D.J., Wei, J.Y., Orchard, M.J., Schrag, D.P., Knoll, A.H., 2004. Large perturbations of the carbon cycle during recovery from the end-Permian extinction. Science 305, 506-509.
Payne, J.L., Turchyn, A.V., Paytan, A., DePaolo, D.J., Lehrmann, D.J., Yu, M., Wei, J., 2010. Calcium isotope constraints on the end-Permian mass extinction. Proceedings of the National Academy of Sciences (U.S.A.) 107, 8543-8548.
Perri, M.C., 1986. A Spathian conodont fauna from the Cencenighe Member of the Werfen Formation (Scythian), southwestern Dolomites, Italy. Bollettino della Società Paleontologica Italiana 24, 23-28.
Perri, M.C., 1991. Conodont biostratigraphy of the Werfen Formation (Lower Triassic),

Southern Alps, Italy. Bollettino della Societa Paleontologica Italiana 30, 23-46.
Perri, M.C., Andraghetti, M., 1987. Permian–Triassic boundary and Early Triassic conodonts from the Southern Alps. Italy. Rivista Italiana di Paleontologia e Stratigrafia 93, 291-328.
Perri, M.C., Farabegoli, E., 2003. Conodonts across the Permian–Triassic boundary in the Southern Alps. Courier Forschungsinstitut Senckenberg 245, 281-313.
Piazza, V., Hammer, Ø., Jattiot, R., 2017. New late Smithian (Early Triassic) ammonoids from the Lusitaniadalen Member, Vikinghøgda Formation, Svalbard. Norwegian Journal of Geology 97(2), 105-117.
Popov, Y.D., 1964. Some Early Triassic ammonoids of northern Caucasus. International Geology Review 6, 700-705.
Posenato, R., 2008. Global correlations of mid Early Triassic events: The Induan/Olenekian boundary in the Dolomites (Italy). Earth-Science Reviews 91, 93-105.
Raup, D.M., 1986. Biological extinction in earth history. Science 231(4745), 1528-1533.
Richoz, S., 2006. Stratigraphie et variations isotopiques du carbone dans le Permien supérieur et le Trias inférieur de quelques localités de la Néotéthys (Turquie, Oman et Iran). Mémoire de Géologie de Lausanne 46, 251 pp.
Richoz, S., Krystyn, L., Baud, A., Brandner, R., Horacek, M., Mohtat-Aghai, P., 2010. Permian–Triassic boundary interval in the Middle East (Iran and N. Oman): Progressive environmental change from detailed carbonate carbon isotope marine curve and sedimentary evolution. Journal of Asian Earth Sciences 39, 236-253.
Romano, C., Goudemand, N., Vennemann, T.W., Ware, D., Schneebeli-Hermann, E., Hochuli, P.A., Brühwiler, T., Brinkmann, W., Bucher, H., 2013. Climatic and biotic upheavals following the end-Permian mass extinction. Nature Geoscience 6, 57-60.
Saito, R., Kaiho, K., Oba, M., Takahashi, S., Chen, Z. Q., Tong, J., 2012. A terrestrial vegetation turnover in the middle of the Early Triassic. Global and Planetary Change 105, 152-159.
Sakuma, H., Tada, R., Ikeda, M., Kashiyama, Y., Ohkouchi, N., Ogawa, N.O., Watanabe, S., Tajika, E., Yamamoto, S., 2012. High resolution lithostratigraphy and organic carbon isotope stratigraphy of the Lower Triassic pelagic sequence in central Japan. Island Arc 21, 79-100.
Samankassou, E., 1995. Early Triassic (Scythian) conodonts from the Werfen Formation, Southern Alps, Italy. Neues Jahrbuch für Geologie und Paläontologie, Monatshefte 4, 248-256.
Schneebeli-Hermann, E., Hochuli, P. A., Bucher, H., Goudemand, N., Brühwiler, T., Galfetti, T., 2012. Palynology of the Lower Triassic succession of Tulong, South Tibet—Evidence for early recovery of gymnosperms. Palaeogeography, Palaeoclimatology, Palaeoecology 339, 12-24.
Schobben, M., Ullmann, C.V., Leda, L., Korn, D., Struck, U., Reimold, W.U., Ghaderi, A., Algeo, T.J., Korte, C., 2016. Discerning primary versus diagenetic signals in carbonate carbon and oxygen isotope records: An example from the Permian–Triassic boundary of Iran. Chemical Geology 422, 94-107.
Sedlacek, A.R.C., Saltzman, M.R., Algeo, T.J., Horacek, M., Brandner, R., Foland, K., Denniston, R.F., 2014. $^{87}Sr/^{86}Sr$ stratigraphy from the Early Triassic of Zal, Iran: Linking temperature to weathering rates and the tempo of ecosystem recovery. Geology 42, 779-

782.
Sephton, M.A., Looy, C.V., Brinkhuis, H., Wignall, P.B., De Leeuw, J.W., Visscher, H., 2005. Catastrophic soil erosion during the end-Permian biotic crisis. Geology 33, 941-944.
Shen, J., Schoepfer, S.D., Feng, Q.L., Zhou, L., Yu, J.X., Song, H.Y., Wei, H.Y., Algeo, T.J., 2015. Marine productivity changes during the end-Permian crisis and Early Triassic recovery. Earth-Science Reviews 149, 136-162.
Shigeta, Y., Kumagae, T., 2016. Spathian (Late Olenekian, Early Triassic) Ammonoids from the Artyom Area, South Primorye, Russian Far East and Implications for the Timing of the Recovery of the Oceanic Environment. Paleontological Research 20, 48-60.
Shigeta, Y., Nakajima, Y., 2017. Discovery of the Early Spathian (Late Olenekian, Early Triassic) Ammonoid *Tirolites* in the Hiraiso Formation, South Kitakami Belt, Northeast Japan. Paleontological Research 21, 37-43.
Shigeta, Y., Zakharov, Y.D., 2009. Systematic Paleontology−Cephalopods. In: Shigeta, Y., Zakharov, Y.D., Maeda, H., Popov, A.M. (Eds.), The Lower Triassic system in the Abrek Bay area, South Primorye, Russia. National Museum of Nature and Science, Tokyo, pp. 44-140.
Shigeta, Y., Zaharov, J.D., Maeda, H., Popov, A.M. (Eds.), 2009. The Lower Triassic System in the Abrek Bay Area, South Primorye, Russia. National Museum of Nature and Science (Tokyo), 218 pp.
Shigeta, Y., Komatsu, T., Maekawa, T., Dang, H.T., 2014. Olenekian (Early Triassic) stratigraphy and fossil assemblages in northeastern Vietnam. National Museum of Nature and Science Monograph 38, Tokyo, Japan.
Signor, P.W., Lipps, J.H., 1982. Sampling bias, gradual extinction patterns, and catastrophes in the fossil record. In: Silver, L.T., Schultz, P.H. (Eds.), Geological Implications of Impacts of Large Asteroids and Comets on the Earth, Geological Society of America Special Paper 190, pp. 291-296.
Silberling, N.J., Tozer, E.T., 1968. Biostratigraphic Classification of the Marine Triassic in North America. Geological Society of America Special Paper 110, 63 pp.
Silva-Tamayo, J.C., Lau, K.V., Jost, A.B., Payne, J. L., Wignall, P. B., Newton, R.J., Eisenhauer, A., Depaolo, D.J., Brown, S., Maher, K., Lehrmann, D.J., Altiner, D., Yu, M.Y., Richoz, S., Paytan, A., 2018. Global perturbation of the marine calcium cycle during the Permian-Triassic transition. Geological Society of America Bulletin 130(7-8), 1323-1338.
Smyshlyaeva, O., Zakharov, Y., 2012. New representatives of the family Melagathiceratidae (Ammonoidea) from the Lower Triassic of South Primorye. Paleontological Journal 46, 142-147.
Song, H.J., Wignall, P.B., Chu, D.L., Tong, J.N., Sun, Y.D., Song, H.Y., He, W.H., Tian, L., 2014. Anoxia/high temperature double whammy during the Permian–Triassic marine crisis and its aftermath. Scientific Reports 4, art. 4132.
Song, H.J., Wignall, P.B., Tong, J.N., Song, H.Y., Chen, J., Chu, D.L., Tian, L., Luo, M., Zong, K.Q., Chen, Y.L., 2015. Integrated Sr isotope variations and global environmental changes through the Late Permian to early Late Triassic. Earth and Planetary Science Letters 424, 140-147.
Song, H.Y., Tong, J.N., Algeo, T.J., Horacek, M., Qiu, H.O., Song, H.J., Tian, L., Chen, Z.Q.,

2013. Large vertical $\delta^{13}C_{DIC}$ gradients in Early Triassic seas of the South China craton: Implications for oceanographic changes related to Siberian Traps volcanism. Global and Planetary Change 105, 7-20.

Song, H.Y., Tong, J.N., Algeo, T.J., Song, H.J., Qiu, H.O., Zhu, Y.Y., Tian, L., Bates, S., Lyons, T.W., Luo, G.M., Kump, L.R., 2014. Early Triassic seawater sulfate drawdown. Geochimica et Cosmochimica Acta 128, 95-113.

Song, H.Y., Du, Y., Algeo, T.J., Tong, J.N., Owens, J.D., Song, H.J., Tian, L., Qiu, H., Zhu, Y.Y., Lyons, T.W., 2019. Cooling-driven oceanic anoxia during the Smithian-Spathian transition (mid-Early Triassic). Earth-Science Reviews, this volume. https://doi.org/10.1016/j.earscirev.2019.01.009

Staesche, U., 1964. Conodonten aus dem Skyth von Südtirol. Neues Jahrbuch für Geologie und Paläontologie, Abhandlungen 119, 247-306.

Stanley, S.M., 2009. Evidence from ammonoids and conodonts for multiple Early Triassic mass extinctions. Proceedings of the National Academy of Sciences (U.S.A.) 106, 15264-15267.

Stebbins, A., Algeo, T.J., Krystyn, L., Rowe, H.D., Brookfield, M., Williams, J., Nye, S.W., Jr., and Hannigan, R., 2018a. Marine sulfur cycle evidence for upwelling and eutrophic stresses during Early Triassic cooling events. Earth-Science Reviews, this volume. https://doi.org/10.1016/j.earscirev.2018.09.007

Stebbins, A., Algeo, T.J., Olsen, C., Sano, H., Rowe, H.D., and Hannigan, R., 2018b. Sulfur-isotope evidence for recovery of seawater sulfate concentrations from a PTB minimum by the Smithian-Spathian transition. Earth-Science Reviews, this volume. https://doi.org/10.1016/j.earscirev.2018.08.010

Sudar, M.N., Jovanović, D., Kolar-Jurkovšek, T., 2007. Late Permian conodonts from Jadar Block (Vardar Zone, northwestern Serbia). Geologica Carpathica 58, 145-152.

Sudar, M.N., Chen, Y., Tea, K.J., Bogdan, J., Divna, J., Marie-Beatrice, F., 2014. Lower Triassic (Olenekian) microfauna from Jadar Block (Gučevo Mt. NW Serbia). Geološki Anali Balkanskog Poluostrva 75, 1-15.

Sun, Y.D., Joachimski, M.M., Wignall, P.B., Yan, C.B., Chen, Y.L., Jiang, H.S., Wang, L.N., Lai, X.L., 2012. Lethally hot temperatures during the Early Triassic greenhouse. Science 338, 366-370.

Sun, Y.D., Joachimski, M.M., Wignall, P.B., Yan, C.B., Chen, Y.L., Jiang, H.S., Wang, L.N., Lai, X.L., 2013. Response to Comment on "Lethally hot temperatures during the Early Triassic greenhouse". Science 339, 1033.

Sweet, W.C., 1970a. Uppermost Permian and Lower Triassic conodonts of the Salt Range and Trans-Indus Ranges, West Pakistan. In: Kummel, B., Teichert, C. (Eds.), Stratigraphic Boundary Problems: Permian and Triassic of West Pakistan 4, pp. 207-275.

Sweet, W.C., 1970b. Permian and Triassic conodonts from a section at Guryul Ravine, Vihi district, Kashmir. University of Kansas Paleontological Contributions, Paper 49, 10 pp.

Tada, R., Watanabe, S., Kashiyama, Y., Tajika, E., Kato, T., Yamamoto, S., Isozaki, Y., Sakuma, H., 2005. High-resolution analysis of Late Paleozoic-Early Mesozoic variability of paleoceanographic system recorded in bedded chert sequence in the inner zone of southwest Japan. Journal of Geography (Chigaku Zasshi) 114, 638-642.

Takahashi, S., Oba, M., Kaiho, K., Yamakita, S., Sakata, S., 2009. Panthalassic oceanic anoxia

at the end of the Early Triassic: A cause of delay in the recovery of life after the end-Permian mass extinction: Palaeogeography, Palaeoclimatology, Palaeoecology 274, 185-195.

Thomazo, C., Vennin, E., Brayard, A., Bour, I., Mathieu, O., Elmeknassi, S., Olivier, N., Escarguel, E., Bylund, K.G., Jenks, J., Stephen, D.A., Fara, E., 2016. A diagenetic control on the Early Triassic Smithian-Spathian carbon isotopic excursions recorded in the marine settings of the Thaynes Group (Utah, USA). Geobiology 14, 1-17.

Thomazo, C., Brayard, A., Elmeknassi, S., Vennin, E., Olivier, N., Caravaca, G., Escarguel, G., Fara, E., Bylund, K.G., Jenks, J.F., Stephen, D.A., Killingsworth, B., Sansjofre, P., Cartigny, P., 2018. Multiple sulfur isotope signals associated with the late Smithian event and the Smithian/Spathian boundary. Earth-Science Reviews, this volume. https://doi.org/10.1016/j.earscirev.2018.06.019

Thorsteinsson, R., Tozer, E.T., 1970. Geology of the Arctic Archipelago. In: Douglas, R.J.W. (Ed.), Geology and Economic Minerals of Canada. Geological Survey of Canada, pp. 547-590.

Tian, C.R., Dai, J., Tian, S.G., 1983. Triassic conodonts. In: Chengdu Institute of Geology and Mineral Resources, Paleontological Atlas of Southwest China, Volume of Microfossils. Geological Publishing House, Beijing, pp. 345-398.

Tian, L., Tong, J.N, Algeo, T.J., Song, H.J., Song, H.Y., Chu, D.L., Shi, L., Bottjer, D.J., 2014. Reconstruction of Early Triassic ocean redox conditions based on framboidal pyrite from the Nanpanjiang Basin, South China. Palaeogeography, Palaeoclimatology, Palaeoecology 412, 68-79.

Tong, J.N., Zhao L.S., 2011. Lower Triassic and Induan-Olenekian Boundary in Chaohu, Anhui Province, South China. Acta Geologica Sinica 85, 399-407.

Tong, J.N., Qiu, H.O., Zhao, L.S., Zuo, J.X., 2002. Lower Triassic inorganic carbon isotope excursion in Chaohu, Anhui Province, China. Journal of China University of Geosciences, 13, 98-106.

Tong, J.N., Zakharov, Y.D., Orchard, M.J., Yin, H.F., Hansen, H.J., 2003. A candidate of the Induan–Olenekian Boundary stratotype in the Tethyan region. Science in China D: Earth Sciences 46, 1182-1200.

Tong, J.N., Zakharov, Y.D., Wu, S.B., 2004. Early Triassic ammonoid succession in Chaohu, Anhui Province. Acta Palaeontologica Sinica 43, 192-204.

Tong, J.N., Hansen, H.J., Zhao, L.S., Zuo, J.X., 2005. A GSSP candidate of the Induan–Olenekian Boundary-stratigraphic sequence of the West Pingdingshan Section, in Chaohu, Anhui Province. Journal of Stratigraphy 29, 205-212.

Tong, J.N., Zuo, J.X., Chen, Z.Q., 2007. Early Triassic carbon isotope excursions from South China: proxies for devastation and restoration of marine ecosystems following the end-Permian mass extinction. Geological Journal 42, 371-389.

Tozer, E.T., 1961. Triassic Stratigraphy and Faunas, Queen Elizabeth Islands, Arctic Archipelago. Geological Survey of Canada Memoir 316, 116 pp.

Tozer, E.T., 1962. Illustrations of Canadian fossils: Triassic of western and Arctic Canada. Geological Survey of Canada Paper 62-19, 26 pp.

Tozer, E.T., 1965. Lower Triassic stages and ammonoid zones of Arctic Canada. Geological Survey of Canada Paper 14, 12 pp.

Tozer, E.T., 1967. A standard for Triassic time. Geological Survey of Canada Bulletin 156, 103 pp.

Tozer, E.T., 1971. Triassic time and ammonoids: problems and proposals. Canadian Journal of Earth Sciences 8, 989-1031.

Tozer, E.T., 1981a. Triassic ammonoidea: classification, evolution and relationship with Permian and Jurassic forms. In: House, M.R., Senior, J.R. (Eds.), The Ammonoidea. The Systematics Association, London, pp. 65-100.

Tozer, E.T., 1981b. Triassic ammonoidea: geographic and stratigraphic distribution. In: House, M.R., Senior, J.R. (Eds.), The Ammonoidea. The Systematics Association, London, pp. 397-431.

Tozer, E.T., 1982. Marine Triassic faunas of North America: their significance for assessing plate and terrane movements. Geologische Rundschau 71, 1077-1104.

Tozer, E.T., 1984. The Trias and its ammonoids: the evolution of a time scale. Geological Survey of Canada Miscellaneous Report 35, 171 pp.

Tozer, E.T., 1994. Canadian Triassic ammonoid faunas. Geological Survey of Canada Bulletin 467, 663 pp.

Tozer, E.T., Calon, T.J., 1990. Triassic ammonoids from Jabal Safra and Wadi Alwa, Oman, and their significance. In: Robertson, A.H.F., Searle, M.P., Ries, A.C. (Eds.), The Geology and Tectonics of the Oman Region. Geological Society of London Special Publication 49, pp. 203-211.

Twitchett, R.J., Barras, C.G., 2004. Trace fossils in the aftermath of mass extinction events. In: McIlroy, D. (Ed.), The Application of Ichnology to Palaeoenvironmental and Stratigraphic Analysis, Geological Society of London Special Publication 228, pp. 397-418.

Vaziri, S.H., 2011. A review on Late Scythian to Middle Anisian ammonoids from the Alam Formation in Nakhlak area, Central Iran. Journal of Science, Islamic Azad University 21, 201–212.

Waagen, W., 1895. Salt-Range fossils. Vol. 2: Fossils from the Ceratite Formation. Palaeontologia Indica 13, 323 pp.

Wang, H.M., Wang, X.L., Li, R.X., Wei, J.Y., 2005. Triassic conodont succession and stage subdivision of the Guandao section, Bianyang Luodian. Acta Palaentologica Sinica 44, 611-626.

Ware, D., Bucher, H., Brayard, A., Schneebeli-Hermann, E., Brühwiler, T., 2015. High-resolution biochronology and diversity dynamics of the Early Triassic ammonoid recovery: the Dienerian faunas of the Northern Indian Margin. Palaeogeography, Palaeoclimatology, Palaeoecology 440, 363-373.

Ware, D., Bucher, H., Brühwiler, T., Schneebeli-Hermann, E., Hochuli, P.A., Roohi, G., Ur-Rehman, K., Yaseen, A., 2017. Griesbachian and Dienerian (Early Triassic) ammonoids from the Salt Range, Pakistan. Fossils and Strata, in press. doi: 10.1130/B31969.1.

Watanabe, K., Kanmera, K., Nakajima, K., 1979. Conodont biostratigraphy in the Kamura limestone (Triassic), Takachiho-cho, Nishiusuki-gun, Miyazaki Prefecture. In: Igo, H., Koike, T. (Eds.), Biostratigraphy of Permian and Triassic Conodonts and Holothurian Sclerites in Japan, Committee of Prof. M. Kanuma Retirement Ceremony, Tokyo, Japan, pp. 127-137.

Weitschat, W., Dagys, A.S., 1989. Triassic biostratigraphy of Svalbard and a comparison with NE-Siberia. Mitteilungen des Geologisch-Paläontologisches Institut der Universität Hamburg 68, 179-213.

Weitschat, W., Lehmann, U., 1978. Biostratigraphy of the uppermost part of the Smithian Stage (Lower Triassic) at the Botneheia, W-Spitsbergen. Mitteilungen des Geologischen-Paläontologischen Institut, Universität Hamburg 48, 85-100.

Wignall, P.B., Twitchett, R.J., 1996. Oceanic anoxia and the end Permian mass extinction. Science 272, 1155-1158.

Wignall, P.B., Bond, D.P., Sun, Y., Grasby, S.E., Beauchamp, B., Joachimski, M.M., Blomeier, D.P., 2016. Ultra-shallow-marine anoxia in an Early Triassic shallow-marine clastic ramp (Spitsbergen) and the suppression of benthic radiation. Geological Magazine 153, 316-331.

Xie, S.C., Pancost, R.D., Huang, X., Jiao, D., Lu, L., Huang, J., Yang, F., Evershed, R.P., 2007. Molecular and isotopic evidence for episodic environmental change across the Permo/Triassic boundary at Meishan in South China. Global and Planetary Change 55, 56-65.

Yan, C.B., Wang, L.N., Jiang, H.S., Wignall, P.B., Sun, Y.D., Chen, Y.L., Lai, X.L., 2013. Uppermost Permian to Lower Triassic conodonts at Bianyang section, Guihzou Province, South China. Palaios 28, 509-522.

Yang, S.R., Wang, X.P., Hao, W.C., 1984. New knowledge on the Lower Triassic of Zuodeng, Tiandong County, Guangxi. In: Selected Papers for the Commemoration of Professor Yue Senxun engaged in Geological Education for 60 Years. Geological Publishing House, Beijing, pp. 105-117.

Yao, A, Kuwahara, K., 1997. Radiolarian faunal change from Late Permian to Middle Triassic times. News of Osaka Micropaleontologists 10, 87-96.

Yin, H.F., Yang, F.Q., Zhang, K.Q., Yang, W.P., 1986. A proposal to the biostratigraphic criterion of Permian/Triassic boundary. Memorie della Societa Geologica Italiana 34, 329-344.

Yin, H.F., Sweet, W.C., Glenister, B.F., Kotlyar, G., Kozur, H., Newell, N.D., Sheng, J.Z., Yang, Z.Y., Zakharov, Y.D., 1996, Recommendation of the Meishan section as Global Stratotype Section and Point for basal boundary of Triassic System. Newsletter on Stratigraphy 34, 81-108.

Yin, H.F., Zhang, K.X., Tong, J.N., Yang, Z.Y., Wu, S.B., 2001. The Global Stratotype Section and Point (GSSP) of the Permian-Triassic boundary. Episodes 24, 102-114.

Zakharov, Y.D., Abnavi, N.M., 2013. The ammonoid recovery after the end-Permian mass extinction: evidence from the Iran-Transcaucasia area, Siberia, Primorye, and Kazakhstan. Acta Palaeontologica Polonica 58, 127-147.

Zakharov, Y.D., Smyshlyaeva, O.P., 2016. New Middle Olenekian (Early Triassic) Ammonoids of South Primorye Paleontological Journal 50, 229-238.

Zakharov, Y.D., Popov, A.M., Buryi, G.I., 2004. Triassic ammonoid succession in South Primorye: 2. Middle Olenekian *Tirolites-Amphistephanites* Zone. Albertiana 29, 29-37.

Zakharov, Y.D., Bondarenko, L.G., Smyshlyaeva, O.P., Andalexander M.P., 2013. Late Smithian (Early Triassic) ammonoids from the *Anasibirites nevolini* zone of South Primorye, Russian Far East. In: Tanner, L.H., Spielmann, J.A., Lucas, S.G. (Eds.), The

Triassic System. New Mexico Museum of Natural History and Science Bulletin 61, pp. 597-612.

Zhang, F.F., Romaniello, S.J., Algeo, T.J., Lau, K.V., Clapham, M.E., Richoz, S., Herrmann, A.D., Smith, H., Horacek, M., Anbar, A.D., 2018. Multiple episodes of extensive oceanic anoxia linked to global warming and continental weathering following the latest Permian mass extinction. Science Advances 4(4), e1602921.

Zhang, L., Zhao, L.S., Chen, Z.Q., Algeo, T.J., Li, Y., Cao, L., 2015. Amelioration of marine environments at the Smithian-Spathian boundary, Early Triassic. Biogeosciences 12, 1597-1613.

Zhang, L., Orchard, M.J., Algeo, T.J., Chen, Z.Q., Lyu, Z.Y., Zhao, L.S., Han, C., Liu, S.J., 2017. An intercalibrated Triassic conodont succession and carbonate carbon isotope profile, Kamura, Japan. Palaeogeography, Palaeoclimatology, Palaeoecology, in press. https://doi.org/10.1016/j.palaeo.2017.09.001.

Zhao, L.S., Tong, J.N., Zuo, J.X., Ming, H.L., 2002. Discussion on Induan-Olenekia Boundary in Chaohu, Auhui Province, China, Journal of China University of Geosciences 3, 141-150.

Zhao, L.S., Tong, J.N., Zuo, J.X., 2003a. Lower Triassic Conodont Biostratigraphical Sequence at West Pingdingshan Section, Chaohu, Anhui Province, China. Earth Science 28, 414-418.

Zhao, L.S., Tong, Jinnan, Orchard, M.J. 2003b. Morphological variation of the conodonts *Platyvillosus* from the Yinkeng Formation in Chaohu, Anhui Province, China. Journal of China University of Geosciences 19, 306-314.

Zhao, L.S., Orchard, M.J., Tong, J.N., 2004. Lower Triassic conodont biostratigraphy and speciation of *Neospathodus waageni* around the Induan-Olenekian Boundary of Chaohu, Anhui Province, China. Albertiana 29, 41-43.

Zhao, L.S., Orchard, M.J., Tong J.N., 2005a. Conodont sequences and its global correlation of the Induan-Olenekian Boundary in West Pingdingshan section, Chaohu, Anhui Province. Albertiana (Part II) 33, 108-111.

Zhao, L.S., Tong, J.N., Orchard, M.J., 2005b. Study on the Lower Triassic Conodont Sequence and the Induan-Olenekian Boundary in Chaohu, Anhui Province. China University of Geosciences Press, 140 pp.

Zhao, L.S., Tong, J.N., Orchard, M.J., Zuo, J.X., 2005c. Lower Triassic conodont zonations of Chaohu area, Anhui Province and their global correlation. Earth Science 30, 624-634.

Zhao, L.S., Orchard, M.J., Tong, J.N., Sun, Z.i., Zuo, J.X., Zhang, S.X., Yun, A.L., 2007a. Lower Triassic conodont sequence in Chaohu, Anhui Province, China and its global correlation. Palaeogeography, Palaeoclimatology, Palaeoecology 252, 24-38.

Zhao, L.S., Tong, J.N., Sun, Z.M., Chang, D.F., Zhang, K.X., Zhang, S.X., Orchard M.J., 2007b. High-Resolution Conodont Biostratigraphy in the Induan-Olenekian Boundary Strata at West Pingdingshan Section, Chaohu, Anhui Province. Earth Science 32, 91-302.

Zhao, L.S., Tong, J.N., Sun, Z.M., Orchard, M.J., 2008a. Detailed Lower Triassic conodont biostratigraphy and its implications at the GSSP candidate of the Induan-Olenekian boundary in Chaohu, Anhui Province. Progress in Natural Science 18, 79-90.

Zhao, L.S., Tong, J.N., Sun, Z.M., Orchard, M.J., 2008b. An update of Conodonts in the

Induan-Olenekian Boundary Strata at West Pingdingshan Section, Chaohu, Anhui Province. Journal of China University of Geosciences 19, 207-216.

Zhao, L.S., Chen, Y.L., Chen, Z.Q., Cao, L., 2013a. Uppermost Permian to Lower Triassic Conodont Zonation from Three Gorges area, South China, Palaios 28, 523-540.

Zhao, L.S., Chen, Z.Q., Algeo, T.J., Chen, J.B., Chen, Y.L., Tong, J.N., Gao, S., Zhou, L., Hu, Z.C., Liu, Y.S., 2013b. Rare-earth element patterns in conodontal bid crowns: Evidence for massive inputs of volcanic ash during the latest Permian biocrisis? Global and Planetary Change 105, 135-151.

Zhao, M.Y., Zheng, Y.F., 2015. The intensity of chemical weathering: geochemical constraints from marine detrital sediments of Triassic age in South China. Chemical Geology 391, 111-122.

Zuo, J.X., Tong, J.N., Qiu, H.O., Zhao, L.S., 2003. Carbon and oxygen isotopic stratigraphic correlation and its paleoenvironment significance during the Lower Triassic, Chaohu, Anhui Province, China. Geology-Geochemistry 31, 26-33.

Zuo, J.X., Tong, J.N., Qiu, H.O., Zhao, L.S., 2004. Carbon and oxygen isotope stratigraphy of the Lower Triassic at Northern Pingdingshan section of Chaohu, Anhui Province, China. Journal of Stratigraphy 28, 35-47.

Zuo, J.X., Tong, J.N., Qiu, H.O., Zhao, L.S., 2006. Carbon isotope composition of the Lower Triassic marine carbonates, Lower Yangtze region, South China. Science in China D−Earth Sciences 49, 225-241.

Figures and captions

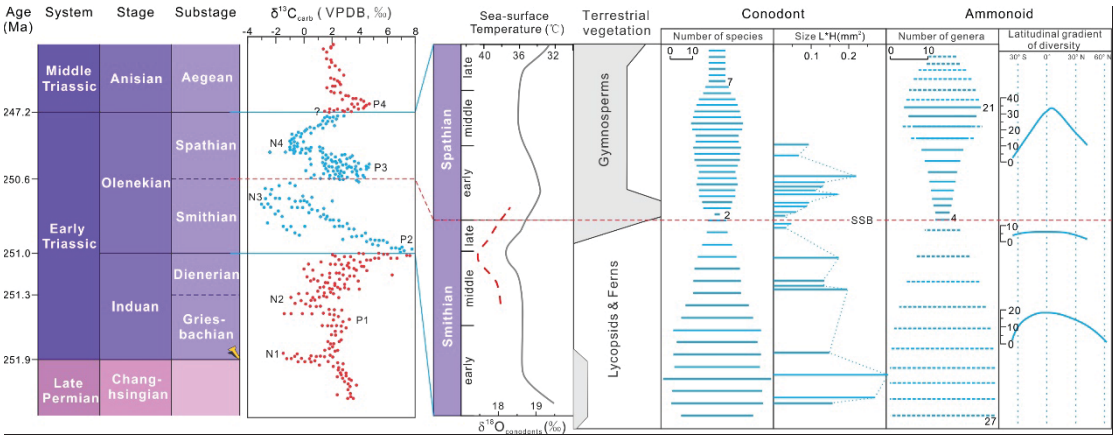

Fig. 1. Simplified carbonate carbon isotopic, climatic (sea-surface temperature) and biotic (floras, conodont and ammonoid) changes during the Smithian and Spathian substages of the Early Triassic. Carbon isotope data are from Payne et al. (2004) and Chen and Benton (2012), with numbering of negative and positive excursions (N1-N4, P1-P4) per Song et al. (2013). The Smithian and Spathian are subdivided into early, middle, and late intervals based on global ammonoid biostratigraphic studies summarized in Jenks et al. (2015). Sea-surface temperature modified after Sun et al. (2012) and Romano et al. (2013). Simplified terrestrial vegetation based on floral data from Hochuli et al. (2016). Conodont and ammonoid diversity profiles from Stanley (2009), which were drawn from global conodont records (Orchard, 2007) and regional (Canadian) ammonoid records (Tozer, 1981a, b, 1994). Conodont size data from Chen-YL et al. (2013), based on *Neospathodus*, *Triassospathodus* and *Novispathodus* taxa in South China (see also Leu et al., 2018). Ammonoid latitudinal gradients from Brayard et al. (2006). The geological time scale (note: non-linear ordinal axis) was simplified and adapted from Burgess et al. (2014) and Shen et al. (2015). SSB = Smithian/Spathian boundary.

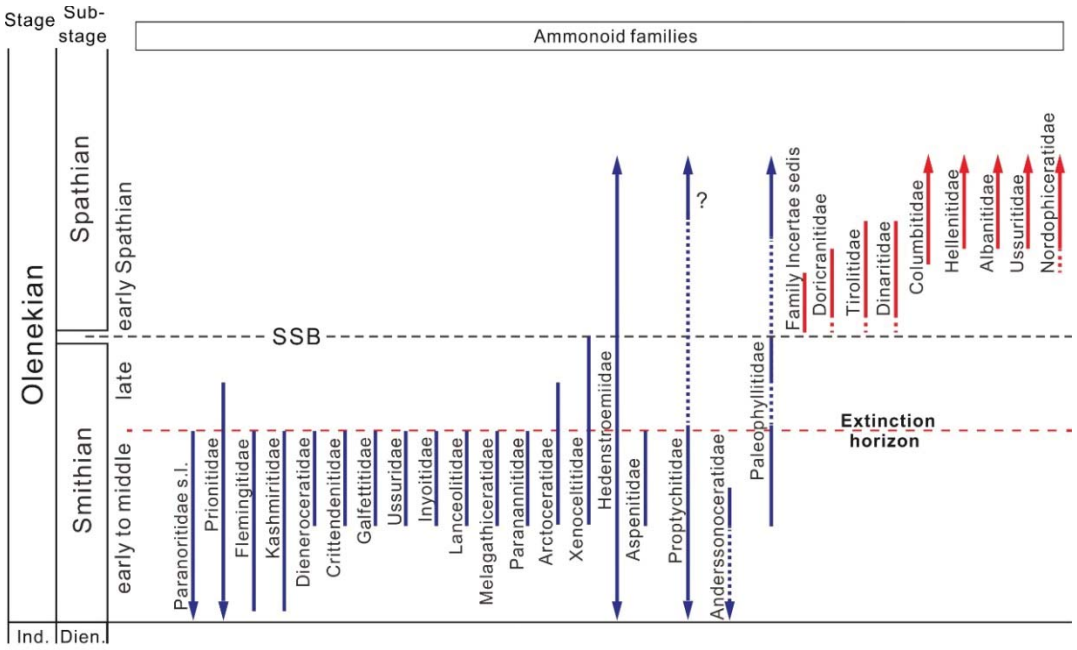

Fig. 2. Stratigraphic ranges of main ammonoid families through the Smithian and early Spathian. Based on ammonoid studies from Brayard et al. (2007b, 2013), Shigeta and Zakharov (2009), Brühwiler et al. (2010c, 2011, 2012a, b), Guex et al. (2010), Smyshlyaeva and Zakharov (2012), Jenks et al. (2013, 2015), Zakharov and Abnavi (2013), Zakharov et al. (2013), Shigeta et al. (2014), Jattiot et al. (2016, 2017), Shigeta and Kumagae (2016), Zakharov and Smyshlyaeva (2016), Shigeta and Nakajima (2017), Ware et al. (2017, 2019), and Jenks and Brayard (2018). Dien. = Dienerian, Ind. = Induan, SSB = Smithian/Spathian boundary.

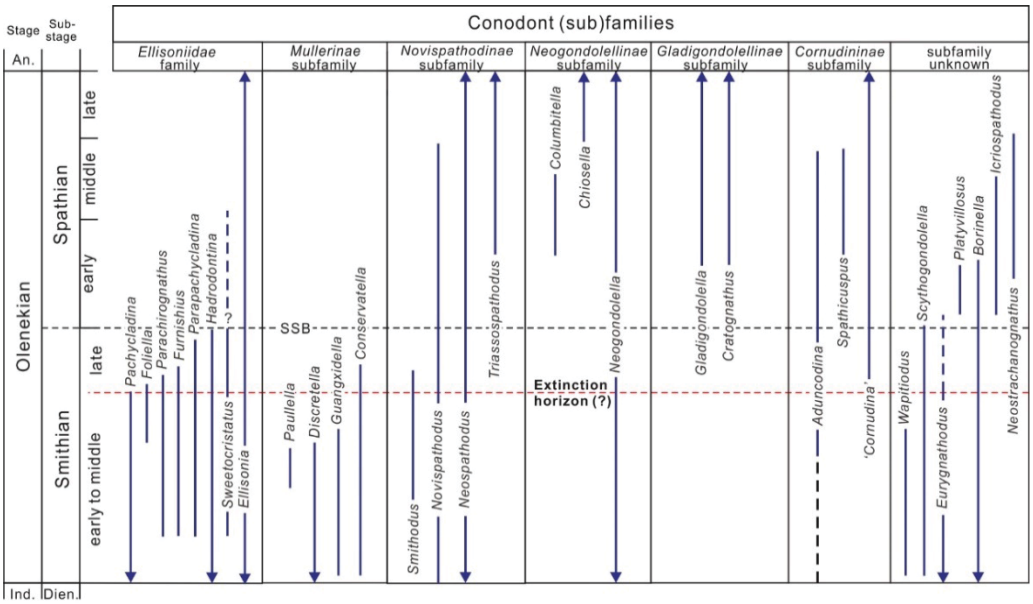

Fig. 3. Stratigraphic ranges of conodont genera through the Smithian and Spathian. Data from Orchard (2007). Dien. = Dienerian, Ind. = Induan, An. = Anisian, SSB = Smithian/Spathian boundary.

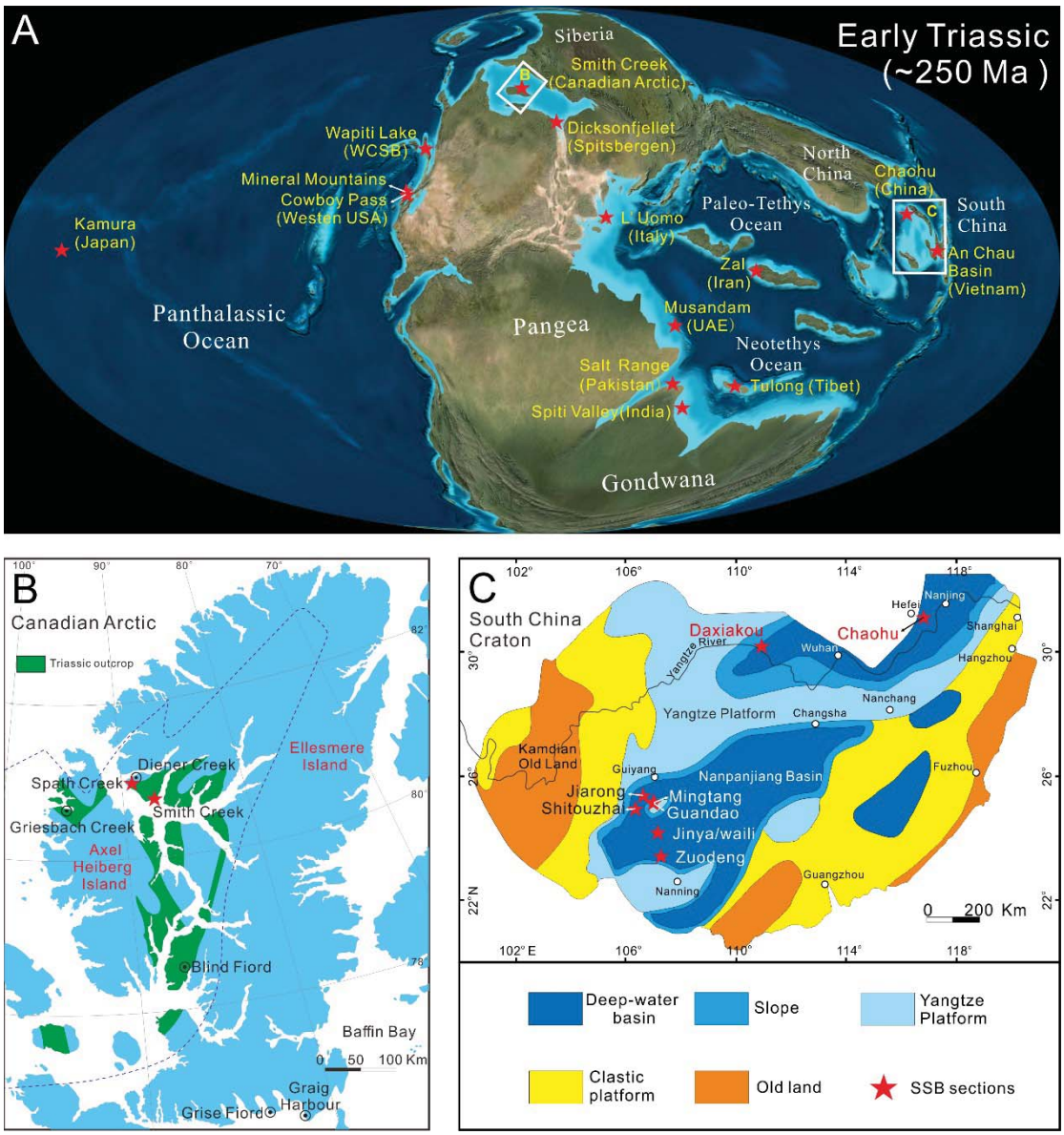

Fig. 4. Paleogeographic maps for key areas of Smithian-Spathian studies: (A) global, (B) Canadian Arctic, and (C) South China (see Bagherpour et al., 2017, for alternative facies distribution). Dotted line in B shows the margin of the Sverdrup Basin (Tozer, 1994). Map sources: base map of A is copyright Ron Blakey, Deep Time Maps; B is from Orchard (2008), and C is from Song et al. (2013).

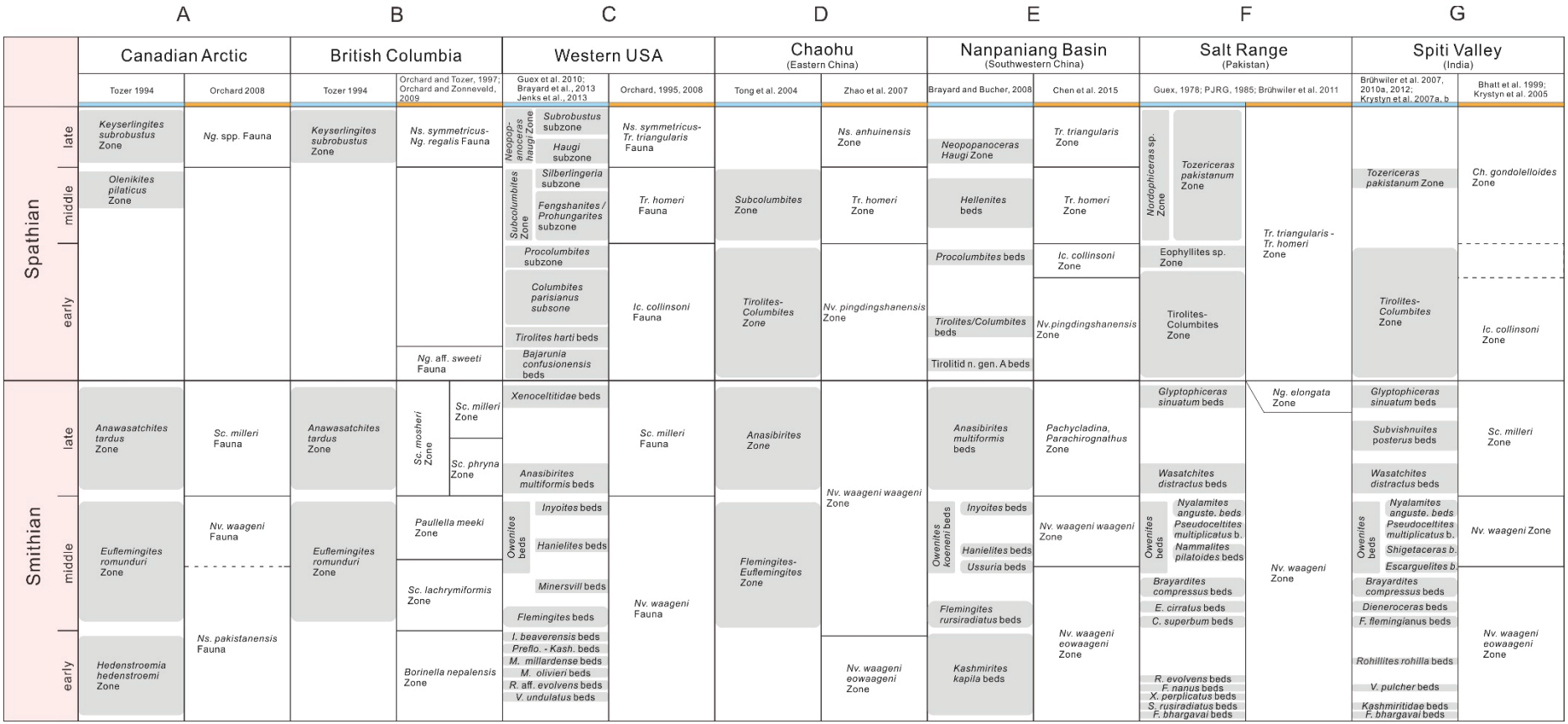

Fig. 5. Simplified correlation of some regional ammonoid-conodont zonation schemes for the Smithian-Spathian substages. Blue and orange bars at tops of columns represent ammonoid and conodont zonations, respectively. Note that ammonoid biozones are usually based on faunal assemblages that are not temporally continuous (see Jenks et al., 2015, for a detailed review), whereas conodont biozones are usually based on first occurrences of key conodont taxa and, thus, generally shown as temporally continuous. The two zonations may therefore not exactly

correlate. Correlations between ammonoid and conodont zonations are based on original published sources and are thus approximate and subject to further refinement (see text for details). Abbreviations (ammonoids): b. = beds; C. = *Clypeoceras*; E. = *Euflemingites*; F. = *Flemingites*; I. = *Inyoites*; Kash. = *Kashmirites*; M. = *Meekoceras*; Preflo = *Preflorianites*; R. = *Radioceras*; S. = *Shamaraites*; Ver. = *Vercherites*. X. = *Xenodiscoides*. Abbreviations (conodonts): Ng. = *Neogondolella*; Sc. = *Scythogondolella*; Ns. = *Neospathodus*; Nv. = *Novispathodus*; Tr. = *Triassospathodus*; Ic. = *Icriospathodus*; Ch. = *Chiosella*.

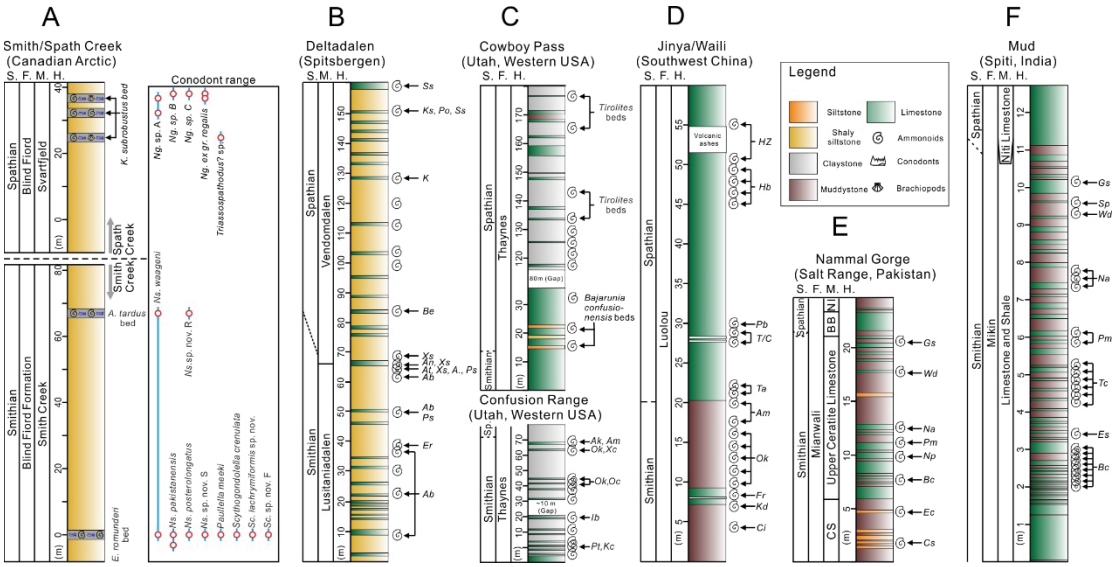

Fig. 6. Distributions of ammonoids and conodonts in some representative SSB sections. Data sources: Smith Creek and Spath Creek from Orchard (2008); Deltadalen from Mørk et al (1999); Cowboy Pass from Guex et al. (2010); Confusion Range from Brayard et al. (2013); Nammal Gorge from Brühwiler et al. (2010, 2011, 2012a); Mud from Brühwiler et al. (2012); and Jinya/Waili from Galfetti et al. (2007b). Abbreviations: S. = Stage, F. = Formation, M. = Member, H. = Height. BB = Bivalve Beds, NI = Niveaux Intermédiaires, A = *Anasibirites* sp., Ab = *Arctoceras blomstrandi*, Ak = *Anasibirites kingianus*, Am = *Anasibirites multiformis*, An = *Arctoprionites nodosus*, At = *Anawasatchites tardus*, Bc = *Brayardites compressus*, Be. = *Bajarunia* ex gr. *euomphala*, Ci = *Clypites* sp. indet, Cs = *Clypeoceras superbum*, Ec = *Euflemingites cirratus*, Er = *Euflemingites romunderi*, Es = *Escarguelites spitiensis*, Fr = *Flemingites rursiradiatus*, Gs = *Glyptophiceras sinuatum*, H = *Hellenites*, HZ = *Haugi* Zone, Ib = *Inyoites beaverensis* sp. nov., K = *Keyserlingites* sp., *Kc* = *Kashmirites confusionensis*, Ks = *Keyserlingites subrobustus*, Na = *Nyalamites angustecostatus*, Np = *Nammalites pilatoides*, Ok = *Owenites carpenteri*, Ok = *Owenites koeneni*, P = *Procolumbites*, Pm = *Pseudoceltites multiplicatus*, Po = *Popovites occidentalis*, Pt = *Preflorianites toulai*, Sp = *Subvishnuites posterus*, Ss = *Svalbardiceras spitzbergense*, Ta = Tirolitid n. gen. A., Tc = *Truempyceras compressum*, T/C = *Tirolites/Columbites*, Wd = *Wasatchites distractus*, Xc = *Xenoceltites cordilleranus*, Xs = *Xenoceltites subevolutus*, Ps = *Pseudosageceras* sp.

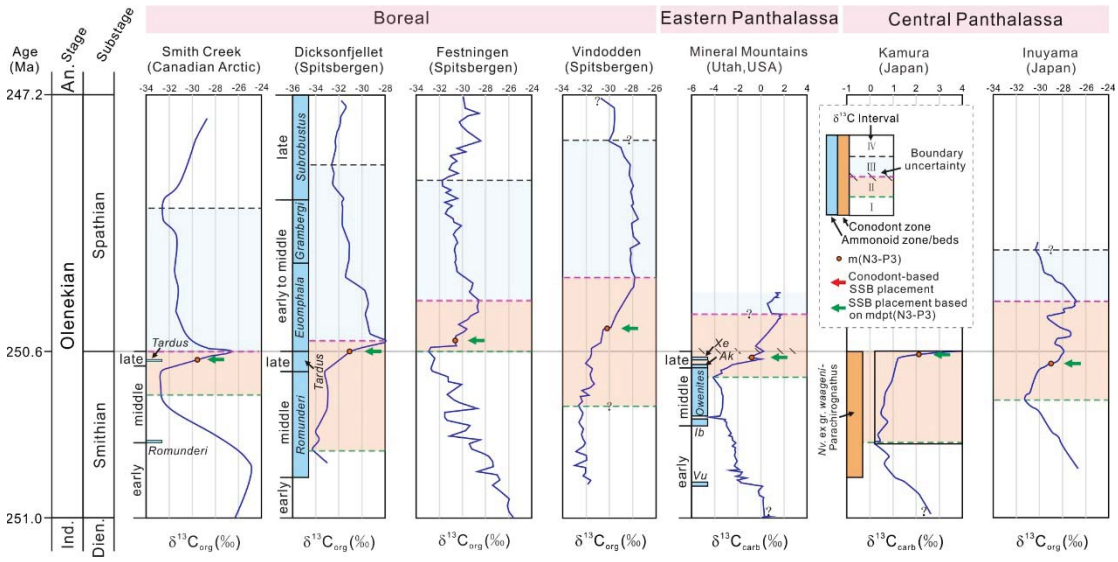

Fig. 7. Detailed correlations of Smithian-Spathian sections in the Boreal and eastern and central Panthalassic regions based on a combination of ammonoid and conodont biostratigraphy and C-isotope chemostratigraphy. Data sources: Smith Creek from Tozer (1967) and Grasby et al. (2013), Dicksonfjellet from Weitschat and Dagys (1989) and Galfetti et al. (2007a), Festningen from Grasby et al. (2016), Vindodden from Wignall et al. (2016), Mineral Mountains from Thomazo et al. (2016), Kamura from Zhang et al. (2017), and Inuyama from Sakuma et al. (2012). The SSB placements shown here are those from the original publications. In this study, we have divided each $\delta^{13}C$ profile into intervals I-IV (for visualization purposes, Interval II is colored pink and Interval III blue) bracketed by correlatable datums (shown as green, red, and black dashed lines). Another correlatable feature is 'mdpt(N3-P3)' (shown as orange dots), which represents the isotopic midpoint between the middle/late Smithian N3 minimum and the earliest Spathian P3 maximum, and which may serve as an auxiliary marker for the SSB. Abbreviations: Vu = *Vercherites undulatus*; I.b. = *Inyoites beaverensis*; O = *Owenites*; Ak = *Anasibirites kingianus*; Xe = *Xenoceltitidae* 'gen. indet.' A.; Dien. = Dienerian, Ind. = Induan, An. = Anisian. See Figure 1 for time scale.

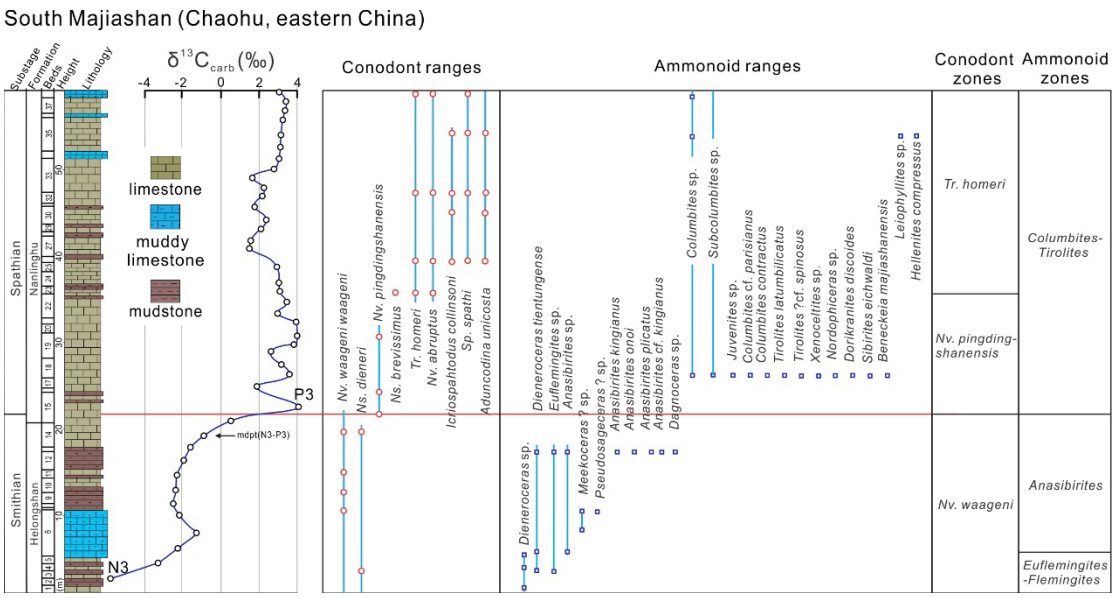

Fig. 8. Conodont, ammonoid and carbon isotopic stratigraphy at South Majiashan section in Chaohu area, eastern China. Data sources: carbon isotope from Tong et al. (2007); conodont ranges from Zhao et al. (2007a); ammonoid ranges from Guo (1982) and Tong et al. (2004). Abbreviations: Ng. = *Neogondolella*; Ns. = *Neospathodus*; Nv. = *Novispathodus*; Tr. = *Triassospathodus*.

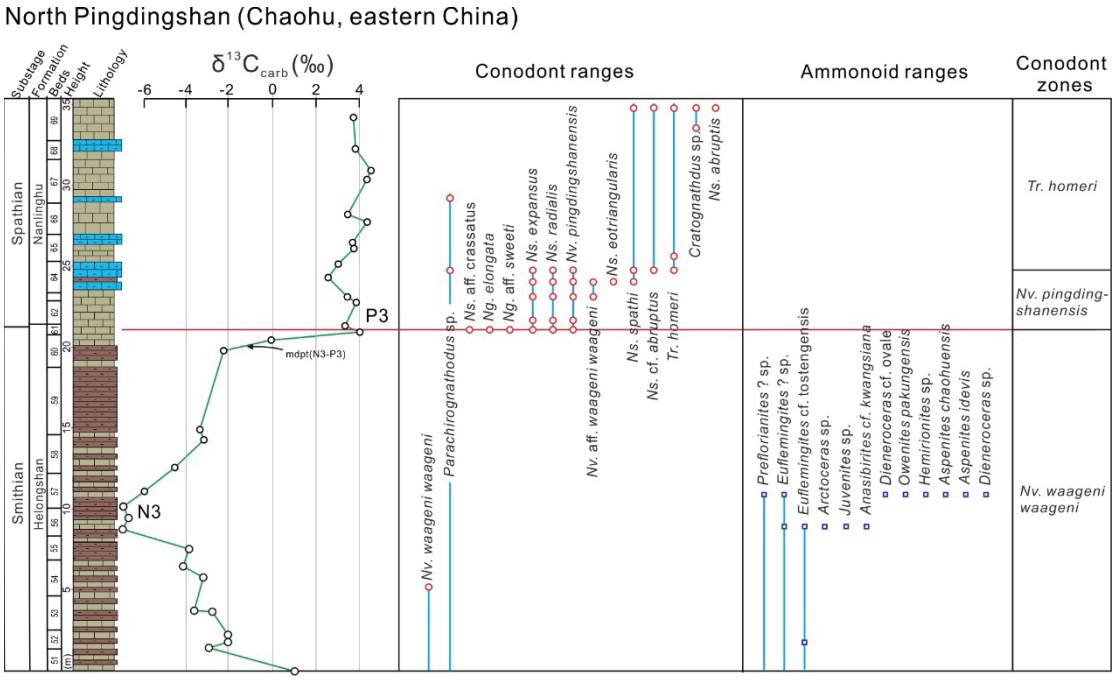

Fig. 9. Conodont, ammonoid and carbon isotopic stratigraphy at North Pingdingshan section in Chaohu area, eastern China. Data sources: carbon isotope from Zuo et al. (2004); conodont and ammonoid ranges from Zhao et al. (2007a). See Figure 8 for legend and abbreviations.

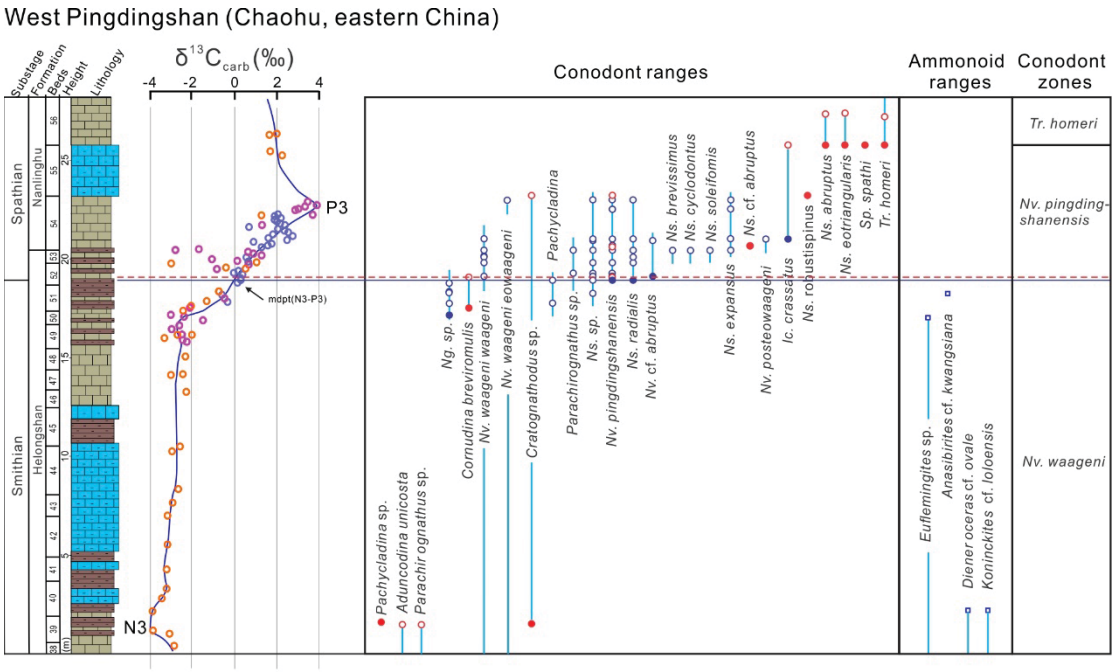

Fig. 10. Conodont, ammonoid and carbon isotopic stratigraphy at West Pingdingshan section in Chaohu area, eastern China. Data sources: carbon isotope from Tong and Zhao (2011) (orange), Liang et al. (2011) (pink) and Zhao and Zheng (2014) (light blue)； conodont ranges from Zhao et al. (2007a) (red circles) and Liang et al. (2011) (blue circles); ammonoid ranges from Zhao et al. (2007a). Placement of the SSB (i.e., first occurrence of *Nv. pingdingshanensis*) by Zhao et al. (2007a) is shown as a red line and the revised datum by Liang et al. (2011) as a blue line. Solid circles represent first occurrences of individual conodont species. See Figure 8 for legend and abbreviations.

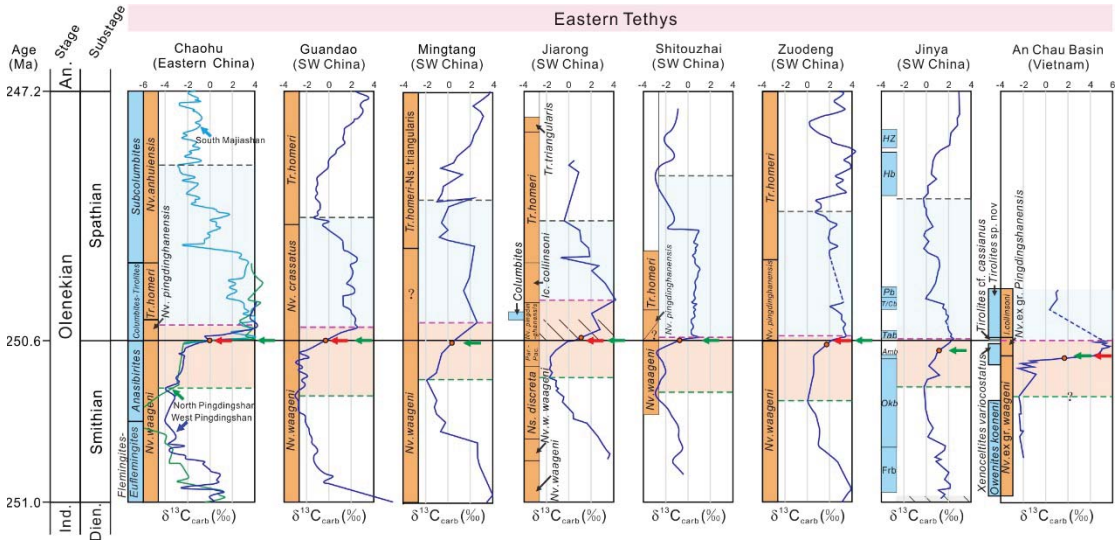

Fig. 11. Detailed correlations of Smithian-Spathian sections in the eastern Tethys region based on a combination of ammonoid and conodont biostratigraphy and C-isotope chemostratigraphy. Data sources: Chaohu from Zuo et al. (2003, 2004), Tong et al. (2004, 2007) and Zhao et al. (2007a); Guandao and Zuodeng from Wang et al. (2005), Tong et al. (2007), and Lehrmann et al. (2015); Mingtang from Liang et al. (2016); Jiarong from Chen-YL et al. (2013, 2015) (note: oblique lines represent uncertainty in SSB placement); Shitouzhai from Zhang et al. (2015); Jinya from Galfetti et al. (2007c); and An Chau Basin from Komatsu et al. (2016). Abbreviations: Dien. = Dienerian, Ind. = Induan, An. = Anisian, HZ = *Haugi* Zone, Hb = *Hellenites* beds, Pb = *Procolumbites* beds, T/Cb = *Tirolites*/*Columbites* beds, TAb = *Tirolitid* n. gen. A. beds, Okb = *Owenites koeneni* beds, Amb = *Anasibirites multiformis* beds, Frb = *Flemingites rursiradiatus* beds. See Figure 1 for timescale and Figure 7 for legend (including green and red arrows).

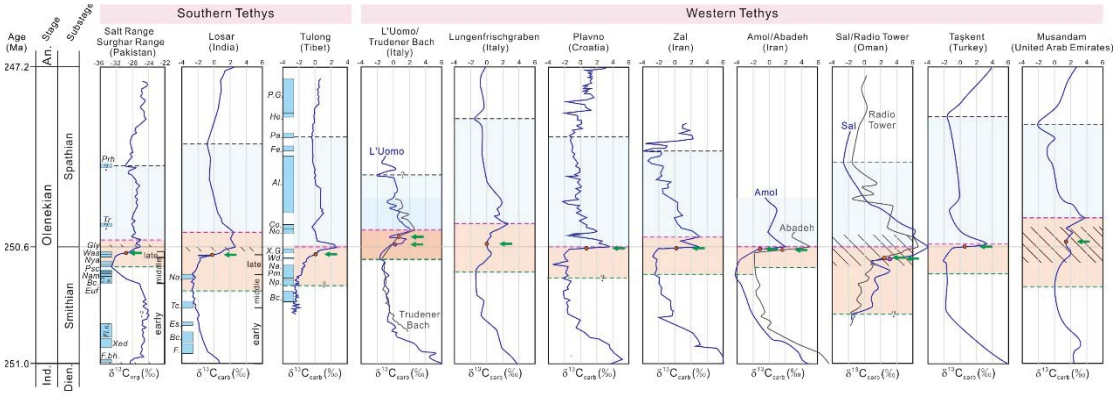

Fig. 12. Detailed correlations of Smithian-Spathian sections in the southern Tethys (North Indian Margin) and western Tethys regions based on a combination of ammonoid and conodont biostratigraphy and C-isotope chemostratigraphy. Data sources: Salt Range and Surghar Range from Hermann et al. (2012) (note: oblique lines represent uncertainty in SSB placement); Losar from Galfetti et al. (2007c); Tulong from Brühwiler et al. (2009, 2010) and Schneebeli-Hermann et al. (2012); L' Uomo from Horacek et al. (2007a); Trudener Bach and Lungenfrischgraben from Horacek et al. (2010); Plavno from Aljinović et al. (2018); Zal, Amol, and Abadeh from Horacek et al. (2007b); Sal from Richoz (2006); Radio Tower from Clarkson et al. (2016); Taşkent from Lau et al. (2016); Musandam from Clarkson et al. (2013). Abbreviations (sub/stages): Dien. = Dienerian, Ind. = Induan, An. = Anisian; (ammonoids): Al. = *Albanitid* n. gen, Bc. = *Brayardites compressus*, Co. = *Columbites*, C.s. = *Clypeoceras superbum*, Es. = *Escarguelites spitiensis*, Euf = *Euflemingites cirratus*, F. = *Flemingites*, F.bh. = *Flemingites bhargavai*, Fe. = *Fengshanites*, Fl.n. = *Flemingites nanus*, Gly = *Glyptophiceras sinatum*, He. = *Hellenites*, Na. = *Nyalamites angustecostatus*, Nam = *Nammalites pilatoides*, No. = *Nordophiceras*, Np. = *Nammalites pilatoides*, Nya = *Nyalamites angustecostatus*, Pa. = *Paragoceras*, P.G. = *Pseudodanubites-Gymnites*, Pm. = *Pseudoceltites multiplicatus*, Prh = *Prohungarites*, Psc = *Pseudoceltites multiplicatus*, Tc. = *Truempyceras compressum*, Tr = *Tirolites*, Was = *Wasatchites distractus*, Wd. = *Wasatchites distractus*, Xed = *Xenodiscoides perplicatus*, X.G. = *Xenoceltites-Glyptophiceras*. See Figure 1 for timescale and Figure 7 for legend (including green and red arrows).

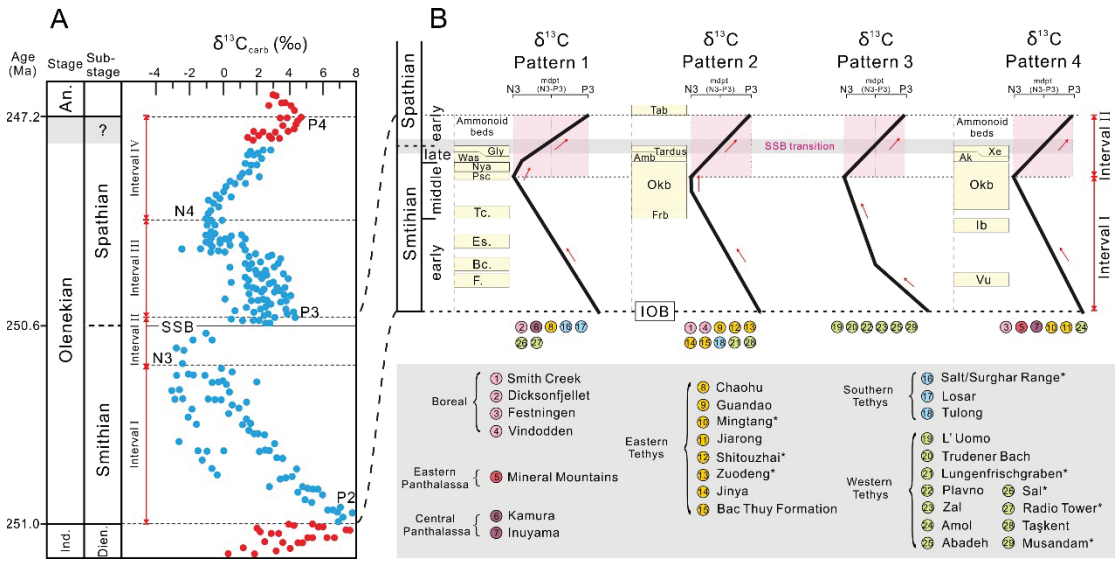

Fig. 13. (A) Carbon-isotope Intervals I to IV of the Olenekian substage. $\delta^{13}C$ data from Payne et al. (2004) and Chen and Benton (2012); N2-N3 and P2-P4 represent $\delta^{13}C$ minima and maxima per Song et al. (2013); and mdpt(N3-P3) is the isotopic midpoint between N3 and P3. (B) $\delta^{13}C$ variation patterns 1 to 4 within the early Smithian to early Spathian (Intervals I-II) based on 29 sections globally; asterisks (*) represent tentative assignments. The pink boxes highlight Interval II, which encompasses the SSB. The early/middle/late subdivisions of the Smithian and Spathian are based on ammonoid biostratigraphic studies as reviewed in Jenks et al. (2015). Representative ammonoid assemblages for Pattern 1 from Salt and Surghar ranges (Hermann et al., 2012) and Losar (Galfetti et al., 2007c), for Pattern 2 from Jinya (Galfetti et al., 2007c), and for Pattern 4 from Mineral Mountains (Thomazo et al., 2016). For abbreviations of ammonoid assemblages, see Figures 7, 11-12. See Figure 1 for other details.

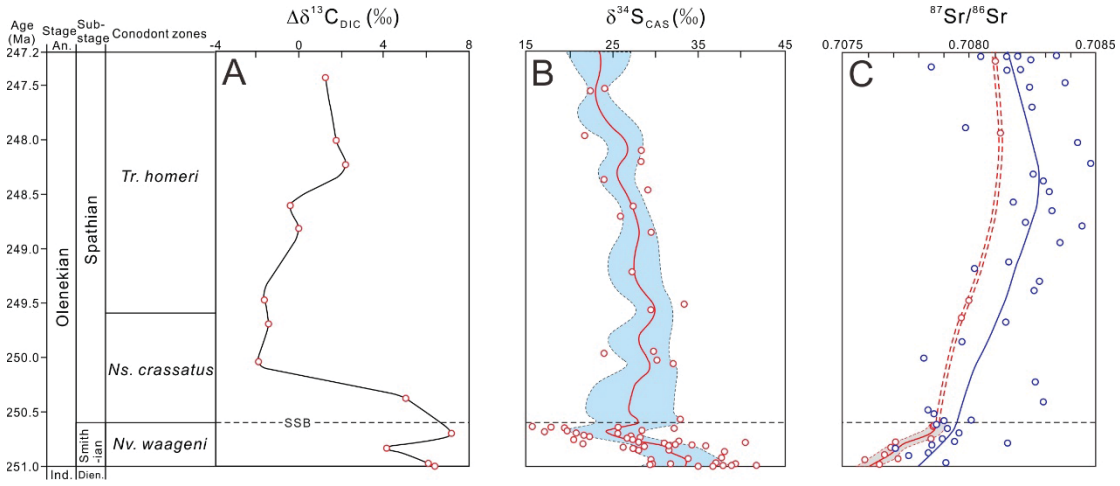

Fig. 14. Some other geochemical records for the Smithian and Spathian: (A) $\Delta\delta^{13}C_{DIC}$ (from Song-HY et al., 2013), (B) $\delta^{34}S_{CAS}$ (from Song-HY et al., 2014), and (C) $^{87}Sr/^{86}Sr$ (dashed red line = Sedlacek et al., 2014; solid blue line = Song-HJ et al., 2015). Conodont zones are from Song-HY et al. (2013, 2014). Dien. = Dienerian, Ind. = Induan, An. = Anisian.

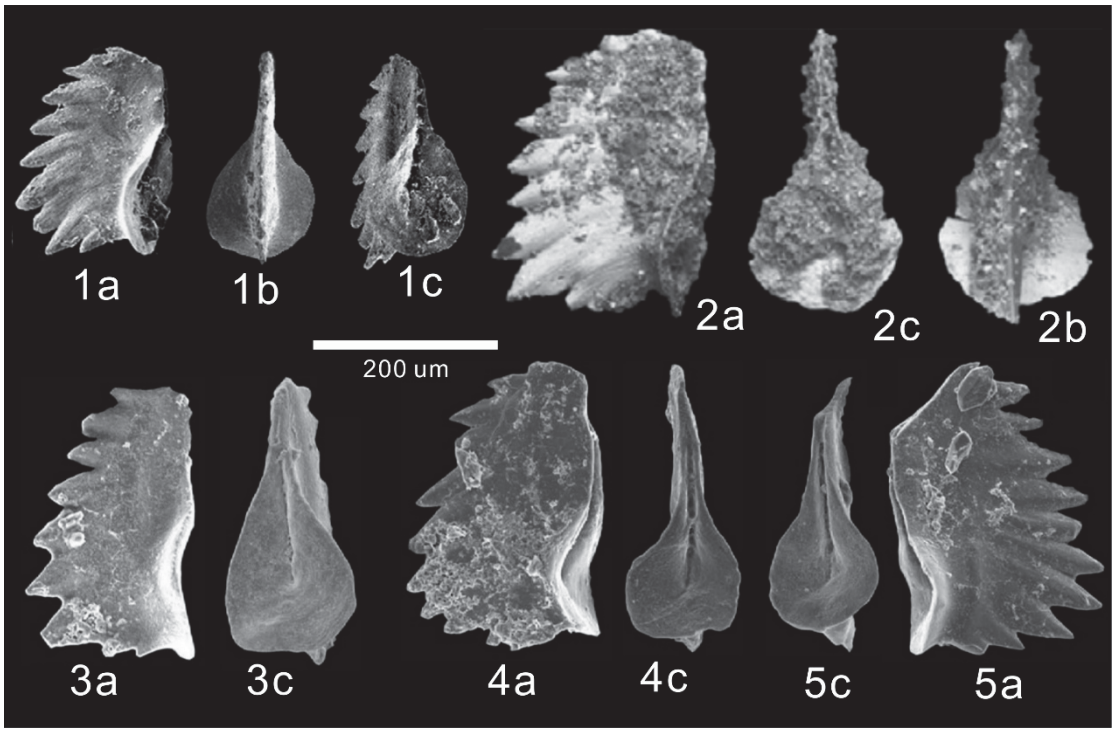

Fig. 15. Photographs of conodont *Novispathodus pingdingshanensis*. a = lateral view; b = upper view; c = lower view. 1) Holotype of *Nv. pingdingshanensis* (CUG03054) from West Pingdingshan, Chaohu area, eastern China (Zhao et al., 2007a); 2) *Nv.* ex. gr. *pingdingshanensis* (MPC25395) from the An Chau Basin, northeastern Vietnam (Komatsu et al., 2016); and 3-5) *Nv. pingdingshanensis* from Jiarong, Nanpanjiang Basin, southwestern China (Chen-YL et al., 2015).

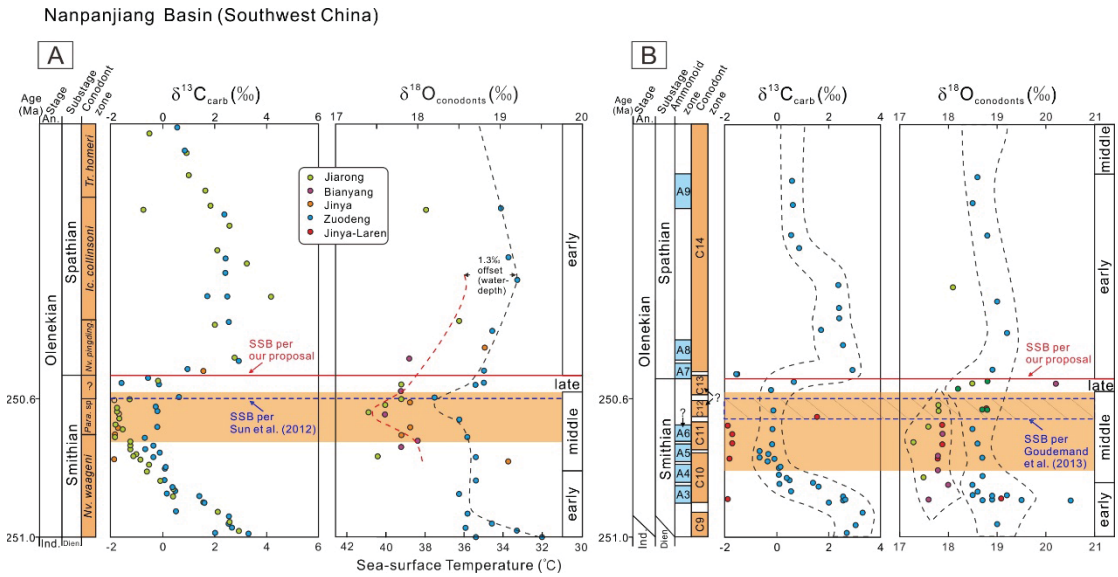

Fig. 16. Comparison of SSB placement based on mdpt(N3-P3) (red solid line; this study) with earlier SSB placements (blue dash lines) of Sun et al. (2012; A) and Goudemand et al. (2013; B). The orange field represents the interval of the Smithian Thermal Maximum (STM). Note that our SSB placement corresponds to a cooling event, as now widely accepted (e.g., Goudemand, 2014b, 2018; Zhang-L et al., 2017; Zhang-F et al., 2018; Stebbins et al., 2018a, b). Abbreviations: *Nv. pingding.* = *Nv. pingdingshanensis*; A3 = *Kashmirites densistriatus*; A4 = *Flemingites rursiradiatus*; A5 = *Owenites koeneni*; A6 = *Anasibirites multiformis*; A7 = Tirolitid n. gen. A; A8 = *Tirolites*/*Columbites*; A9 = *Procolumbites*; C9 = *Neospathodus dieneri*; C10 = *Novispathodus waageni*; C11 = *Parachirognathus* sp.; C12 = *Nv. pingdingshanensis*; C13 = *Icriospathodus collinsoni*; C14 = *Triassospathodus homeri*/*Ns. symmetricus*. See Figure 1 for other details.